R-09-07

Low pH self compacting concrete for deposition tunnel plugs

Carsten Vogt, Björn Lagerblad, Kjell Wallin, Franziska Baldy
Swedish Cement and Concrete Research Institute (CBI)

Jan-Erik Jonasson, Luleå Technical University (LTU)

April 2009

Svensk Kärnbränslehantering AB
Swedish Nuclear Fuel
and Waste Management Co

Box 250, SE-101 24 Stockholm
Phone +46 8 459 84 00

ISSN 1402-3091
SKB Rapport R-09-07

Low pH self compacting concrete for deposition tunnel plugs

Carsten Vogt, Björn Lagerblad, Kjell Wallin, Franziska Baldy
Swedish Cement and Concrete Research Institute (CBI)

Jan-Erik Jonasson, Luleå Technical University (LTU)

April 2009

Summary

The temporary plugs in the entrance of the deposition tunnel have three purposes, i.e. to bring about a water pressure in the deposition holes as quickly as possible in order to facilitate the wetting of the buffer, to reduce the groundwater's pressure gradient in the backfill so that piping is prevented, and to keep the backfill in place during the operating phase until the main tunnel has been backfilled.

In the repository concept, low-pH-concrete shall be used instead of conventional concrete. A low-pH concrete is a concrete with a leachate pH below 11, which is lower than in normal concrete (pH > 12.5). The low-pH concrete developed is achieved by replacing 40% by weight of the cement with silica fume. According to the current understanding, low-pH concrete should not disturb the function of the bentonite. This is accomplished by avoiding the development of a high-pH leachate by replacing leachable calcium compounds with silica in the low-pH-concrete.

There are different demands on the concrete in fresh and hardened state in order to fulfil its purpose. The geometry of the plug requires the fresh concrete to be self-compacting. The method of placement requires that the fresh concrete keeps its self-compacting properties for at least two hours. All components of the mix design must be commercially available and it must be possible to produce the concrete in a normal concrete factory. The concrete shall release low exothermic heat during curing. The volume changes of the young and mature concrete shall be minimised. The properties of the young and mature concrete need to be quantified in order to design and construct the plugs so that they fulfil the intended purpose.

Low-pH concrete with self-compacting properties has been developed and is presented in the report. The low-pH SCC (Self-Compacting Concrete) contains ordinary Portland cement, densified silica fume, limestone filler, superplasticizer, high quality natural fine aggregates and average quality crushed coarse aggregate. Two mix designs were tested, one mix design with 200 kg of binder (cement and silica fume) per cubic meter concrete (B200) and one with 300 kg of binder (B300). The low-pH SCC has high flowability, combined with good stability. Due to the low amount of cement in the low-pH SCC, the heat development due to hydration was low. The strength development was slow at early age but after 28 days, the compressive strength was 53 MPa (B200) and 71 MPa (B300). After 3 months, B200 has a compressive strength of about 75 MPa and B300 of about 100 MPa. The tensile strength of mature low-pH SCC is similar to mature conventional concrete. The properties of mature low-pH SCC do not differ significantly from conventional concrete other than a higher ultimate strength development. The established models for Young's modulus, compressive strength, tensile strength, stress-strain and creep are valid. The creep ratio is low when the concrete is mature. There is no large difference between the two mix designs; however, the mix B300 has a higher final compressive strength, Young's modulus and tensile strength. The higher early volume changes of B300 lead to higher stresses at young age when fully restrained.

Evaluation of the obtained results using mathematical models, established for traditional concrete, was possible. A setup of input data for finite element calculations was established. To what extent the differences between the two mix designs influence the development of stresses and consequently the risk of crack development in the plugs needs to be evaluated by further numerical modelling.

Sammanfattning

De temporära pluggarna i deponeringstunnelns mynning har tre syften, nämligen att så snabbt som möjligt få till stånd ett vattentryck i deponeringshålen för att underlätta buffertens bevätning, att minska grundvattnets tryckgradient i återfyllningen så att kanalbildning förhindras samt att hålla återfyllningen på plats under driftskedet till dess att övriga utrymmen har återfyllts.

I slutförvaret för använt kärnbränsle ska låg-pH-betong användas i stället för konventionell betong, för att i möjligaste mån undvika negativa effekter på bentonitens funktion. Låg-pH-betong är betong med ett pH lägre än 11, medan vanlig betong har ett pH på omkring 12,5. I den låg-pH-betong som utvecklats har 40 viktsprocent av cementen ersatts med silikastoft för att sänka pH-värdet hos läckvattnet från den färdiga betongen.

Det finns olika krav som ställs på den färska och hårdnade betongen för att den ska fylla sin funktion. Pluggens geometri kräver att betongen är självkompakterande och gjutningsmetodiken kräver dessutom att betongen behåller sina självkompakterande egenskaper under minst två timmar. Alla beståndsdelar som ingår i betongreceptet måste finnas tillgänglig på marknaden och betongen måste kunna blandas i en vanlig betongfabrik. Betongen ska dessutom utveckla låg värme när den härdar. Volymändringar i såväl den färska som den hårdnade betongen ska minimeras. Egenskaperna hos den härdade och mogna betongen skall kvantifieras så det går att beräkna och tillverka pluggar som uppfyller funktionskraven.

Självkompakterande låg-pH-betong (SCC) innehåller Portlandcement, silikastoft, kalkstensfiller, flytmedel, naturgrus av hög kvalité och krossballast av genomsnittlig kvalité. Två betongrecept, ett med 200 kg bindemedel (cement och silikastoft) per kubikmeter betong (B200) och ett med 300 kg bindemedel (B300), har testats. Låg-pH-SCC har bra flytbarhet kombinerad med god stabilitet. Värmeutvecklingen under härdningen är låg eftersom halten av cement är låg.

Hållfasthetsutvecklingen är långsam i början men efter 28 dygn har B200 uppnått 53 MPa i tryckhållfasthet och B300 71 MPa. Efter 3 månader har B200 uppnått cirka 75 MPa i tryckhållfasthet och B300 cirka 100 MPa. Draghållfastheten hos låg-pH-SCC är jämförbar med den hos konventionell betong. Mogen låg-pH-SCC skiljer sig inte avsevärt från konventionell betong, bortsett från högre sluthållfasthet. Etablerade modeller för elasticitetsmodul, tryckhållfasthet, draghållfasthet, spänning- deformationsrelation och krypning gäller. Krypningen är liten för mogen låg-pH-SCC. Skillnaden mellan B200 och B300 är inte nämnvärt stor, men B300 har högre tryckhållfasthet, elasticitetsmodul och draghållfasthet än B 200. Eftersom B300 har större volymändringar i det unga skedet leder detta till större dragspänningar i ung ålder om rörelse förhindras.

Försöksresultaten kan utvärderas med etablerade samband som utvecklats för konventionell betong. En uppsättning ingångsparametrar för numeriska beräkningar skapades. Vilken betydelse skillnaden mellan de två betongrecepten har på utveckling av spänningar och sprickor i pluggen måste avgöras med hjälp av ytterligare beräkningar.

Contents

1 Orientation

CBI was asked by Swedish Nuclear Waste Management (SKB) to help in the development of a low pH concrete to construct plugs in order to seal off deposition tunnels in a repository for nuclear waste.

In the deposition tunnels, concrete plugs restrain the tunnel backfill and act as part of the deposition tunnel sealing system. The plugs limit water movement but are not considered the primary water seal for deposition tunnels. The plugs shall withstand a hydraulic pressure of 4 MPa plus 2 MPa swelling pressure from the bentonite backfill, see /Dahlström et al. 2008/, and shall be free of continuous cracks or gaps.

A prototype plug has already been built with conventional self compacting concrete with compressive strength of 50 MPa, see /Dahlström et al. 2008/. It is designed as a reinforced convex concrete plug with a diameter of a little more than 5 m and an overall plug thickness of approximately 1.3 m, see Figure 1-1. The plug is reinforced due to the expected load on the structure. Water cooling pipes were cast in to reduce the likelihood of temperature induced cracking.

In the repository concept described by SKB, low pH concrete shall be used instead of conventional concrete. According to current understanding, the use of low pH concrete should not disturb the function of the bentonite. A low pH concrete is a concrete with a pH lower (pH < 11) than normal concrete (pH > 12.5). The low pH concrete developed in this program is achieved by replacing 40% by weight of the binder with silica fume. However, reducing the amount of low pH concrete used in a repository is still recommended to reduce the possible influence of leachate on bentonite.

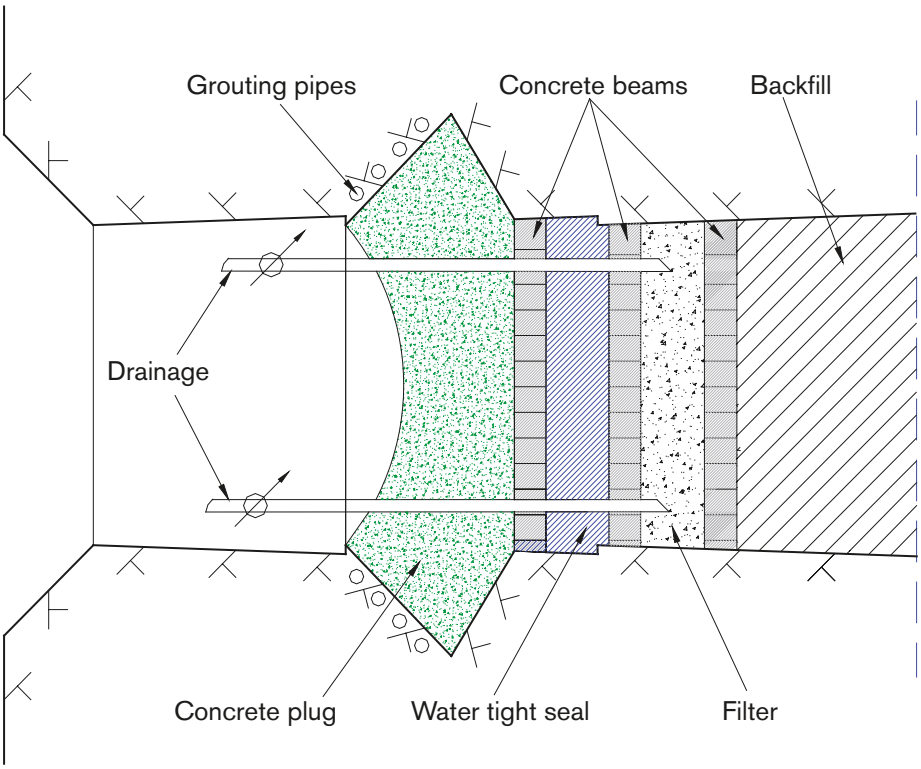

Figure 1-1. *SKB basic design for arch shaped concrete plugs, see /Dahlström et al. 2008/.*

There are several processes in fresh and hardening concrete which cause volume reduction and can result in cracking of a structure. The cement hydration itself is a process that results in reaction products with less volume than the ingredients. Loss of water due to drying is another reason for volume changes of concrete. Usually, volume changes of concrete are summarised as different types of shrinkage, e.g. chemical shrinkage, autogenous shrinkage and drying shrinkage. The mechanisms and theories as well as the consequences are described in the literature; see e.g. /Taylor 1997, Lea 2000, Neville 1994/.

In large volume constructions, another aspect that has to be considered is thermal cracking. In the fresh concrete, the exothermal process of the cement hydration will increase the temperature in the concrete and cause expansion of the fresh and hardening concrete. Later, the subsequent cooling will shrink the hardened concrete, resulting in tensile stresses. There will be temperature gradients within the plug which may cause internal cracking in the concrete. The temperature gradients and temperature raise must be minimized and therefore low heat cement is usually used in large volume constructions. Alternatively, one can cool the fresh concrete before casting or use cooling pipes. For more information on thermal cracking of concrete, see e.g. /Emborg 1989/ or other relevant literature.

All relevant material parameters are mostly known and considered for normal concrete in structural calculations or crack risk analysis. The material parameters are not known for low pH concrete. To be able to plan and construct a plug with low pH concrete, the thermal, viscoelastic and shrinkage properties are required for calculations.

2 Research program

2.1 Demands on the low pH concrete

The following demands on the concrete to be used in the plug were identified before the work started:

1. It shall be pumpable.
2. It shall be self-compacting and keep its self-compacting properties for at least 2 hours.
3. It shall be possible to be produced in a normal concrete factory.
4. It shall have a final compressive strength of at least 50 MPa.
5. It shall give as low exothermic heat as possible to minimize cooling measures. The amount of binder shall be kept low to minimize heat development and shrinkage.
6. The components shall be commercially available.
7. The concrete must give a pH of less than 11 to the groundwater when leached.
8. The concrete is allowed to contain organic superplasticizer but the amount shall be minimised. No other organic components are allowed.

2.2 Overall research program

The low pH concrete development for the plugs involves several stages where different aspects are tested. It will be iterative where failure in one stage may force the program to go back to a previous stage (Figure 2-1).

Stages

1. Development of mix design (includes laboratory trials).
2. Testing of mix design at a concrete factory.
3. Revision of mix design if necessary.
4. Testing and quantification of concrete properties.
5. Structural design with low pH concrete material parameters.
6. Revision of concrete mix design if necessary. To be done using interpolation between the two tested mixes from stage 1 to 3.
7. Casting of full size plug in an Äspö tunnel.

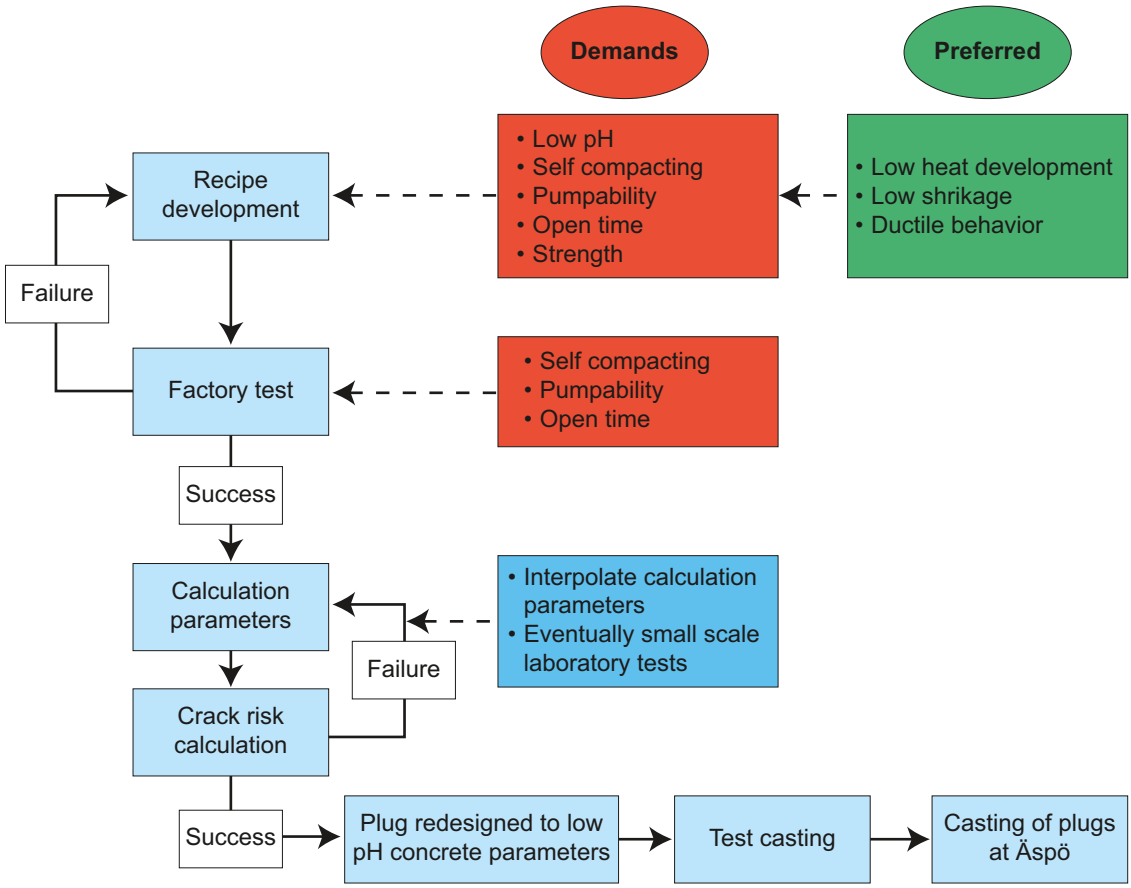

Figure 2-1. *Flow chart of development process of plug concrete.*

3 Development of mix design

3.1 Introduction

The basic concept of how to make a low pH concrete is known from other projects. A pH of 11 can be achieved by composing the binder of at least 35 to 40 wt. % silica fume which is an active pozzolana that reacts with Portland cement in such a way that it changes the chemical properties of the cement paste.

Volume changes do occur for several reasons in fresh and hardening concrete; see /Taylor 1997, Lea 2000, Neville 1994/. The consequences on different constructions are important. A free body may not be influenced at all while a restrained body may crack. The plug is restrained by the surrounding rock. Therefore different types of volume changes like thermal expansion and different types of shrinkage may cause cracking and development of free space between concrete and rock. To minimize volume changes the concrete should contain a minimum of cement as the exothermic cement reactions will cause thermal shrinkage/cracking. The cement used in Sweden for constructing mass concrete constructions like the plug is a CEM I MH, SH, LA (moderate heat, sulphate resistant and low alkali) according to /SS-EN 197-1 2000/. Anläggningscement from Cementa fulfils these requirements.

In other projects, different types of low pH concrete have been developed and tested. Thus some basic knowledge is available:

1. It is possible to make a self compacting low pH concrete.
2. The low pH concrete is more viscous than ordinary concrete, which makes it more difficult to pump.
3. It is possible to reduce the amount of binder to low contents if ultra fine filler is added.
4. The strength is at least similar to ordinary concrete with the same amount of binder or higher.
5. The shrinkage is higher than that of ordinary concrete.
6. The shrinkage (autogenous) lasts for a longer period than that of ordinary concrete.

Self-compacting concrete (SCC) is a concrete which is able to flow under force of gravity only, fills the formwork completely and achieves full compaction without additional compacting work /EFNARC 2005/. It is usually considered to have different properties than conventional concrete in the fresh state but similar properties when hardened /EFNARC 2005/. This is not completely correct. There is research data which indicates that self-compacting concrete:

1. Has a higher creep ratio than conventional concrete /Reinhardt and Wuestholz 2007/.
2. Is more sensitive to early volume changes due to its high content of fine powder /Esping 2007/.

Therefore, the early volume changes and creep properties of low pH SCC should be examined.

For the further development within the research program, two concrete mix designs should be tested, incorporating different amounts of binder. The amount of binder should be minimised as much as possible. Problems with pumpability due to high viscosity of the concrete may occur if the binder content is reduced too much. Two binder contents are suggested with about 200 and 300 kg of binder per m^3 of concrete. In the following, the mix with 200 kg of binder is denoted B200 and the mix with 300 kg of binder is denoted B300. While both mix designs require filler, this is especially true of the mix design with 200 kg of binder. Quartz filler is normally used but this may cause problems (silicosis) at the concrete factory, so other fillers were tested. The strength development can be expected to be fairly slow. Thus the final strength should be measured after 91 days. Leaching tests were not included in this program.

3.2 Composition of different mixes depending on the fresh concrete properties

One important factor for the successful installation of the plugs are the self compacting properties of the mixes. There are different ways of achieving self-compacting properties for concrete. One common method is to increase the amount of paste in the concrete by adding fillers. Another possibility is the addition of VMA (viscosity modifying agent), but the safety assessment analysis of the repository requires minimising of the amount of organic components in the concrete. Therefore it was decided to develop filler-based self compacting low pH concrete. In the report, this material is denoted low pH SCC.

3.2.1 Mix components

One of the basic requirements on the mix composition was that the components should be commercially available and the production of the concrete should be possible in a normal mixing plant. Therefore it was decided to concentrate on limestone as filler material as this is the most commonly used filler material in Sweden. The other components used are cement CEM I, silica fume, natural fine aggregates (0–8 mm) and crushed coarse aggregates (8–16 mm) as well as polycarboxylate based superplasticizer. Quartzfiller M 300 was used in some test mixes for comparison. The basic chemical composition of all materials is given in Table 3-1.

Different requirements on the aggregates were identified, see Table 3-2. The coarse aggregate was considered to be of minor importance for the properties of especially the fresh concrete. It should meet the requirements for concrete aggregate in /SS-EN 12620 2008/. The coarse aggregate used in this project was crushed granite of average quality from the Stockholm area. Therefore it should be easy to find similar or better material for the production of the plugs. The fine aggregate was considered to be more important for the quality of the concrete. Therefore, natural sand of high quality with a well distributed grading curve from the Äspö area was used. This sand contains rather high amounts of fine material, which should be beneficial for the stability of the low pH SCC.

The grading curves of fine and coarse aggregates are displayed in Figure 3-1. If a change of aggregate source is required for some reasons, it is important to choose similar material in order to maintain the properties of the self compacting low pH concrete. Usually, a natural variation of 3–5 wt. % is considered acceptable in concrete production. The grading curves of the aggregates should be within this variation.

If one intends to change the type of filler or cement, it should be noted that the substitution material needs to be of similar fineness and chemical composition. That implies that another type of sulphate resistant low alkali cement or limestone filler of similar fineness from other manufacturers could be used without major changes in mix design and concrete properties. However, some additional testing would be necessary.

Table 3-1. Basic chemical components and manufacturers of the materials incorporated in the low pH SCC.

Material	Components	Manufacturer
Anläggningscement CEM I 42.5 MH/SR/LA	CaO, SiO_2, Al_2O_3, Fe_2O_3	Cementa
Silica Fume	SiO_2	Elkem, Fesil
Limestone filler Limus 25 and 40	$CaCO_3$	Nordkalk
Quartz filler M 300	SiO_2	Sibelco
Granitic aggregates	Granitic rock composition	local
Superplasticizer Glenium 51	Polycarboxylate solution, 35% dry content	BASF

Table 3-2. Requirements on the aggregates in the low pH SCC.

	Fine aggregate	Coarse aggregate
Relevant standard	/SS-EN 12620 2008/	/SS-EN 12620 2008/
Type	natural	Natural or crushed
Grading	Close to curve A /betonghandbok 1994/	

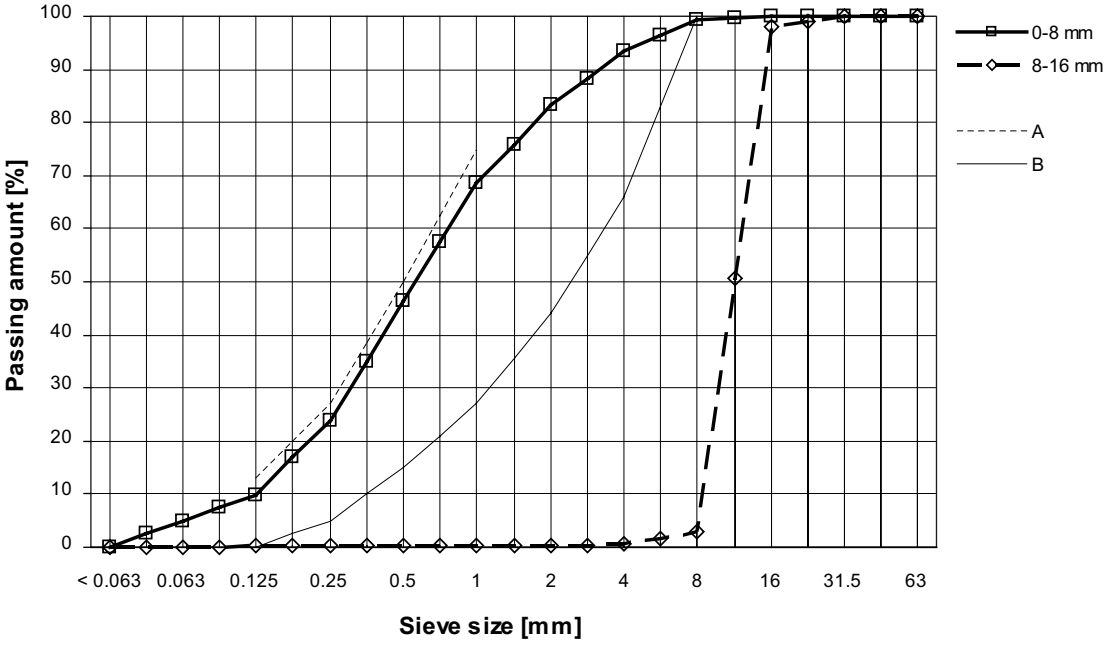

Figure 3-1. *Grading curve of fine (0–8 mm) and coarse (8–16 mm) aggregate. Curves A and B are the limiting grading curves for suitable fine aggregate 0–8 mm according to /Betonghandbok Material 1994/.*

3.2.2 Mix development and fresh concrete properties

Measuring the rheology of self-compacting concrete in a concrete viscometer is a well established procedure in laboratories and is used all over the world in developing and evaluating the properties of fresh self-compacting concrete. The methodology that was used in this program was to test different mix compositions in a concrete viscometer (ConTec 4) and adjust the mix until sufficient rheological parameters were measured. In addition to the rheological measurements, the slump flow was measured at different points of time after mixing and the mixed concrete was visually inspected (Figure 3-2).

/Wallevik 2007/ establishes a relationship between yield value and viscosity of concrete mixes required to achieve self compacting properties. If the rheological properties of a mix composition are measured and the resulting point in a yield value – viscosity diagram lies within the dashed curve, one has an indication that the mix may have sufficient self compacting properties. The dashed curve in Figure 3-3 and Figure 3-5 is based on rheological measurements of self compacting concrete in different countries with different concepts of making SCC and gives an idea about the ratio between yield value and viscosity that gives workable SCC compositions. Compositions high above the dashed line may have too low flowability, while concrete with rheological parameters far below the line can show separation. The low pH SCC has a much higher content of silica fume and lower cement content; therefore it may have different properties compared to conventional SCC. However, when measuring the rheological properties of the initial mixes that were considered workable, it could be seen that there were no big differences compared to normal SCC. Mixes which were separating or too stiff could not be measured and are not presented.

Figure 3-2. *Slump flow test, note the evenly distributed coarse aggregate.*

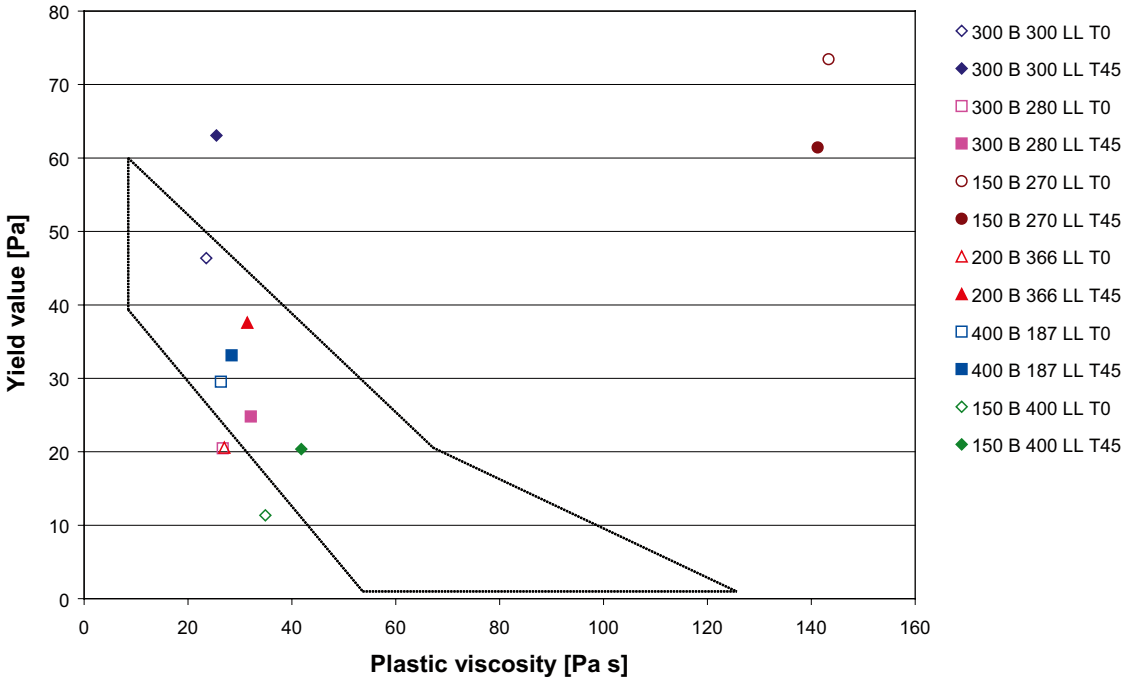

Figure 3-3. *Measured rheological parameters of some initial mixes with different amounts of different limestone fillers, different binder contents, and different water-binder ratios. Test carried out directly after mixing and 45 min after mixing. The amount of binder is given as the first number; amount of limestone as second and time after mixing is the third. The dashed line describes the area of favourable yield value – viscosity combinations for SCC according to /Wallewik 2007/.*

It can be seen in Figure 3-3 that the mix with 200 kg of binder and 366 kg of limestone filler as well as the one with 300 kg of binder and 280 kg of limestone filler showed sufficient workability. Therefore those mixes were optimised in several steps which are not presented here and the resulting mix compositions for B200 and B300 can be seen in Table 3-3. Taking into account the amount of water in those mixes, the ratio between water and binder plus filler is close to 0.30. This number is similar to conventional high quality filler-based SCC. In order to increase the stability of B200 and B300, limestone filler Limus 25, which is more fine-grained than Limus 40, was used. The filler content was adjusted to give a water- powder ratio of 0.29. The water content for the mixes B200 and B300 was kept constant; consequently the water binder ratio differs.

The mixing order for the low pH SCC has to be altered compared to conventional SCC. This is contributed to high content of densified silica fume which needs to be dispersed, see /Lagerblad and Utkin 1993/.

Table 3-3. Mix composition of the optimized mixes, chosen for more intensive testing.

Kg/m³	B200	B 300
CEM I 42.5 MH/SR/LA	120	180
Silica fume (densified)	80	120
Water	165	165
Limestone filler L25	369	269
Sand 0–8 mm	1,037	1,035
Gravel 8–16 mm	558	557
Glenium 51	6.38	7.08
water/cement	1.375	0.917
water/binder	0.825	0.55
water/powder	0.29	0.29

Table 3-4. Mixing order of low pH SCC in laboratory.

1	Aggregates and silica fume
2	Mixing
3	Cement and limestone filler
4	Mixing
5	Water and superplasticizer
6	Final mixing

The required mixing time depends on the efficiency of the mixer but can be expected to be at least two times longer than for conventional SCC. Intensive mixing is required to achieve homogeneous concrete, especially with such high contents of silica fume.

Figure 3-4 shows that the loss in slump flow is rather small, presumably due to the high amount of plasticizer per cement unit. The dosage of plasticizer is higher than for normal SCC but this is required due to the large specific surface of the silica fume.

Figure 3-5 shows the development of the rheological parameters yield value and viscosity over time. Mixes B200 and B300 were tested. Figure 3-6 shows that the loss of workability for B200 with time is acceptable; and addition of superplasticizer raised the slump flow to the initial value. The low pH SCC can be expected to be workable for at least 4 hours, provided that the concrete is mixed all the time and addition of superplasticizer is possible. The results mainly show that the yield value increases with time, but that the viscosity of the mixes is almost constant. That is very beneficial regarding the open time (period of time a batch of concrete is workable) of the low pH SCC as the yield value of a SCC mix can be influenced by superplasticizer. Even though it may seem that the tested mixes (Figure 3-5) loose their self-compacting properties rather rapidly, this did not prove to be the case. The mixes kept a high slump flow (compare Figure 3-4 and Figure 3-5) even though the measured yield stress increased. This can be explained by the fact that the concrete was resting in the viscometer, thus building up an inner structure, while the concrete that was tested on slump flow was mixed gently all the time.

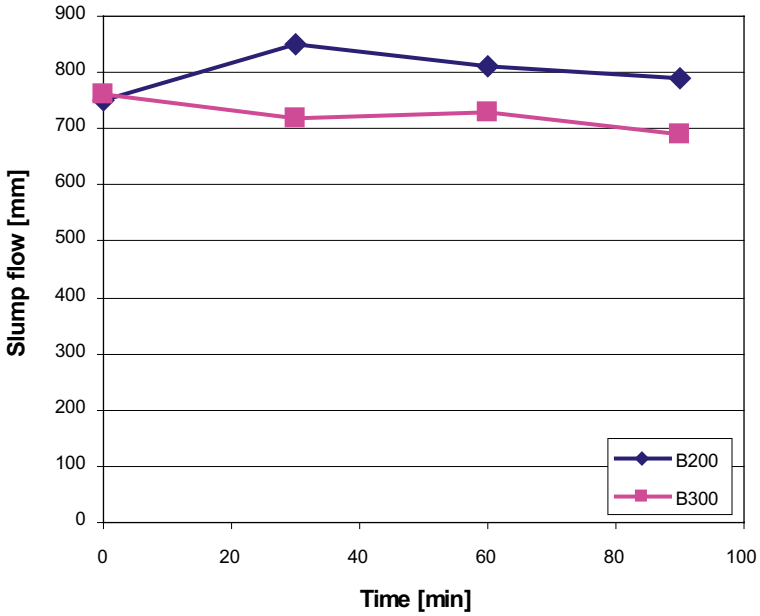

Figure 3-4. *Slump flow value versus time for the optimised mix compositions B200 and B300.*

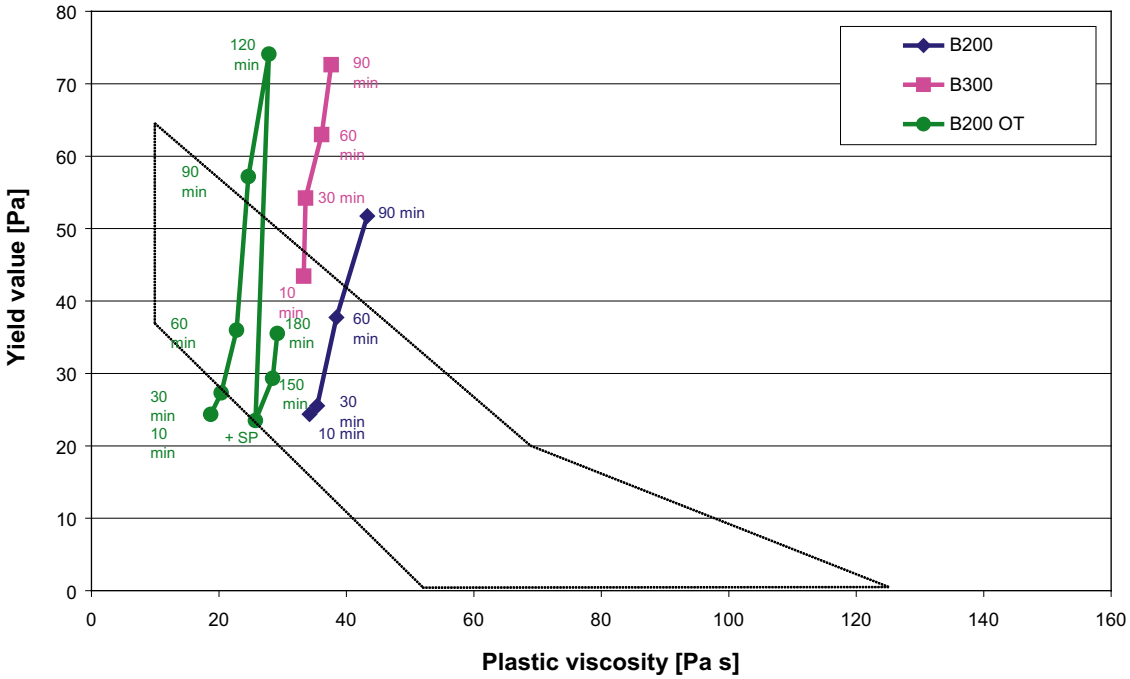

Figure 3-5. *Rheological parameters for the optimized mixes B200 and B300 at different points of time after mixing. B200 OT is an additional mix of B200 investigated for 180 minutes where superplasticizer was added after 120 minutes. The dashed line describes the area of favourable yield value – viscosity combinations for SCC according to /Wallewik 2007/.*

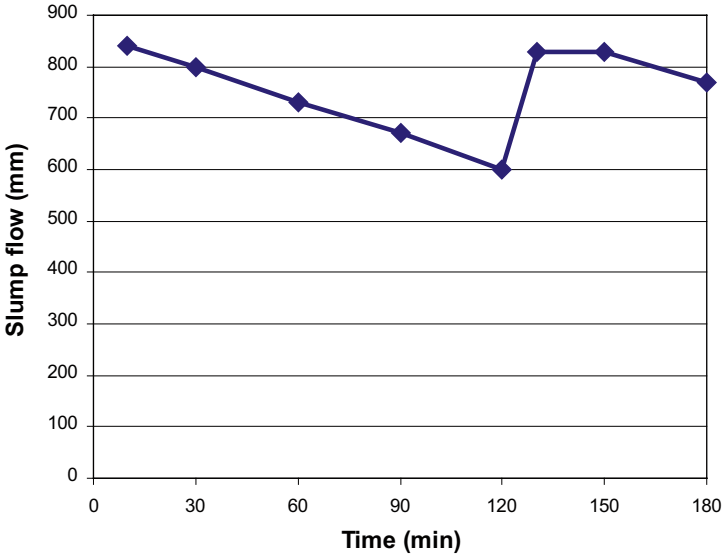

Figure 3-6. *Slump flow over time for mix B200; after 120 minutes with addition of superplasticizer.*

3.3 Hardened concrete properties

3.3.1 Compressive and splitting tensile strength

The compressive strength (Figure 3-7 and Table 3-5) was tested using cubes of 100 × 100 × 100 mm^3 according to /SS-EN 12390-3 2001/. The samples were stored in water at three different temperatures, 5°C, 20°C and 35°C. The splitting tensile strength (Table 3-5) was tested using cubes of 150 × 150 × 150 mm^3 according to /SS-EN 12390-6 2000/ on samples cured at 20°C at 100% RH.

Figure 3-7 shows the development of the compressive strength at different temperatures for the tested mix designs. It can be seen that the increased binder content in B300 leads to higher compressive strength. This is most pronounced at an age of 91 days, B200 has compressive strength (recalculated to 150 mm cubes) of about 75 MPa and B300 of 100 MPa at 20°C. The strength development is slow for all mix designs, compared to normal concrete. However, the final strength is much higher than for traditional concrete with similar water binder ratio and binder content. Traditional concrete with the same water/binder and binder content as B200 would have a compressive strength at 91 days of around 20 MPa /Neville 1994/.

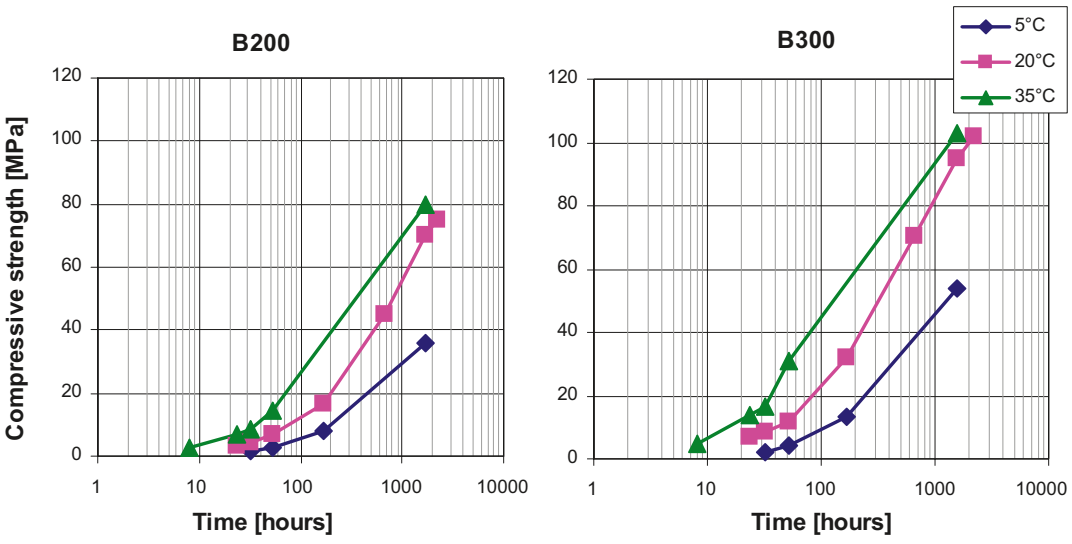

Figure 3-7. *Compressive strength development of B200 and B300, stored at 3 different temperatures; time axis is logarithmic, 2,184 h = 91 days.*

Table 3-5. Splitting tensile strength and compressive strength for mixes B200 and B300. Compressive strength recalculated from 100 mm cubes to equivalent values for 150 mm cube according to EN 206-1.

	B200		B300	
Compressive strength	28 days	91 days	28 days	91 days
Mean value [MPa]	43.4	72.6	68.1	98.7
Lowest value [MPa]	42.5	71.6	66.2	97.8
Splitting tensile strength				
Mean value [MPa]	4.2	5.7	5.5	6.27
Lowest value [MPa]	3.88	5.52	5.03	6.0

The differences in the rate of strength increase and ultimate strength compared to traditional concrete must be taken into account when modelling the plug construction in order to simulate the correct mechanical behaviour of the low pH SCC.

In Table 3-6 the values for compressive strength and calculated tensile strength of B200 and B300 were compared to standard calculation parameters for concrete strength from /EN 1992-1-1 EC2 2004/. The compressive strength values obtained for water cured cubes of 100 mm were first converted to equivalent values for cubes of 150 mm and then an equivalent to cylinder compressive strength. The coefficients used can be found in /SS-EN 206-1 2001/. The correlation factor between central tensile strength and splitting tensile strength given in /Betonghandbok Material 1994/ differs between 0.7 and 1.0. A conservative evaluation using a factor of 0.7 is chosen here.

Table 3-6. Transformation of splitting tensile strength to tensile strength and comparison with values from /EN 1992-1-1 EC2 2004/.

	B200	B300
28 day parameters		
Tested parameters		
Compressive strength (150 mm cube) [MPa]	43	68
Calculated compressive strength (cylinder) [MPa]	34	54
Splitting tensile strength [MPa]	4.2	5.5
Tensile strength = 0.7*splitting tensile strength [MPa]	2.94	3.85
Parameters from EN 1992-1-1		
Concrete strength class (acc. to SS-EN 206-1)	C 30/37	C 50/60
Compressive strength (cylinder) [MPa]	30	50
Tensile strength [MPa]	2.9	4.1
91 day parameters		
Tested parameters		
Compressive strength (150 mm cube) [MPa]	73	99
Calculated compressive strength (cylinder) [MPa]	58	79
Splitting tensile strength [MPa]	5.7	6.3
Tensile strength = 0.7*splitting tensile strength [MPa]	4.0	4.4
Parameters from EN 1992-1-1		
Concrete strength class (acc. to SS-EN 206-1)	C 55/67	C 70/85
Compressive strength (cylinder) [MPa]	55	70
Tensile strength [MPa]	4.2	4.6

Low pH SCC has similar relationship between compressive strength and tensile strength as the standard calculation parameters in EN 1992-1-1 imply.

3.3.2 Resistance against water penetration

The resistance against water penetration was tested according to /SS-EN 12390-8 2000/ after 3 months of water curing on samples of 150 × 150 × 150 mm^3. The measured water penetration was 5 mm for B200 and 3 mm for B300. The low pH SCC meets the requirements in /Betonghandbok Material 1994/ of less than 50 mm water penetration and can be considered to be water tight. However, water transport may still occur in cracks or in the contact zone between rock and concrete.

3.3.3 Heat development during hydration

The heat development during hydration is an important input parameter in crack risk calculations for young concrete. The equipment shown in Figure 3-8 was used to evaluate the heat development of the different mixes. In combination with strength development and viscoelastic material parameters, these values will be used as input parameters in calculating the thermal crack risk for the plugs.

Figure 3-9 shows the measured heat development for B200 and B300. The temperature increased about 7°C for B200 and about 9°C for B300 in the semi-adiabatic calorimeter. These are very low values compared to conventional concrete. /Ekerfors 1995/ measured temperature rise of 40–45°C for conventional concrete. The low heat development of low pH SCC correlates well with the slow strength development.

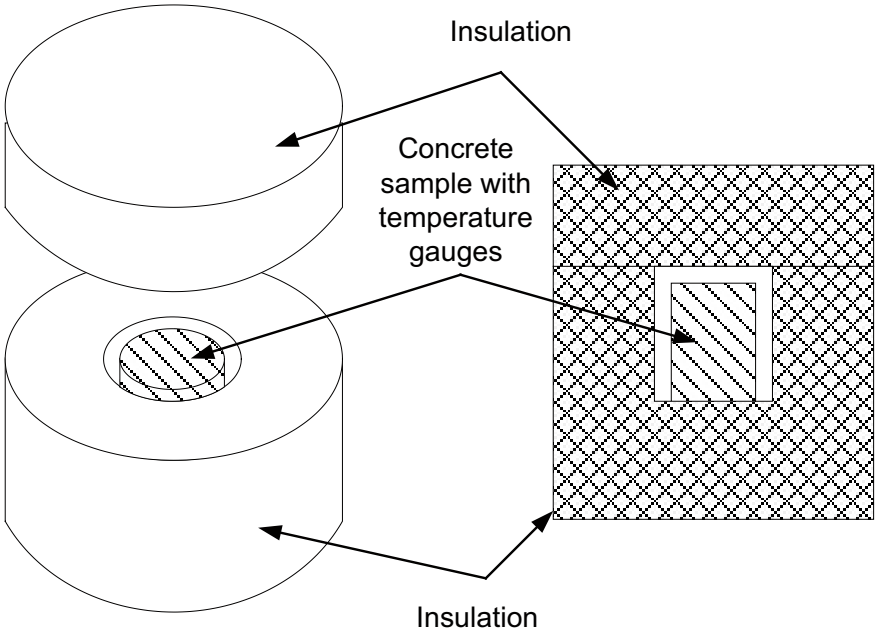

Figure 3-8. *Semi-adiabatic equipment used for measurement of heat development during hydration, see /Ekerfors 1995/.*

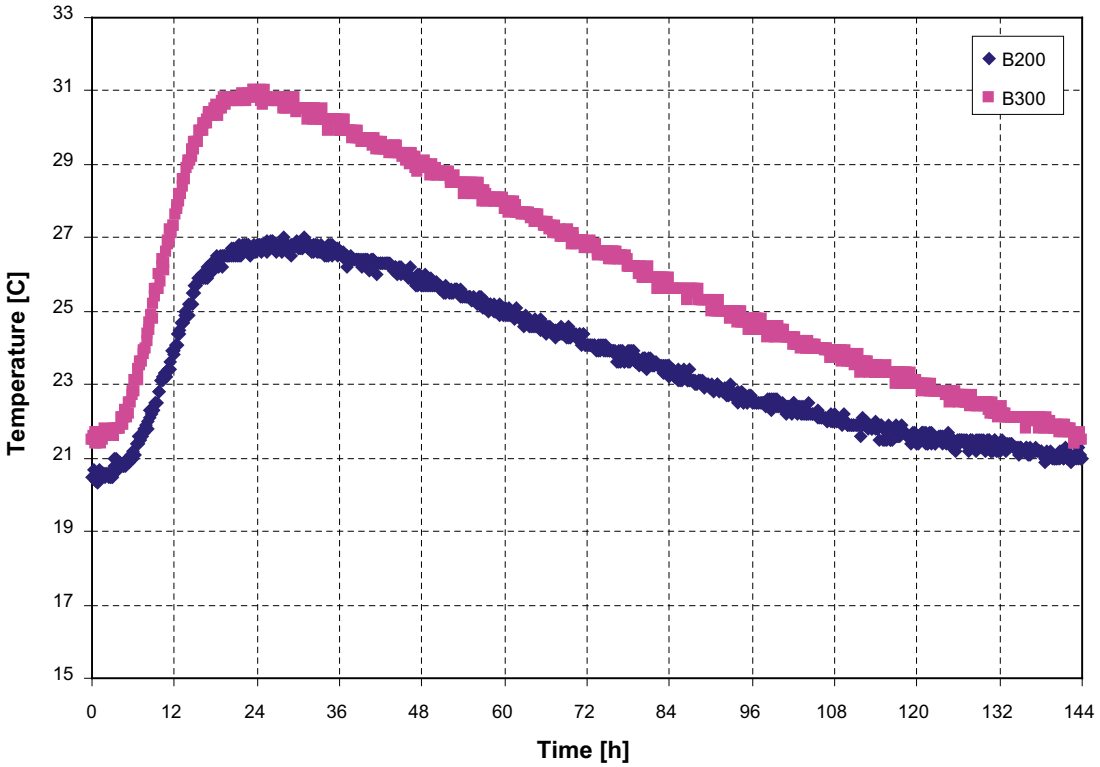

Figure 3-9. *Heat development for B200 and B300. The heat development was measured in the semi-adiabatic calorimeter.*

3.3.4 Shrinkage

The shrinkage properties of the low pH SCC were considered to be of major importance for the performance of the plug construction. Therefore, shrinkage was tested with different methods. When testing shrinkage, the environment the concrete will be kept in has to be taken into consideration. The plugs will be installed in tunnels with changing humidity. However, the plug is a massive construction and only the surfaces of the plug may be influenced by the environment. As the majority of the plug volume will not be influenced by the environment, shrinkage under sealed conditions was considered to be the relevant property to study. The literature, e.g. /Taylor 1997/, defines shrinkage under sealed conditions as autogenous shrinkage.

The shrinkage measurement according to Swedish standard /SS 13 72 15 2000/ starts at a concrete age of 7 days. No information is obtained for the first 7 days. This was regarded to be unsatisfying for the low pH SCC plugs. Therefore, shrinkage measurements were started as early as possible. There are methods which allow to measure volume changes of concrete almost immediately after mixing; other methods require certain strength for the concrete to be tested. Problems can occur when comparing the results of those different shrinkage measurement methods, as all of them use different physical principals and have various sources of error.

In this investigation, the autogenous shrinkage was measured in three different ways; two of them are described in /Esping 2007/ and the third method was a modified standard test /SS 13 72 15 2000/.

First, volumetric measurement of autogenous shrinkage was performed on samples in a tight flexible latex membrane submerged in a bath of water (see Figure 3-10). The samples' change in volume was measured by the change in weight (reduced buoyancy, according to Archimedes' principle). The measurement started about 30 minutes after mixing.

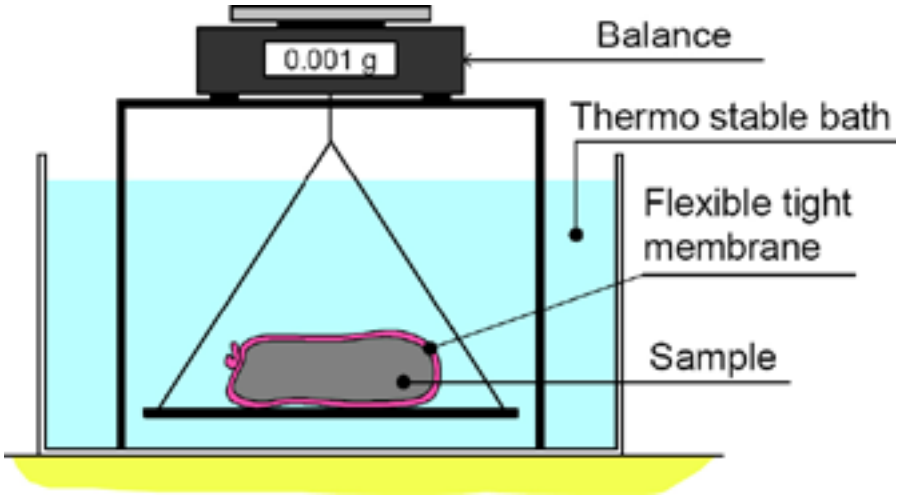

Figure 3-10. *Illustration of volumetric autogenous shrinkage measurement by reduced buoyancy technique (method 1), from /Esping 2007/.*

The second method that was used to measure the early autogenous shrinkage of concrete is the use of a digital dilatometer (see Figure 3-11). The method and equipment is described in /Esping 2007/. The measurement starts about one hour after mixing. The concrete specimen to be measured is cast into a flexible plastic tube and placed into a measuring frame.

In a third method, standard beams /SS 13 72 15 2000/ of 100 × 100 × 400 mm^3 were demoulded one day after casting. Half of the samples were sealed with special gas-tight butyl tape. The other half of the samples was stored with free surface in 50% RH. Shrinkage and weight measurements started 24 hours after casting.

The results from the measurements with reduced buoyancy (method 1) (Figure 3-12) show that there is a large volume change during the first 6 h for both mixes. Later, B300 shrinks at a slower speed than B200. This is presumably due to the development of a denser microstructure as curing progresses. As B300 with more binder and lower water to binder ratio has a faster development of microstructure and strength, the volume change will slow down earlier in the hardening process. Re-calculating the volume change to length change in order to compare with other shrinkage measuring methods, the correlation factor determined is shape dependent. A factor of around 3 (valid for a cube) can be assumed for the irregular shape of the sample within the membrane. The length change for both mixes after 24 hours is approximately 1.3 mm/m.

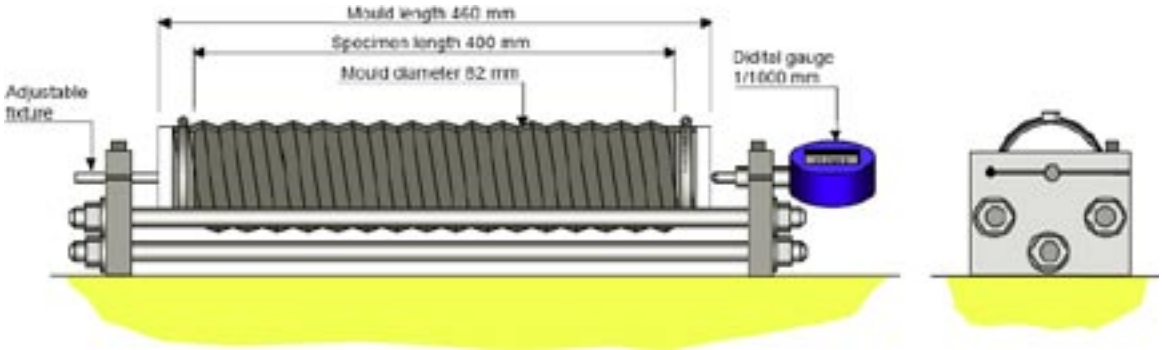

Figure 3-11. *Dilatometer (method 2) for measurement of early autogenouse shrinkage of concrete according to /Esping 2007/.*

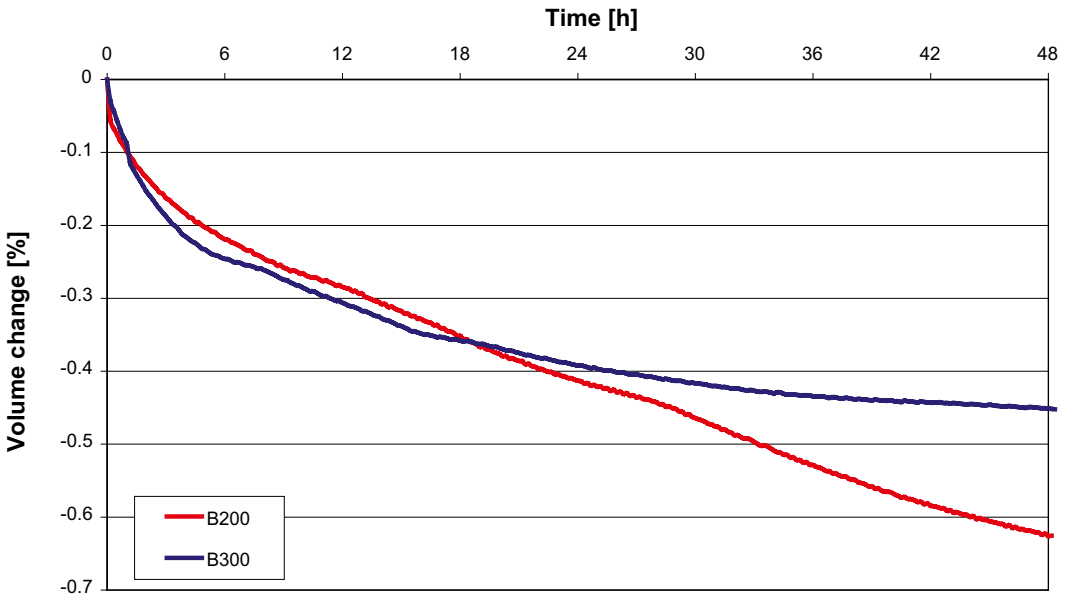

Figure 3-12. *Early volume change of small concrete samples, measured under water in water tight membrane with reduced buoyancy (method 1).*

The shrinkage of B200 and B300 were measured with the dilatometer (method 2) for a long period of time. Figure 3-13 shows the total shrinkage of low pH SCC measured with the dilatometer. The total deformation measured after about 4.5 months is approximately 1.2 mm/m. A large part (about 2/3) of the total deformation occurred during the first 24 hours of measurement. Therefore the measured data was split into two separate diagrams, where the first 24 hours (Figure 3-14) and the following period of time are displayed (Figure 3-15). It can be seen in Figure 3-14 that the deformation during the first 24 hours is almost the same for the two tested mix designs. That can be explained by the identical water content and water to powder ratio (powder = cement + silica fume + limestone filler) of both mixes. Other researchers had similar findings, e.g. /Esping 2007/. When analyzing the shrinkage after 24 hours, the different composition of the mixes results in different shrinkage values. Figure 3-15 shows that the mix with more binder has a higher shrinkage. The recorded shrinkage curves indicate that the shrinkage of low pH SCC is a process that goes on for a long time. When comparing the shrinkage values of sealed beam specimens (method 3) (Figure 3-16) and specimen in the plastic tubes (method 2) (Figure 3-15), the shrinkage of the samples in the plastic tubes (method 2) is more than double the shrinkage of the sealed beams (method 3). This is a result of different degree of sealing for the different samples.

Figure 3-17 show the weight loss for the different specimens. The sealed beams loose almost no weight while both, samples in plastic tubes and unsealed beams loose large amounts of water. Therefore the sealed beams can be considered to be measurements of sealed shrinkage while both unsealed beams and samples in plastic tubes resemble different degrees of drying shrinkage. Obviously, the plastic tube is not as impermeable to moisture as the butyl tape.

The shrinkage value of the sealed beams (method 3) (Figure 3-16) is remarkably low, about 0.28 mm/m for B300 and 0.17 mm/m for B200. However, the measurement (method 3) started after 24 hours, so the actual total deformation is larger. The shrinkage of the unsealed beams is about the same for both mixes, as both, autogenous and drying shrinkage are recorded in that test. That means that the drying shrinkage of B200 must be higher than the drying shrinkage of B300.

It seems that the dilatometer is only suitable for measurement of the early deformations. Later the permeable plastic tube allows water to evaporate. The sealed beams proved to be water tight. The sealed beams are suitable for measurement of shrinkage under sealed conditions after 24 hours. A combined shrinkage curve of dilatometer measurement for the first 24 hours and sealed beams for the following period of time may be the most realistic description of the autogenous shrinkage for the plug.

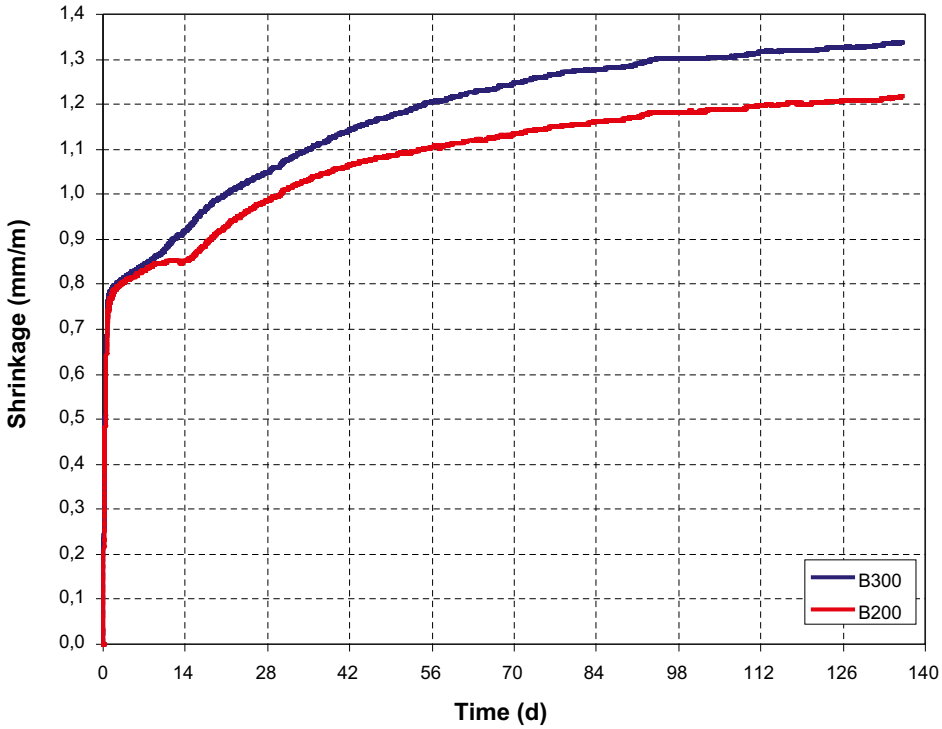

Figure 3-13. *Total shrinkage measured with dilatometer (method 2), start of measurement 1 hour after casting.*

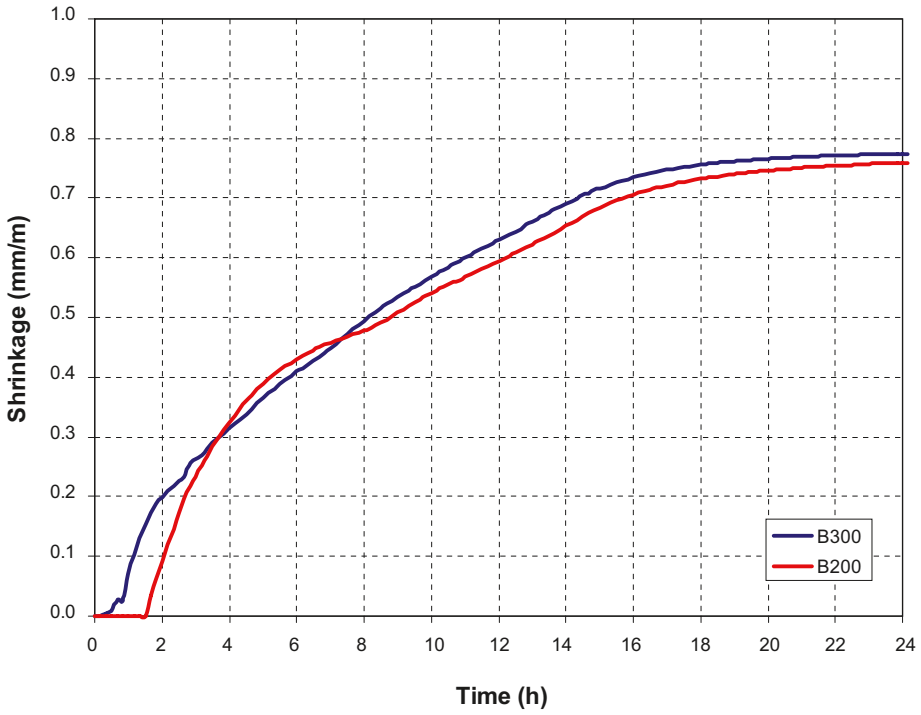

Figure 3-14. *Early shrinkage (up to 24 h) of B200 and B300 measured with dilatometer (method 2), average of 2 specimens.*

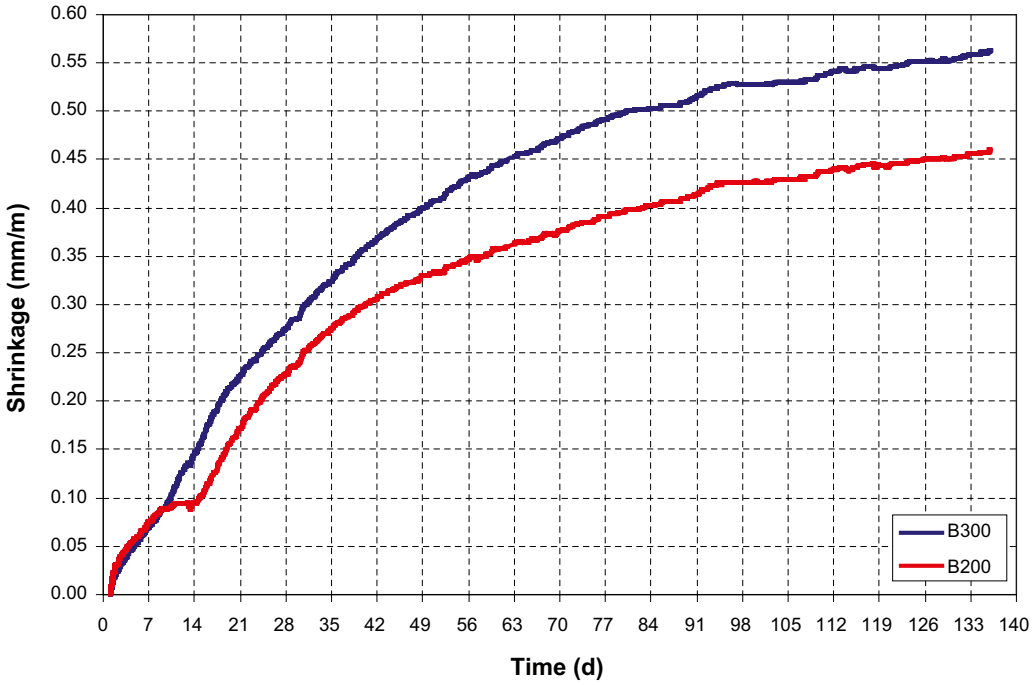

Figure 3-15. *Shrinkage B200 and B300 measured with dilatometer (method 2), starting point 24 hours after casting, average of 2 specimens.*

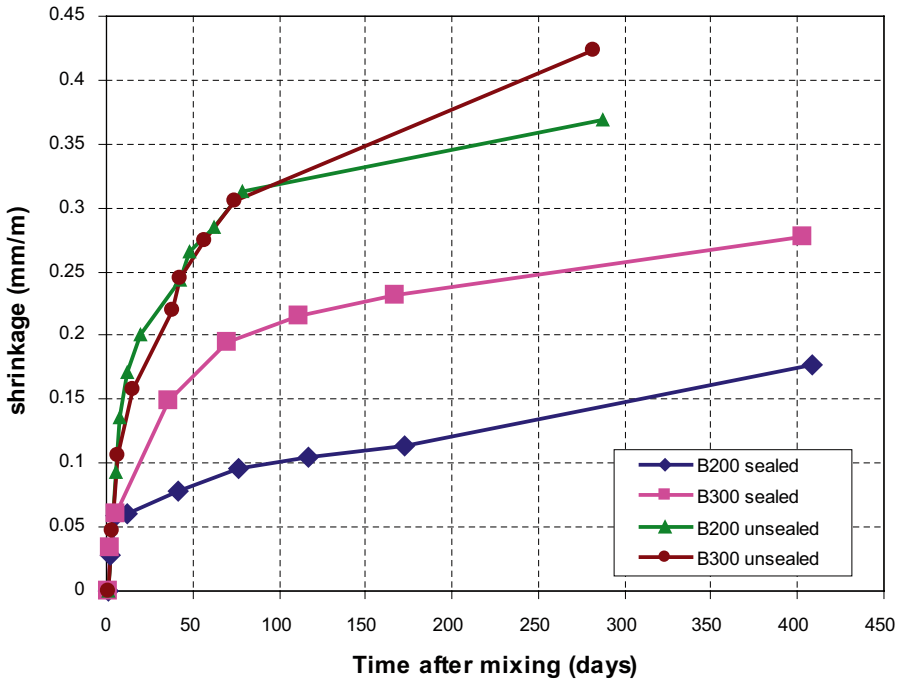

Figure 3-16. *Shrinkage of beam specimens (method 3), comparison of sealed and unsealed samples. The starting point of the measurement is 24 h (1 day) after casting. The curves do not start at time = 0.*

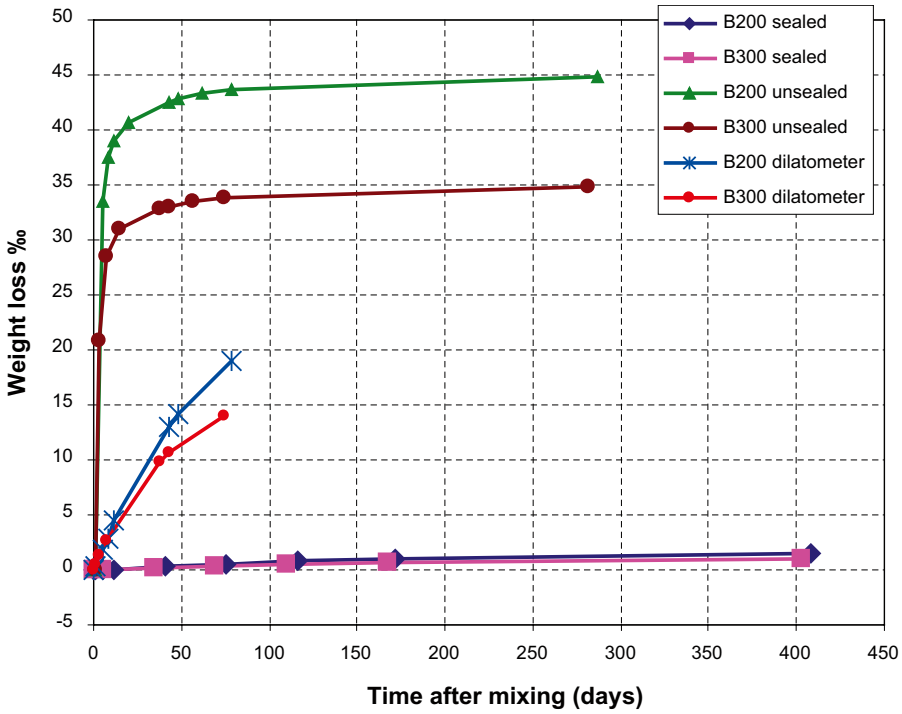

Figure 3-17. *Weight loss of specimens in dilatometer (method 2), sealed and unsealed beam specimens (method 3).*

3.3.5 Microstructure

The microstructure of both mixes was studied on thin sections in a light microscope and on highly polished samples in a Scanning Electron Microscope (SEM). The samples were taken from mature concrete (older than 3 months).

The analysis of the thin sections showed a homogeneous paste structure with well distributed filler. The paste was very dense; comparison of the porosity with reference samples gave a corresponding porosity to a water- cement ratio of 0.4 for the low pH SCC with 200 kg of binder and between 0.35 to 0.4 for the concrete with 300 kg of binder. Small amounts of undispersed silica fume samples were found in both samples.

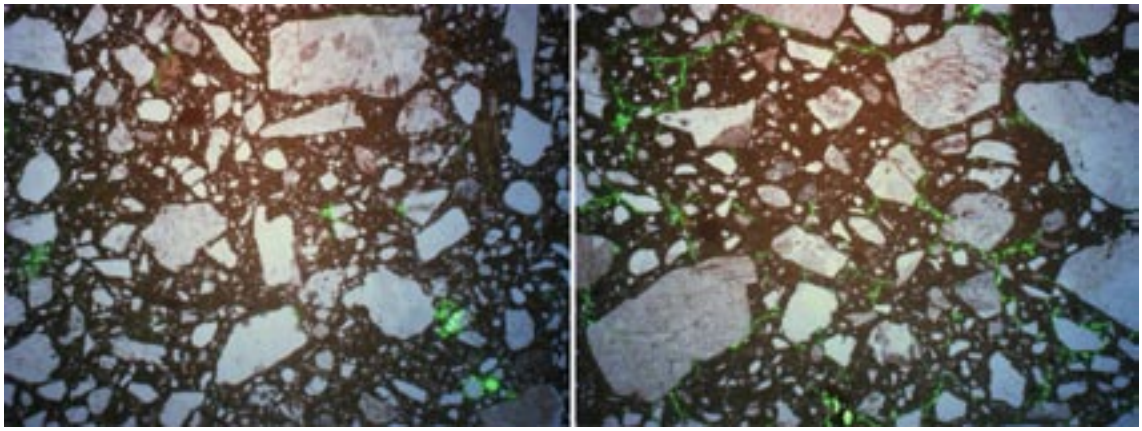

Figure 3-18. *Thin section in light microscope, B200 (left) and B300 (right). The green colour represents epoxy dye in larger pores and micro cracks.*

SEM analysis allows much higher resolution than light microscopy. At the same time, the chemical composition can be analysed, using energy-dispersive X-ray spectroscopy analysis (EDX). Figure 3-19 and Figure 3-20 show a homogeneous distribution of filler and fine aggregate. The interfacial transition zones around the larger aggregate grains are very thin, small limestone particles are situated close to the coarser grains. This indicates a good dispersion of the large amount of fines in the low pH SCC. The limestone filler becomes an integrated part of the paste which explains the high compressive strength. The porosity of the paste is low and only few unhydrated cement grains can be found.

The chemical analysis shows that the samples were well hydrated. In both mixes the analysed CaO/SiO_2 ratio was close to the theoretical value of approximately 0.75 (Table 3-7). That value can be calculated from the content of CaO in the cement, the content of SiO_2 in the cement and SiO_2 from the silica fume. For the cement used and the binder composition of 60% cement and 40% silica fume, the CaO/SiO_2 ratio will be approximately 0.75 at equilibrium (completely hydrated). The variation of the CaO/SiO_2 ratio between analysis close to unhydrated cement grains and paste away from cement grains illustrates that the analysed samples were not fully hydrated. Variations in calcium content result from unhydrated cement grains and the high content of limestone filler. All other analysed quantities of oxides are in the expected range.

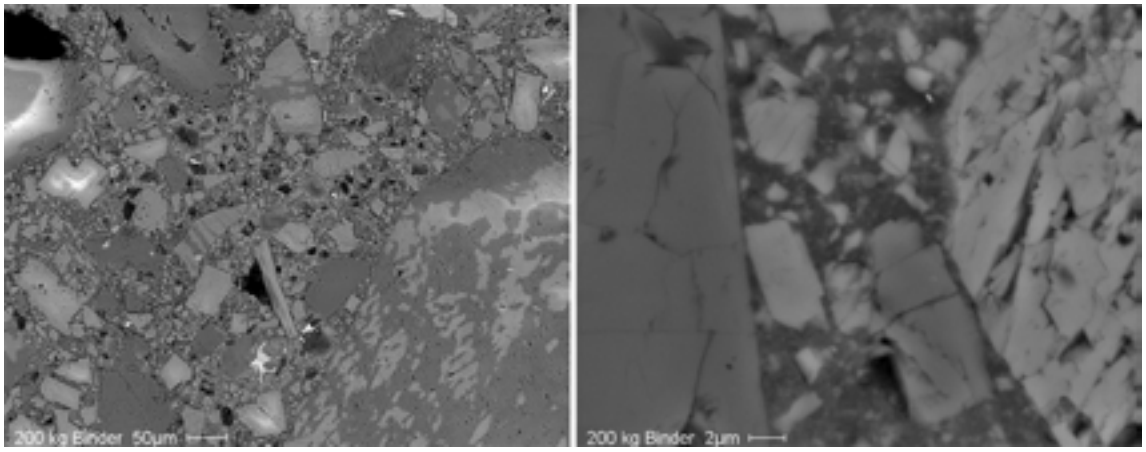

Figure 3-19. *SEM picture of B200, low magnification (left) and high magnification close to aggregate (right).*

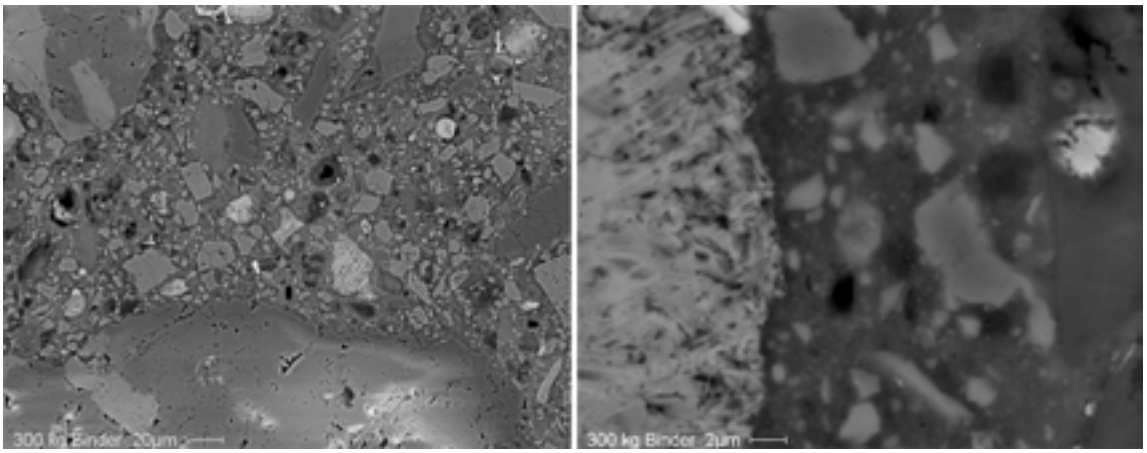

Figure 3-20. *SEM picture of B300, low magnification (left) and high magnification close to unhydrated cement grain (right).*

Table 3-7. Chemical composition of low pH SCC analysed with EDX in SEM.

	B200		B300	
	Close to cement grain	Paste	Close to cement grain	Paste
Na_2O	0.33	0.40	0.49	0.29
MgO	0.85	0.96	0.89	1.02
Al_2O_3	3.60	3.11	2.61	2.65
SiO_2	48.64	49.64	51.98	53.54
SO_3	0.99	1.12	1.25	1.58
K_2O	0.66	0.76	0.64	0.44
CaO	41.38	40.65	39.33	37.60
Fe_2O_3	3.55	3.36	2.83	2.88
Total	**100.00**	**100.00**	**100.00**	**100.00**
CaO/SiO_2	0.85	0.82	0.76	0.70

3.4 Mix design summary

It was possible to develop low pH concrete with self compacting fresh concrete properties. The mix compositions incorporate limestone filler, Ordinary Portland cement, densified silica fume, superplasticizer, high quality natural fine aggregates and average quality crushed coarse aggregate.

With the help of a concrete viscometer, the mix composition was adjusted to achieve high flowability of the concrete, combined with good stability. The developed mixes have a long open time and respond to the addition of superplasticizer when the slump flow decreases with time.

The amount of binder was lowered as much as possible, while maintaining good stability of the fresh concrete. Consequently, the heat of hydration is low. The strength development was slow at early age but after 28 days, the compressive strength in the initial tests (recalculated to 150 mm cubes) was 43 MPa (B200) and 68 MPa (B300). After 3 months, B200 has a compressive strength of almost 75 MPa and B300 of 100 MPa. The tensile strength of mature low pH SCC is similar to that of mature conventional concrete.

The early volume changes were rather high but the shrinkage values for sealed conditions were low. The autogenous shrinkage of B200 is lower than B300. The shrinkage of the unsealed beams shows similar values for both mix designs.

The analysis of the microstructure shows a dense paste with homogeneously distributed filler particles.

The concrete has very good resistance to water penetration.

4 Testing at concrete factory

4.1 Introduction

In order to determine the suitability of the low pH SCC under practical working conditions, it was decided to test the mixes B200 and B300 in a larger scale.

For logistical reasons this test was performed at a mobile concrete producer. This concrete producer does not use traditional mixing equipment but uses truck mixers (Figure 4-1). Presumably the mixing efficiency of these mixers is lower compared to conventional mixers. The test can therefore be seen as a worst case scenario. If the test is successful with this type of mixing equipment, almost every other kind of sufficiently powerful mixer should be able to mix the low pH SCC.

Figure 4-1. *Truck mixer used in the factory test.*

4.2 Fresh concrete

The mobile concrete producer did not have a silo for the limestone filler, so the filler had to be added from big bags manually. Therefore the mixing order shown in Table 4-1 was used. The batch sizes were chosen to incorporate 1,000 kg of limestone filler each (= 1 big bag of filler). On account of this, 2.71 m^3 of B200 and 3.72 m^3 of B300 were mixed.

The moisture content of the fine aggregate was determined with an electronic device and the water content adjusted accordingly. Superplasticizer was added in two steps, one part with the mixing water and the remaining part was added later, as necessary. When the slump flow and the pumpability were tested, the concrete seemed not to be stable and coarse aggregate separated, even though the amount of superplasticizer was much lower than in the laboratory tests.

As too high water content can be the cause of an instable SCC, the moisture content of the fine aggregates was again determined manually. The result of this test showed higher moisture content of the fine aggregates than measured initially; consequently the first two mixes contained too much water (see Table 4-2). The higher water content of the aggregate increases the water-powder ratio and lowers the stability of the low pH SCC. The reason for the difference in determined aggregate moisture with different measuring devices may be that the aggregate was stored outside and partly frozen.

Table 4-1. Mixing order for factory test.

1	Coarse aggregates and silica fume
2	Mixing
3	Limestone filler
4	Mixing
5	Cement, water and ½ of superplasticizer
6	Mixing
7	Fine aggregate
8	½ of superplasticizer
9	Mixing

Table 4-2. Fresh concrete properties, aggregate moisture and required amount of plasticizer.

	Mix 1 200 kg –1	**Mix 2 300 kg –1**	**Mix 3 200 kg –2**	**Mix 4 300 kg –2**
Aggregate moisture content	1.5%*	1.5%*	3.2%**	3.2%**
relative water content compared to mix design	+ 8 kg/m^3	+ 8 kg/m^3	ok	ok
Glenium 51	4.5 kg/m^3	4.04 kg/m^3	4.06 kg/m^3	5.4 kg/m^3
Relative amount of Glenium 51 to amount in laboratory	71%	58%	65%	77%
Concrete temperature	15°C	13°C	13.5°C	12.5°C
Slump flow in mm after water addition (min)	700 (25)	460 (20)	550 (10)	500 (10)
After transport simulation (min)	730 (50)	500 (45)	660 (35)	640 (25)
After pump (min)	–	570 (48)	–	–
Air content after pump	–	–	3.2%	2.9%

* moisture content of aggregate determined with electronic device, presumably too low due to partly frozen aggregate

** moisture content of aggregate determined manually

Adjusting the content of mixing water for mixes 3 and 4 (see Table 4-2) in accordance to the above finding resulted in a stable low pH SCC with good workability. It was also obvious that the slump flow increased with continued mixing. Presumably the truck mixer was less efficient than the laboratory mixer and the concrete became more homogeneous with time.

No difficulties occurred when pumping the low pH SCC using a relatively small pump and a thin (2.5'') hose (Figure 4-2). Usually 4'' hoses are used on building sites.

In order to evaluate the stability of the low pH SCC against aggregate separation and the suitability for bulky constructions, cylindrical steel moulds (diameter of 0.85 m, height of 3.0 m) were instrumented with temperature sensors and filled with low pH SCC (Figure 4-3). This is about 1/50 of the volume of a plug. Development of heat of hydration, settlement and hardened concrete properties were investigated.

After approximately 30 minutes of transport simulation, low pH SCC from mix 3 and mix 4 were pumped into their respective moulds, and no mechanical compaction in any form was applied. After the moulds were filled, a linear variable displacement transducer (LVDT) was installed at the top of each column and the measurement of settlement started (Figure 4-4).

Cube samples were cast for compressive strength tests to compare with drill cores from the columns.

Figure 4-2. *Pumping test with small pump and 2.5" hose.*

Figure 4-3. *Two cylindrical steel moulds, diameter 0.85 m and height 3 m, instrumented with temperature gauges and one LVDT at the top to measure the settlement, were filled with low pH SCC.*

Figure 4-4. *LVDT installed at the top of each mould to measure the settlement over time.*

4.3 Hardened concrete

The temperature development (Figure 4-5) was recorded for both cast columns. This data will be used to fine-tune the material parameters for computer modelling of temperature development. A maximum temperature rise of about 13°C was recorded for B300. B200 showed an increase of about 10°C in temperature at the centre of the column during curing. The peak temperature occurred about 24 hours after casting.

The settlement measurements are basically combined measurement of both settlement and early volume changes in the concrete. The shape of the curves is similar to the measurement of early autogenous shrinkage with the digital dilatometer (Figure 3-14). However, the measured magnitude of deformation (Figure 4-6) differs remarkably between the mixes. This is different from the measurements in the dilatometer.

The reason for the difference in early deformation between the two mixes, measured on the columns, is not clear. Further investigations could be helpful to understand this phenomenon which may be important for the decision of which mix design to choose.

The effect of the early volume changes could be seen when removing the formwork from the columns after one week. There was a visible gap (approximately 1 mm) between mould and concrete, see Figure 4-7. The consequences of the early volume changes for the performance of the plugs should be included in the evaluation. However, it should be mentioned that large early volume changes are not specific for low pH SCC, other researchers, e.g. /Esping 2007/, found similar results for conventional SCC.

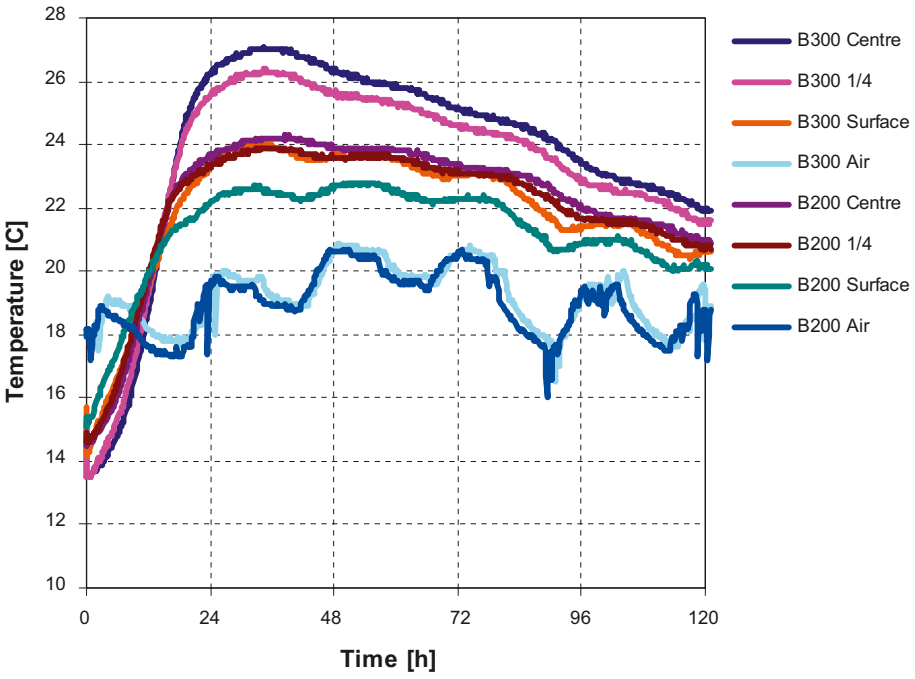

Figure 4-5. *Temperature measurement of columns. The temperature gauges were installed at 1.5 m height in the columns. They were placed in the centre, at ¼ of the diameter and close to the edge of the mould. Additional temperature gauges recorded the air temperature adjacent to the columns.*

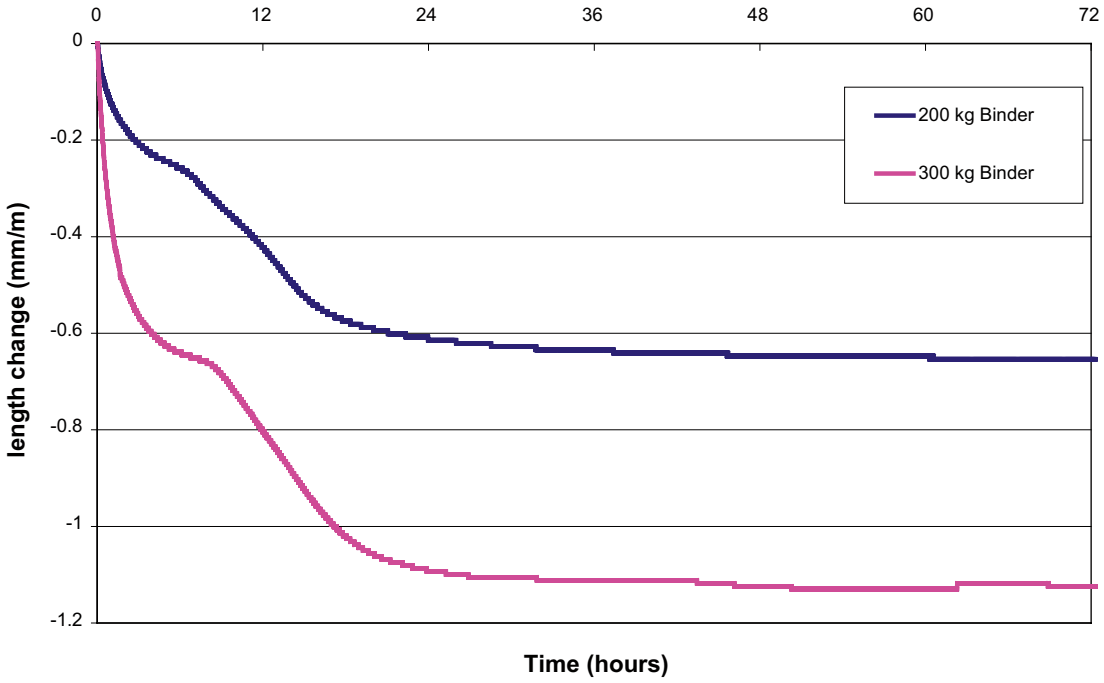

Figure 4-6. *Measurement of settlement for low pH SCC with 200 kg and 300 kg of binder for the first 3 days after casting. The measurement started 10 min after casting of the column.*

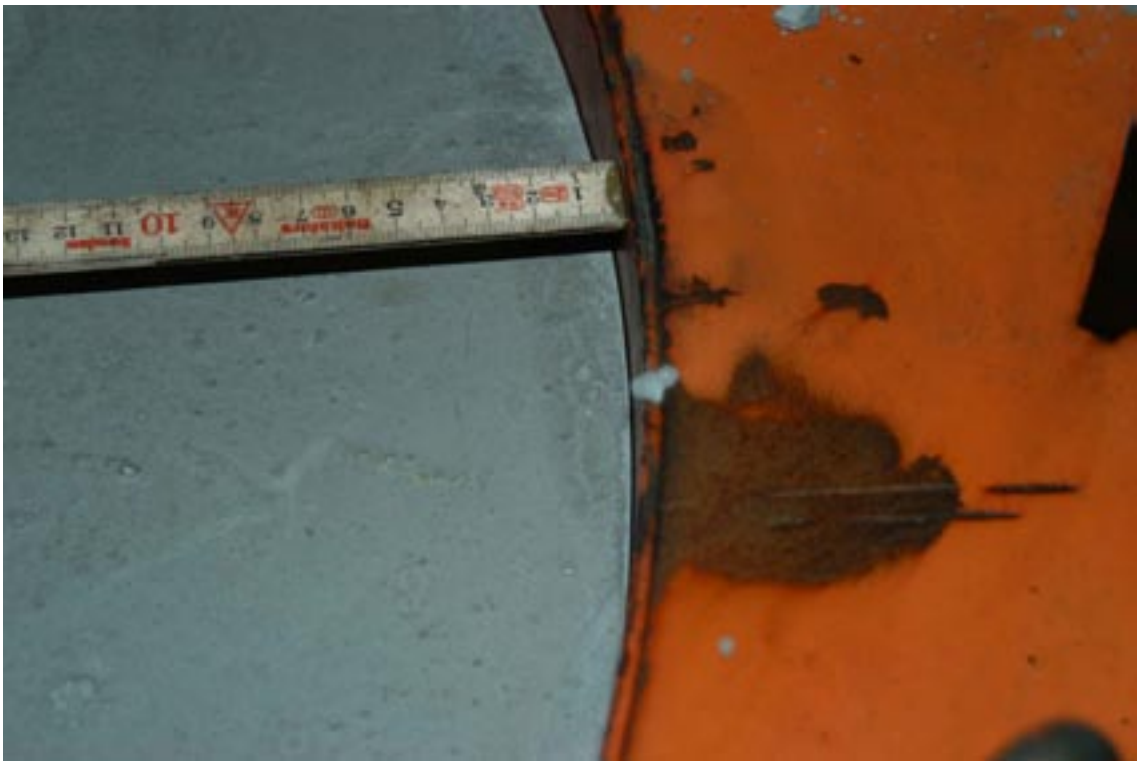

Figure 4-7. *Gap between steel mould and concrete, one week after casting.*

The compressive strength, splitting tensile strength, density and air content were determined for the cube samples and drilled cores. There is no significant difference in either strength or density compared to the laboratory samples. The compressive strength in the columns was slightly lower than in the cube samples (Table 4-3). The density and compressive strength values at the column top are slightly lower than at the lower part of the column, suggesting loss of water by evaporation at the top of the column. The measurement of the air content in the hardened concrete shows a constant air distribution over height of the columns. Visual inspection of the drill cores did not show uneven aggregate distribution, suggesting water evaporation may be the cause of the strength variation.

The microstructure of both mix designs was investigated on thin section from the drill cores taken at mid-height of the columns (+1,500 mm). They were compared to the thin sections prepared on laboratory samples. Figure 4-8 and Figure 4-9 show that the air content is higher in the samples from the factory tests. It can be seen that the microstructure of B200 is much more inhomogeneous in the sample from the factory test. There are porous zones around the aggregate grains and also in the paste. At higher resolution it was seen that conglomerates of limestone filler close to the surface of the aggregate grains are the cause for the increased porosity. Presumably this is a result of the mixing order that was used in the factory test. In laboratory, the limestone filler and cement were mixed at the same time into the concrete. In the factory test, the limestone filler was added prior to the cement. This was a mistake and should have been avoided, because it is known to give agglomeration of filler around the aggregates. The agglomeration of limestone filler around the aggregate is a result of opposite electrical charge of limestone filler and granitoid aggregate. Addition of cement turns the electrical charge of the granitoid aggregate due to the higher pH, resulting in repulsion of aggregate grains and filler particles.

The microstructure of B300 is almost equal for laboratory sample and sample from the factory test. One difference is the higher air content in the sample from the factory tests. Both thin sections show some microcracks in the paste of the concrete. However, there was no agglomeration of limestone filler around the coarser aggregate grains. The reason for this is not clear, this may be a localized effect in the area sampled or may be due to another unknown reason.

The observed amount of undispersed silica fume in both mixes was slightly higher in the factory tests than in the laboratory samples but no reason for concern. Presumably the mixing of coarse aggregate and silica fume lead to sufficient dispersion of the densified silica fume granules.

Table 4-3. Properties of hardened low pH SCC, determined on cubes and drilled cores after 28 days.

	B200	B300
Compressive strength of cube samples [MPa]	48.5	73
Density of cube samples [kg/m^3]	2,300	2,315
Splitting tensile strength of cube samples	4.1	5.4
Compressive strength and density of drilled cores	44.5	59.5 [x)]
(Column height +0 mm = bottom)	2,330	2,360
Compressive strength and density of drilled cores	44.5	66.5
(Column height +500 mm)	2,270	2,330
Air content in hardened concrete	4.6%	2.8%
Compressive strength and density of drilled cores	44.0	70.0
(Column height +1,500 mm)	2,260	2,320
Air content in hardened concrete	3.6%	2.8%
Compressive strength and density of drilled cores	37.0	62.5
(Column height +2,500 mm)	2,250	2,300
Air content in hardened concrete	3.5%	2.9%
Compressive strength and density of drilled cores	39.5	54.5
(Column height +3,000 mm = top)	2,300	2,270

[x)] Sample showed traces of excess of form oil, resulting in reduced strength.

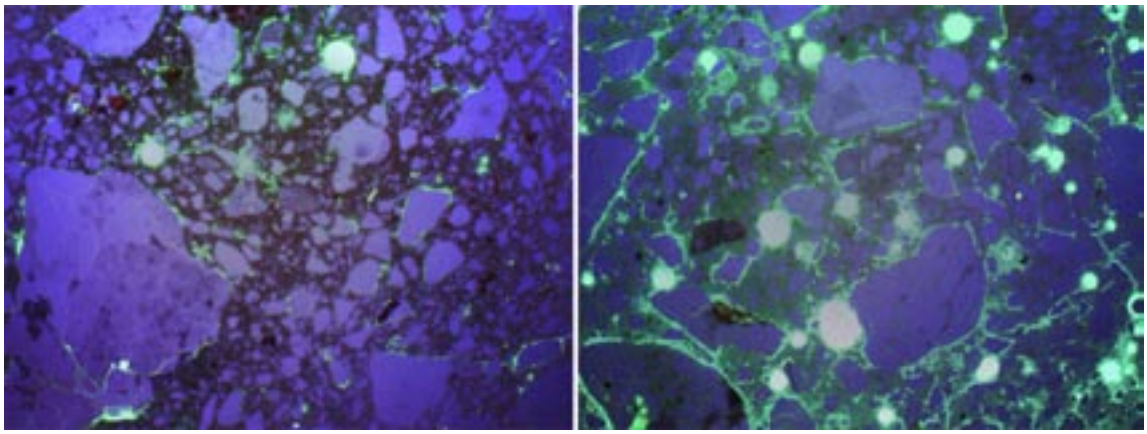

Figure 4-8. *Thin section of laboratory sample (left) and sample from columns (right) of B200.*

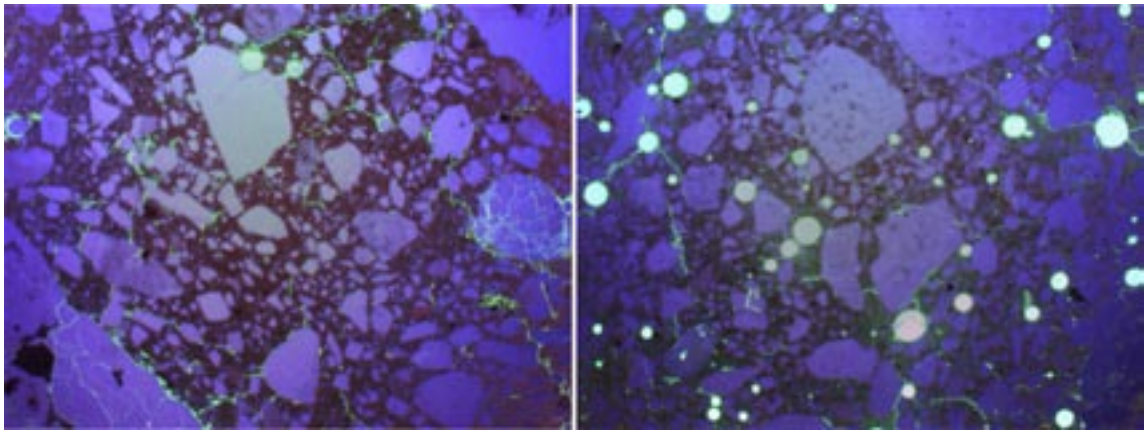

Figure 4-9. *Thin section of laboratory sample (left) and sample from columns (right) of B300.*

4.4 Summary of factory testing

The results of the factory tests show that mixing at full scale with rather inefficient mixing equipment can be accomplished and still gives sufficient results. Pumping with a small hose was possible without problems. The importance of correct determination of aggregate moisture on fresh concrete properties was demonstrated. Accurate measurement of aggregate moisture is important to achieve the desired fresh concrete properties. Less superplasticizer was required in the factory test than in the laboratory, which is probably a result of longer mixing time and lower ambient temperature. It was found that the slump increases with mixing time and after pumping.

After investigating the hardened concrete properties, it was found that similar compressive and splitting tensile strength was achieved from factory tests and laboratory tests. The drilled cores from the columns showed well distributed coarse aggregate over column height. The compressive strength and density was slightly lower at the top of the column compared to the bottom.

The analysis of the microstructure showed that, especially for the concrete with 200 kg of binder, agglomeration of limestone filler around the aggregate grains occurred. This resulted from the mixing order, when limestone filler was added before cement. In the future, this can be easily avoided by using the same mixing order as in the laboratory. This illustrates the importance of the correct mixing order to achieve the desired concrete properties.

Rather large early volume changes were recorded, the reason and possible measures to reduce those should be investigated further.

The mixing tests at the mobile concrete plant showed that no major changes of the mix designs are required. The amount of superplasticizer had to be adjusted but this is normal procedure when a mix design is taken from laboratory to full scale. The fresh concrete properties were sufficient for the desired SCC use and no large differences to the laboratory results could be found when analysing the hardened concrete. Consequently, the mix design was not revised.

5 Testing and quantification of properties for young and mature concrete

5.1 Preface

The main objective of this report is to map the evaluated properties of the concrete mixes B200 and B300 with respect to young and hardened concrete. This gives the basis to assess stress growth in the following conditions.

1) The young concrete, from casting and the first months thereafter. This comprises calculations of eigenstresses due to effects of the heat of hydration and the autogenous shrinkage, which can be realized with the computer program /ConTeSt Pro 3.2 2008/. Data files for this computer program are prepared based on the evaluation of test results shown in this report.
2) The hardened concrete, from the age of external loading of the plug (approximately three months after casting) up to the time of interest for long-term effects in the structural calculations. This comprises calculation of stresses caused by the load situation during the serviceability state of the construction. The data for this purpose are shown in this report, and it includes strength growth in compression and tension, Poisson´s ratio, development of Young's modulus, and creep ratios for variable load durations and variable loading times.

5.2 Young concrete

5.2.1 Background

Cracking of concrete during the young concrete phase must be avoided in order to minimize the risk of durability problems in the future, such as water tightness and corrosion risk of the reinforcement. Estimation of the risk of early age cracking requires knowledge of the combined effects from temperature development and mechanical behaviour during the hydration.

Theoretical and experimental methods with the purpose of mapping required young concrete properties to be able to carry out calculations concerning risks of thermal as well as moisture induced stresses have been derived and evaluated at Luleå University of Technology (LTU) during a long period /Emborg 1989, Jonasson 1994, Westman 1999, Hedlund 2000, Groth 2000, Nilsson 2003, Larson 2003 and Carlswärd 2006/.

The tests performed here are in accordance with an established "standard" procedure at LTU to map properties for usage in temperature and stress calculations. In this report only the most essential formulas are given to be able to understand the meaning of presented data.

The following areas (sections 6.2.1.1 to 6.2.1.6) have been evaluated based on tests:

- maturity functions;
- heat of hydration;
- strength growth at variable temperature;
- Young´s modulus and early age creep;
- free deformation at variable temperature; and
- stress growth at totally restraint conditions.

Maturity function

The properties of the young concrete are expressed in accordance with the so called maturity concept, here applied with the temperature equivalent time, t_e, as the independent parameter. The concept originates from /Nurse 1949, Saul 1951/, and it was first introduced in Sweden by /Bergström 1953/:

$$t_e = \beta_\Delta \int_t \beta_T \cdot dt + t_{e,0} \tag{5-1}$$

where β_Δ = adjustment factor to be used for different admixtures [–], here = 1, β_T = temperature sensitivity factor [–], see further Eq. (5-2), t = clock time [h], and $t_{e,0}$ = starting time of t_e (at $t = 0$) to be used for different admixtures [–], here = 0.

β_T is often called the maturity function, which can be expressed /Freisleben and Pedersen 1977, Byfors 1980/ by:

$$\beta_T = \begin{cases} \exp\left[\theta \cdot \left(\frac{1}{293} - \frac{1}{T+273}\right)\right] & \text{for T} > -10\ ^\circ C \\ 0 & \text{for T} \le -10\ ^\circ C \end{cases} \tag{5-2}$$

where θ = "activation temperature" [K] = (formally:) activation energy divided by general gas constant, which here is expressed /Jonasson 1984/ by:

$$\theta = \theta_{ref} \cdot \left(\frac{30}{T+10}\right)^{\kappa_3} \tag{5-3}$$

where θ_{ref} [K] and κ_3 are fitting parameters according to best fit with test data.

Heat of hydration

The test procedures are fully described in /Ekerfors 1995, Ekerfors and Jonasson 2000/, and test data are evaluated regarding generated heat for the total binder content, as expressed by Eq. (5-3) /Jonasson 1984/.

$$W_B = \frac{W_{tot}}{B} = W_U \cdot \exp\left[-\lambda_1 \cdot \left(\ln(1+\frac{t_e}{t_1})\right)^{\kappa_1}\right] \tag{5-4}$$

where W_B = generated heat by weight of binder as a function of equivalent time [J/kg], B = binder content, here the sum of cement and fly ash content [kg/m^3], W_{tot} = generated heat at testing [J], W_U = ultimate generated heat by weight of binder [J/kg], and λ_1 [–], t_1 [h] and κ_1 [–] are fitting parameters.

Strength growth at variable temperature

The strength growth at variable temperature has been tested according to the procedure described in /Ekerfors 1995/. The strength growth for all tested mixes is evaluated according to Eq. (5-5), where the lower formula has been proposed by /Kanstad et al. 1999/ as a slight modification of the expression for strength growth in the European Standard /EN 1992-1-1 EC2 2004/, where $t_s = 0$ is used.

The upper formula in Eq. (5-5) for $t_e \le t_A$ is intended for very early age strength estimations to be able to assess trowelling and slipform actions, but here no measurements are performed in this region.

$$f_{cc}(t_e) = \begin{cases} (t_e / t_A)^{n_A} \cdot f_A & \text{for } 0 \le t_e < t_A \\ \exp\left[s \cdot \left(1 - \sqrt{\frac{672 - t_S}{t_e - t_S}} \right) \right] \cdot f_{cc,28} & \text{for } t_e \ge t_A \end{cases} \quad (5\text{-}5)$$

where f_{cc} = compressive strength as a function of equivalent time [MPa], $f_{cc,28}$ = 28-days compressive strength [MPa], s [–] and t_S [h] are fitting parameters, t_A = (here chosen to be) = $1.5 \cdot t_S$ = equivalent time when shifting from the upper to the lower formula [h], f_A is the compressive strength at $t_e = t_A$, calculated by the lower formula [MPa].

Young's modulus and early age creep

When deformations at loading are measured, the total deformation is the true material parameter, but, in engineering practice it is common to distinguish between "elastic" and "creep" deformation. The differentiation between the types of deformation can be done in many different ways and can also be adapted to the application in question. As long as the total deformation is in accordance with the measurements it is only a question of how detailed the information is in the time scale. For young concrete, and applications with respect to stresses caused by inelastic deformations at variable temperature and moisture state, the "elastic" time duration, Δt_0, is here chosen to be 0.001d /Emborg 1989, Westman 1999/. Hereby, the Young's modulus at loading age t_0, $E(t_0)$, can be expressed by:

$$E(t_0) = \frac{1}{J(\Delta t_0, t_0)} = \frac{1}{J(0.001, t_0)} \quad (5\text{-}6)$$

where $J(0.001,t_0)$ is the measured deformation 0.001d (≈ 1.5 minutes) after loading [1/Pa], and t_0 = equivalent age at loading [d].

The total deformation, $J(\Delta t_{load},t_0)$, can now be expressed by:

$$J(\Delta t_{load}, t_0) = \frac{1}{E_0(t_0)} + \Delta J(\Delta t_{load}, t_0) \quad (5\text{-}7)$$

where $\Delta l_{load} = t - t_0$ = load duration, [d], $\Delta J(\Delta t_{load},t_0)$ = "creep" part of the total deformation [1/Pa].

The Young's modulus is here expressed, see /Larson 2003/ by:

$$E_c(t_0) = \left[\exp\left\{ s_E \cdot \left(1 - \sqrt{\frac{28 - t_{SE}}{t_0 - t_{SE}}} \right) \right\} \right]^{0.5} \cdot E_{28d} \quad (5\text{-}8)$$

where t_0 = equivalent age at loading [d], t_{SE} = equivalent time, where deformations start to create stresses [d], E_{28} = Young's modulus at equivalent time = 28d [GPa], and s_E = shape parameter for the growth of the Young's modulus [–].

With two straight lines in the logarithmic time scale /Larson 2003/ the creep portion can be formulated as:

$$\Delta J(\Delta t_{load}, t_0) = \begin{cases} a_1 \cdot \log\left(\dfrac{\Delta t_{load}}{\Delta t_0}\right) & \text{for } \Delta t_0 \le \Delta t_{load} < \Delta t_1 \\ a_1 \cdot \log\left(\dfrac{\Delta t_1}{\Delta t_0}\right) + a_2 \cdot \log\left(\dfrac{\Delta t_{load}}{\Delta t_1}\right) & \text{for } \Delta t_{load} \ge \Delta t_1 \end{cases} \quad (5\text{-}9)$$

where Δt_1 = time duration for the distinct break point in the creep behaviour [d], a_1 and a_2 are inclinations, dependent on the loading ages, in the linear-logarithmic plot of the creep behaviour [10^{-12}/(Pa log-unit)].

Free deformation at variable temperature

The tests are performed to determine the free deformation of newly cast concrete at variable temperature. The measured deformation is a combined effect of temperature and moisture changes in the concrete. The problem is to separate the deformation into a thermal deformation related to temperature changes and an autogenous deformation not directly dependent on the temperature changes /Bjøntegaard 2000/. Bjøntegaard measured the thermal deformation by a saw-toothed variation of the temperature, and considered the remainder as an "experimentally determined autogenous deformation" valid for the studied mix. This procedure has been used by /Bosjnak 2001, Atrushi 2003, Ji 2008/. This evaluation was done in a similar way without direct measurements of the thermal deformation. The thermal dilation coefficient of hardening concrete was chosen as a constant, and the remainder is modelled as a maturity related autogenous shrinkage. The evaluation was accomplished by a fitting technique based on the measured total deformation for a "realistic" (0.7 m wall structure) temperature curve. The model is described in /Hedlund 2000/ and expressed by:

$$\varepsilon_{\text{tot}} = \varepsilon_T^o + \varepsilon_{SH}^o \quad (5\text{-}10)$$

$$\varepsilon_T^o = \Delta T \cdot \alpha_{\text{T}} \quad (5\text{-}11)$$

$$\varepsilon_{SH}^o = \begin{cases} 0 & \text{for } t_e \le t_{s1} \\ \dfrac{t_e - t_{s1}}{t_{s2} - t_{s1}} \cdot \varepsilon_{s1} & \text{for } t_{s1} < t_e \le t_{s2} \\ \varepsilon_{s1} + \exp\left[-\left(\dfrac{t_{SH}}{t_e - t_{s2}}\right)^{\eta_{SH}}\right] \cdot \varepsilon_{s2} & \text{for } t_e > t_{s2} \end{cases} \quad (5\text{-}12)$$

where ε_{tot} = the measured strain [–], ε_T^o = the stress free strain related to changes in temperature [–], ε_{SH}^o = the stress free strain not related to changes in temperature [–], ΔT = change in temperature [°C], α_T = thermal dilation coefficient [1/°C], t_{s1} [h], t_{s2} [h], ε_{s1} [–] ε_{s2} [–], t_{SH} [h] and η_{SH} [–] are fitting parameters.

Stress growth at full restrained conditions

In the Temperature Stress Testing Machine (TSTM), the stress to strength ratio can be determined at full restrained conditions. Specimens are located in a totally rigid frame and heated in accordance with a "realistic" temperature development, which is calculated with parameters evaluated for the tested concrete mix applied to a 0.7 m thick wall at indoor conditions. The induced stresses in the fully restrained concrete specimen are measured. The test set-up and

performance is fully described in /Westman 1999/. The results from the TSTM test are a combined effect from all parameters that influence the hardening phase under restraint conditions. When comparing measured and calculated stresses, it might be regarded as a "check point" if the evaluated parameters are able to reflect the measured stress development.

If the specimen cracks the stress at failure represents a "structural" tensile strength at the moment of cracking. If a crack does not appear after reaching a peak value in the measured stress, the specimen is loaded to cracking, and again the stress at failure represents a structural tensile strength for the tested concrete. The tensile strength is related to the compressive strength according to:

$$f_{ct} = (f_{cc} / f_{cc}^{ref})^{\beta_1} \cdot f_{ct}^{ref} \tag{5-13}$$

where f_{ct} = tensile strength [MPa], f_{cc}^{ref} = reference compressive strength [MPa], f_{ct}^{ref} = reference tensile strength [MPa}, and β_1 = exponent [–].

The stress-strain curve used in the calculation is illustrated in Figure 5-1, and α_{ct} denotes the upper limit of the linear stress-strain at 1st loading. Remaining denotations in Figure 5-1 are: σ = (uniaxial) stress in the concrete [MPa], ε_m = strain related to stresses in concrete (= "material" strain) [–], ε_0 is the strain related to a linear behaviour all the way up to $\sigma = f_{ct}$.

Finally, in many investigations there has been observed a phenomenon which was denoted transient creep at variable temperature and humidity /Bažant and Chern 1985/ or stress-induced deformations /Thelandersson 1987/. For young concrete this was introduced in a simplified manner by /Jonasson 1994/ as:

$$\Delta\varepsilon_T = \Delta\varepsilon_T^o \cdot (1 + \rho_T \cdot \frac{\sigma}{f_{ct}} \cdot sign(\Delta T)) \tag{5-14}$$

and

$$\Delta\varepsilon_{SH} = \Delta\varepsilon_{SH}^o \cdot (1 + \rho_\varphi \cdot \frac{\sigma}{f_{ct}} \cdot sign(\Delta T)) \tag{5-15}$$

where Δ denotes a change associated with a time step (Δt), ε_T = strain related to a temperature variation at a stress level of σ/f_{ct} (≥ 0) [–], σ = stress in the concrete [MPa], ε_φ = strain not related to a temperature variation at a stress level of σ/f_{ct} (≥ 0) [–], T = temperature [°C].

When a discrepancy is observed between the measured (TSTM) and calculated stresses using material related parameters evaluated in accordance with Eqs. (5-3) – (5-13), the numerical modelling checks whether non-zero (> 0) values of ρ_T and/or ρ_φ are able to give a better fit. /Ji 2008/ actually measured transient creep both for a young and a mature concrete and presented the results using Eq. (5-14).

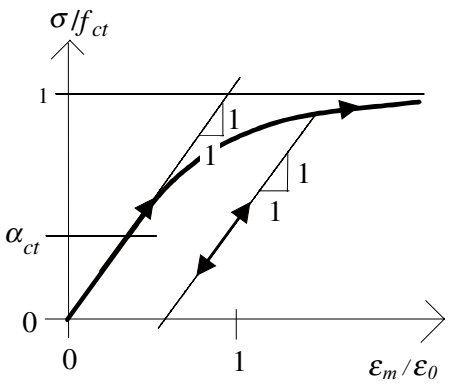

Figure 5-1. *Non-linear stress-strain curve for the concrete in tension.*

5.2.2 Mix designs

The mix design for B200 is shown in Table 5-1, and for B300 in Table 5-2. The assumed air content was 20 l/m^3, but measurements showed that the actual air content was 11 l/m^3 for B200 and 9 l/m^3 for B300, which is corrected for in both tables.

With the corrected values based on measured air contents the following binder contents are calculated:

B200: $B_{corr} = C_{corr} + SF_{corr} = 121.10 + 80.74 = 201.84$ kg/m^3

B300: $B_{corr} = C_{corr} + SF_{corr} = 182.02 + 121.35 = 303.37$ kg/m^3

Table 5-1. Mix design for B200.

Component	Nominal* weight [kg/m^3]	Density [kg/m^3]	Volume with measured air content [m^3]	Corrected weight with measured air content [kg/m^3]
Cement (C)	120	3,200	0.038	121.10
Silica fume (SF)	80	2,230	0.036	80.74
Water	165	1,000	0.167	166.52
Limus 25	369	2,760	0.135	372.39
FM	6.38	1,100	0.006	6.44
Aggregate, 0–8 mm	1,037.2	2,650	0.395	1,046.69
Aggregate, 8–16 mm	558.2	2,650	0.213	563.60
Air	0	0	0.011**	0
Sum of all components	**2,336**	**–**	**1.000**	**2,357**

*) For an assumed air content of 20 l/m^3

**) Measured air content = 11 l/m^3

Table 5-2. Mix design for concrete B300.

Component	Nominal* weight [kg/m^3]	Density [kg/m^3]	Volume with measured air content [m^3]	Corrected weight with measured air content [kg/m^3]
Cement (C)	180	3,200	0.057	182.02
Silica fume (SF)	120	2,230	0.054	121.35
Water	165	1,000	0.167	166.85
Limus 25	269	2,760	0.099	272.02
FM	7.06	1,100	0.006	7.14
Aggregate, 0–8 mm	1,035.3	2,650	0.395	1,046.94
Aggregate, 8–16 mm	557.3	2,650	0.213	563.74
Air	0	0	0.009**	0
Sum of all components	**2,334**	**–**	**1.000**	**2,360**

*) For an assumed air content of 20 l/m^3

**) Measured air content = 9 l/m^3

5.2.3 Maturity and strength growth

For determination of parameters (θ_{ref} and κ_3) to express the "maturity" function (Eq. 5-3), strength measurements are performed for four temperature levels: 5, 20, 35, and 50°C, respectively. The measured temperatures are shown in Figure 5-2.

The measured compressive strengths for the curing conditions shown in Figure 5-2 are presented in Figure 5-3. For each recipe all cubes are taken from one batch to avoid possible variations from different mix procedures.

Based on the results in Figure 5-2 and Figure 5-3, the temperature sensitivity function can be established according to the method in /Ekerfors and Jonasson 2000/, see Figure 5-4, and the evaluated parameters to be used in Eq. (5-3) are presented in Table 5-3. In this evaluation procedure only the part of the stress growth in Figure 5-3, where a straight line is relevant, is studied.

With respect to the maturity concept, the actual time is recalculated as the equivalent time according to Eq. (5-1) and the resulting strength curves are presented in Figure 5-5, and the evaluated parameters according to Eq. (5-5) are given in Table 5-4.

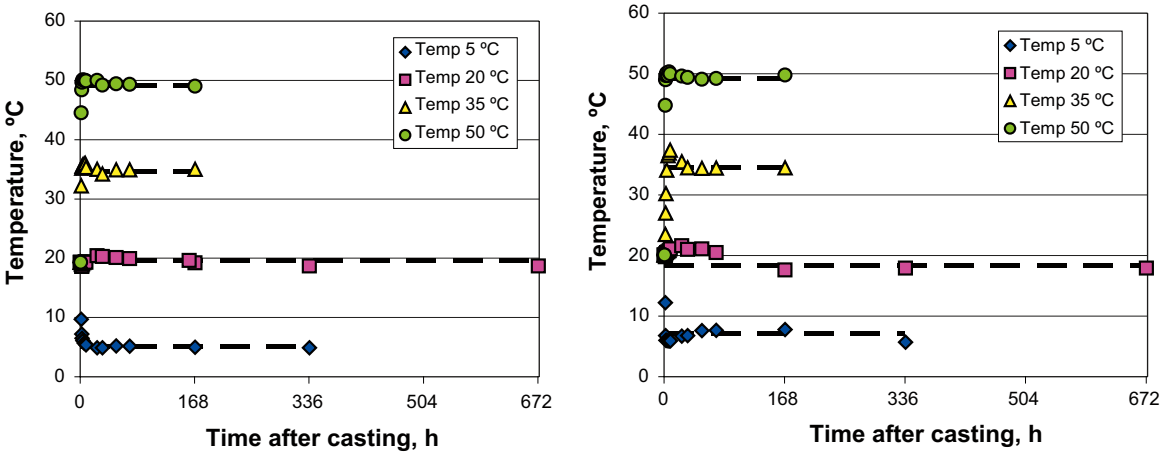

a) B200 b) B300

Figure 5-2. *Curing temperatures for concretes cubes in water. The dashed lines represent the average curing temperature for each level.*

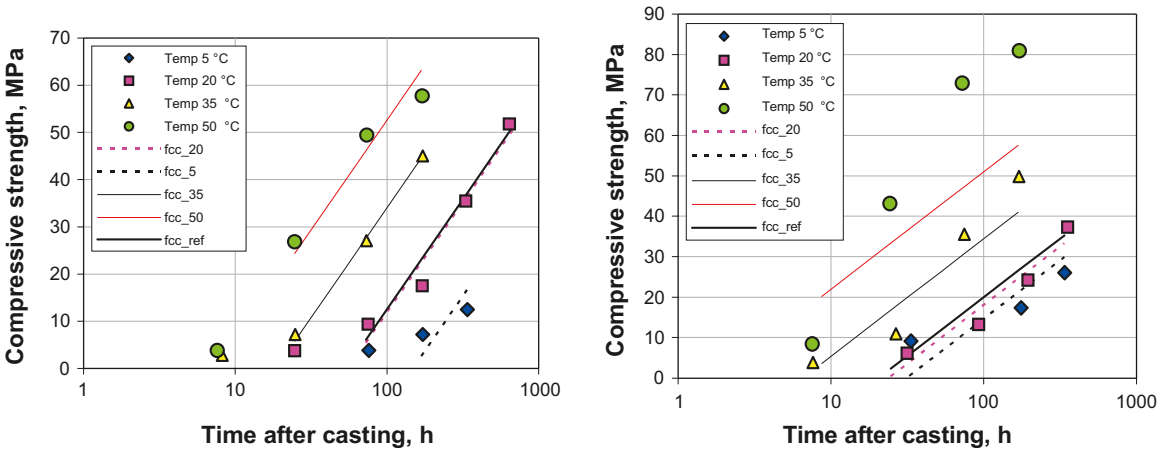

a) B200 b) B300

Figure 5-3. *Measured compressive strengths for cubes 100 × 100 × 100 mm for the conditions in Figure 5-2. The dashed lines represent best fits for each temperature level as a part of the evaluation process. Fcc = compressive strength of cubes.*

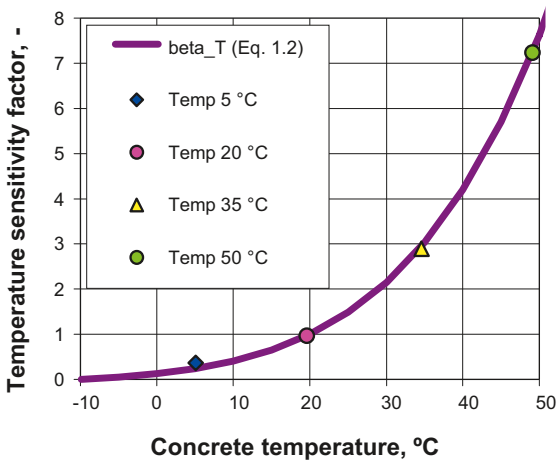

a) B200

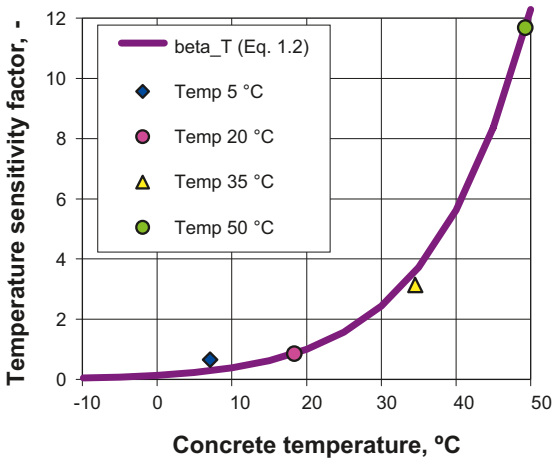

b) B300

Figure 5-4. *Temperature sensitivity based on information from Figure 5-3 and Figure 5-3.*

Table 5-3. Parameters for the temperature sensitivity using Eq. (5-3) for concrete mixes B200 and B300.

Concrete mix	Parameters using Eq. (5-3)	
	θ_{ref} [K]	κ_3 [–]
B200	7,079	0.144
B300	7,913	0

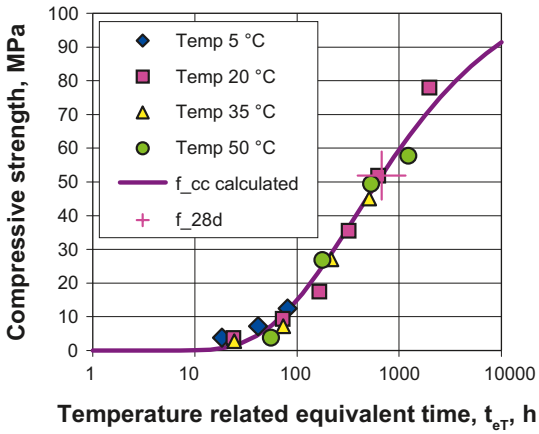

a) B200

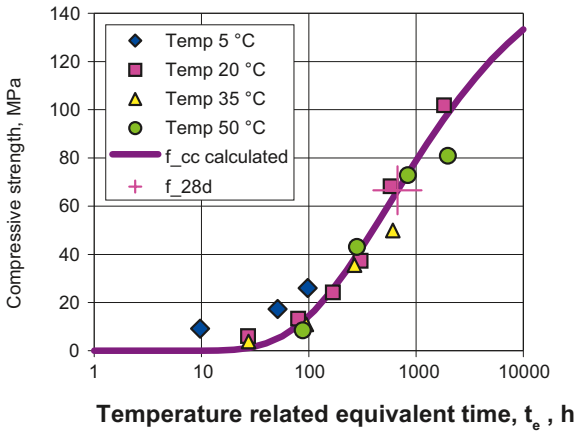

b) B300

Figure 5-5. *Strength growth (recalculated to 150 mm cubes) calculated according to Eq. (5-5). Equivalent time calculated according to Eq. (5-1).*

Table 5-4. Parameters for compressive strength using Eq. (5-5) for concrete mixes B200 and B300.

Concrete mix	Parameters using Eq. (5-5)				
	$f_{cc,28}$ [MPa]	s [–]	t_S [h]	t_A [h]	n_A [–]
B200	51.833	0.7647	3.2615	4.8922	3
B300	66.55	0.9370	4	6	3

5.2.4 Heat of hydration

For both mix designs the concrete temperature development was registered inside two semi-adiabats. If no heat is released to the surrounding from a body, the situation is defined as adiabatic. For the equipment used here, the concrete specimen is covered with insulation materials, and during the hydration period some heat will be released to the surroundings. This latter type of equipment is defined as semi-adiabat. After the temperature from the heat of hydration has returned to a level close to the environmental air temperature, the test specimen is heated with a heater mat around the test specimen to a temperature somewhat higher than the peak temperature from hydration. The cooling period after the second heating gives the basis to evaluate the so called cooling ratio, which afterwards is used to determine the total generated heat inside the concrete expressed by:

$$W_{tot} = \rho_c c_c \left(T - T_{start} + a \int_0^t (T - T_{air}) dt \right) \qquad (5\text{-}16)$$

where W_{tot} = specific heat of hydration for the concrete by concrete volume [J/m^3], T = measured concrete temperature [°C], T_{start} = starting concrete temperature (= casting temperature) [°C], T_{air} = environmental temperature in the air [°C], t = clock time[h], a = cooling ratio [1/h], ρ_c = concrete density [kg/m^3], and c_c = specific heat capacity of the concrete by cement weight [J/(kg °C)].

Evaluated cooling periods are shown in Figure 5-6, and the resulting cooling ratios are presented in Table 5-5.

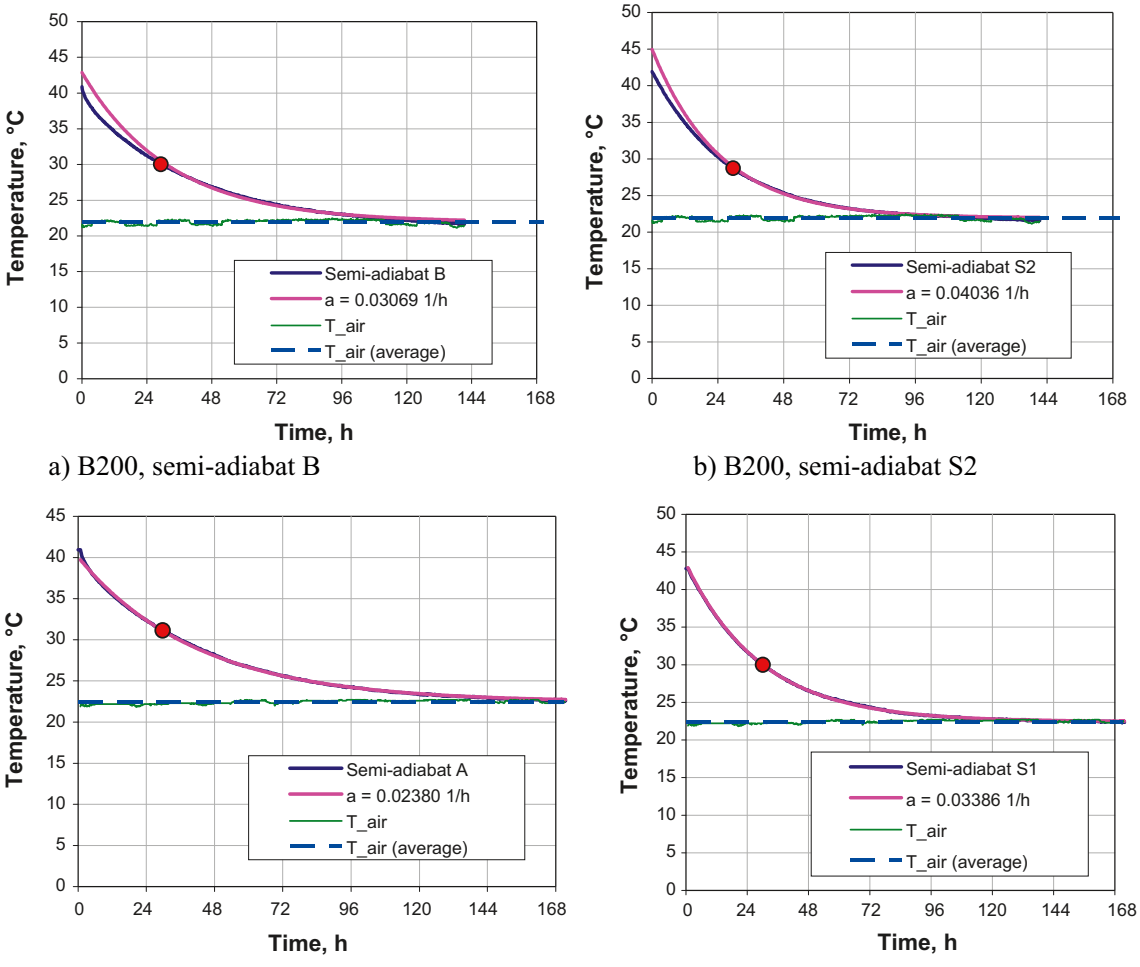

a) B200, semi-adiabat B

b) B200, semi-adiabat S2

c) B300, semi-adiabat A

d) B300, semi-adiabat S1

Figure 5-6. *Measured cooling ratios a [1/h], for concretes B200 and B300 in 4 different semi-adiabatic calorimeters, 2 measurements for each mix.*

Table 5-5. Cooling ratios in two semi-adiabatic calorimeters for each concrete mix B200 and B300.

Concrete mix	Cooling ratios to be used in Eq. (5-16)	
	Semi-adiabat I	*Semi-adiabat II*
B200	B: a = 0.030686 1/h	S2: a = 0.040364 1/h
B300	A: a = 0.023804 1/h	S1: a = 0.033861 1/h

With the combined use of measured concrete temperatures and adjustments based on evaluated cooling ratios, the real heat of hydration can be calculated according to Eq. (5-16). Then the specific heat of hydration by cement weight can be calculated in accordance with Eq. (5-4), see the resulting curves in Figure 5-7, and the calculated numerical parameters in Table 5-6.

Table 5-6. Parameters for heat of hydration using Eq. (5-4) for concrete mixes B200 and B300.

Concrete mix	Parameters in Eq. (5-4)			
	W_u, J/kg	λ_1, –	t_1, h	κ_1, –
B200	610480	1	68.914	0.5191
B300	445008	1	77.676	0.4945

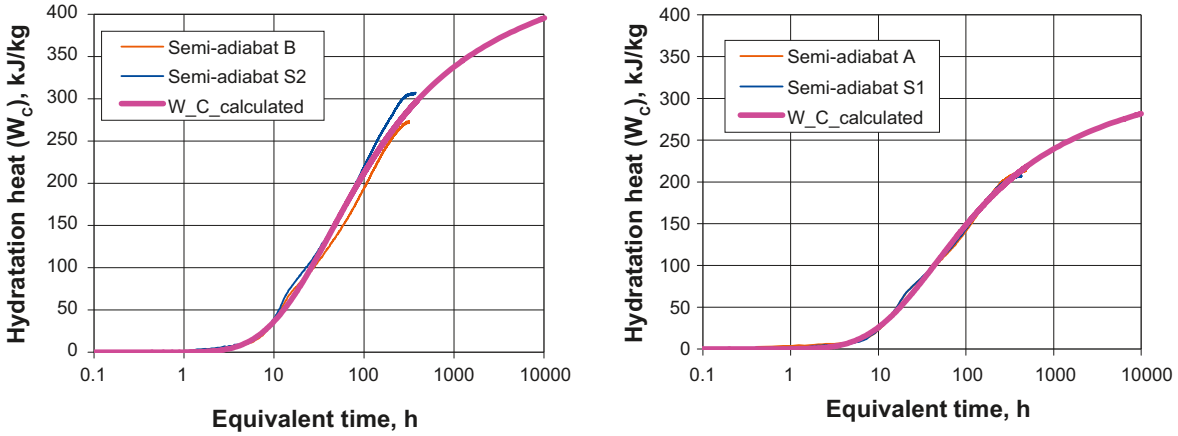

a) B200 b) B300

Figure 5-7. *Heat of hydration by weight of binder content for concrete mixes B200 and B300 in 4 different semi-adiabatic calorimeters, 2 measurements for each mix. Equivalent time calculated according to Eq. (5-1).*

5.2.5 Free deformation at variable temperature

The curve fits to measured free movements, using Eqs. (5-10)–(5-12), are shown in Figure 5-8, and the evaluated parameters are presented in Table 5-7.

For B300, the deformation sensor came loose during testing and no measurements were made. The calculated deformation in Figure 5-8 d) is therefore not fitted, but, as later can be seen in shown in Section 5.2.7, the calculated stresses show approximately the same agreement to the measured stresses as for B200. This indicates that the calculated deformation in Figure 5-8 d) is in the right magnitude.

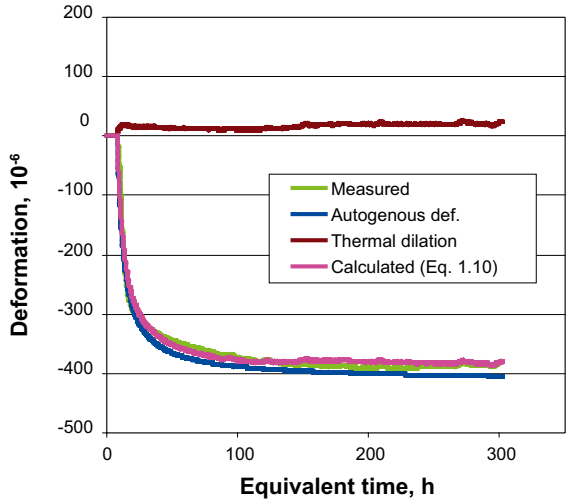

a) B200, almost constant temperature

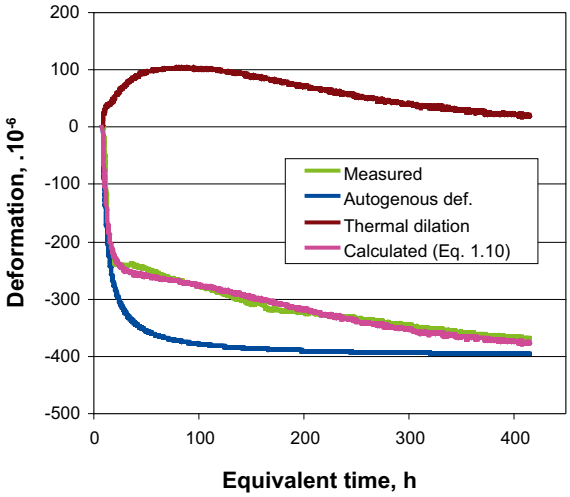

b) B200, variable temperature

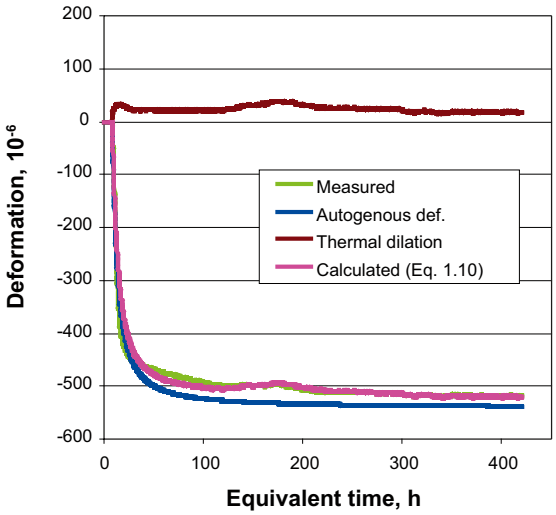

c) B300, almost constant temperature

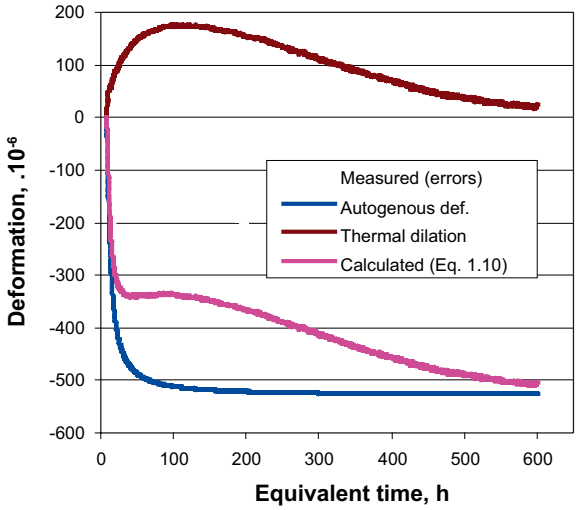

d) B300, variable temperature

Figure 5-8. *Free movements for concrete mixes B200 and B300. Figure a) and c) measured at almost constant temperature, figure b) and d) measured at temperature that develops when casting a 0.7 m thick wall. Curves for measured data, calculated deformation from heat development, calculated autogenous deformation and calculated total deformation. All calculated deformations according to Eq. (5-10)–(5-12). Equivalent time calculated according to Eq. (5-1).*

Table 5-7. Parameters for free deformations using Eqs. (5-10)–(5-12) for concrete mixes B200 and B300.

Concrete mix	Parameters using Eqs. (5-10) – (5-12)						
	α_T [10^{-6}/°C]	t_{s1} [h]	t_{s2} [h]	ε_{s1} [10^{-6}]	ε_{s2} [10^{-6}]	t_{SH} [h]	η_{SH} [–]
B200	11.1	4	6	0	–518	3.25	0.90
B300	13.0	4	6	0	–555	5.00	1.18

5.2.6 Young's modulus and early age creep

Young's moduli calculated using Eq. (5-8) are shown in Figure 5-9 with the fitted parameters presented in Table 5-8.

The creep deformations using Eq. (5-9) is shown in Figure 5-10 for concrete B200 and B300, and the fitted inclinations a_1 and a_2 are presented in Table 5-9.

With the help of the computer program RELAX /Jonasson and Westman 2001/ the deformations according to Figure 5-10 were recalculated to a relaxation spectra for each mix, and the resulting relaxation moduli are put into the material data files to be used in the computer program /ConTeSt Pro 3.2 2008/.

Table 5-8. Parameters for the Young's modulus up to 28 days of curing, using Eq.(5-8) for concrete mixes B200 and B300.

Concrete mix	Parameters using Eq. (5-8)		
	E_{28d} [GPa]	s_E [–]	t_{SE} [d]
B200	24.5	0.287	0.5
B300	28.9	0.263	0.5

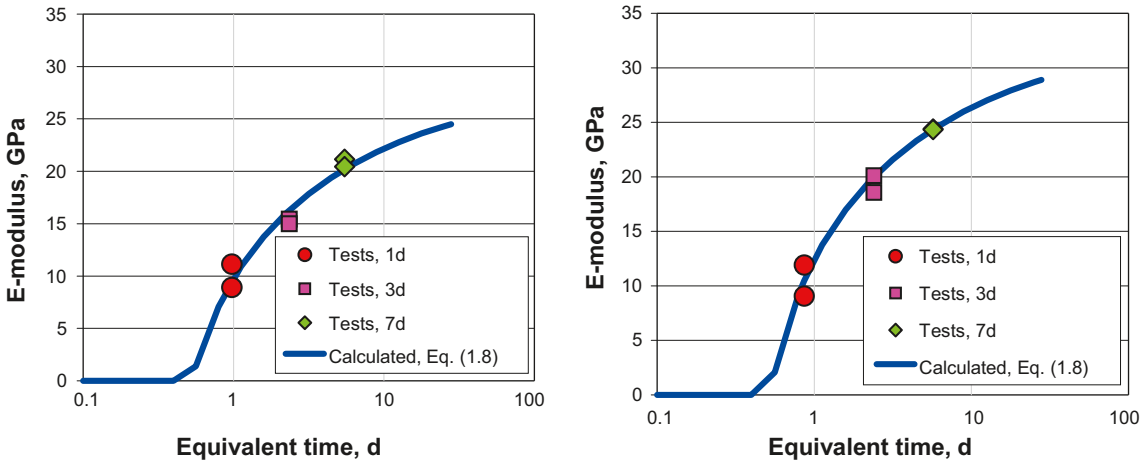

a) B200 b) B300

Figure 5-9. *Young's modulus according to Eq. (5-8) for concrete mixes B200 and B300. Test values for 1 day, 3 days and 7 days of curing and the calculated development of the young's modulus over time using Eq (5-8). Equivalent time calculated according to Eq. (5-1).*

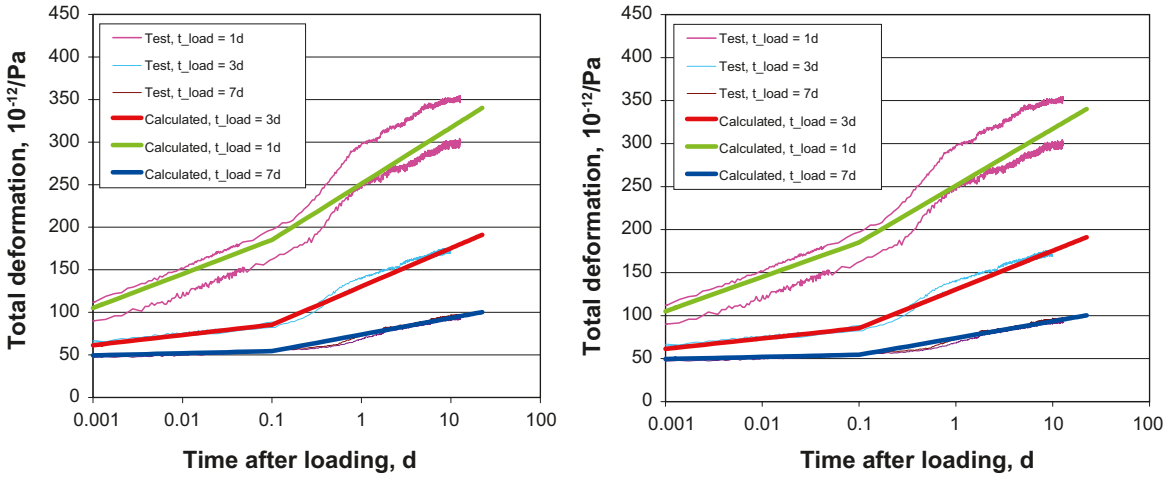

a) B200 b) B300

Figure 5-10. *Creep deformations for concrete mixes B200 and B300 for sample age 1 day, 3 days and 7 days, measured on two samples for each test. Calculated creep according to Eq. (5-9) with parameters determined from tests.*

Table 5-9. Parameters for the creep deformations using Eq. (5-9) for concrete mixes B200 and B300.

Concrete mix	Parameters using Eq. (5-9)			
	t_0 [d]	Δt_1 [d]	a_1 [10^{-12}/(Pa log-unit)]	a_2 [10^{-12}/(Pa log-unit)]
B200	0.9755	0.1	40	66
	2.3479		12	45
	5.4785		2.5	19.5
B300	0.8625	0.1	28	35
	2.4009		6	23
	5.7179		3	12

5.2.7 Stresses at total restraint

The testing in the stress rig at Luleå University of Technology gives information on strength growth in the tested concrete as well the development of the tensile strength /Westman 1999/. The resulting tensile strength parameters, see Eq. (5-13), are presented in Table 5-10.

For the use of the stress-strain curve illustrated in Figure 5-1 $\alpha_{ct} = 0.9$ has been adopted for concrete mixes B200 and B300.

Calculated and measured stresses are compared in Figure 5-11 for the mixes B200 and B300. The agreement between the calculated and measured stresses in Figure 5-11 is satisfactory, and most likely the use of calculated parameters can be used in future crack analysis, as the calculated stresses seem to capture the general behaviour of both concrete mix B200 and B300.

A final comment may be that some of the parameters for the low pH SCC studied are not like other “normal” concretes analysed before, as the shrinkage deformation is rather high and the temperature deformations rather low. For normal reference concrete, the very early age period, about one day, shows compression stresses before the stresses changes into tension /Westman 1999, Hedlund 2000/, but, as can seen in Figure 5-11, the concretes tested here are in tension throughout the test period.

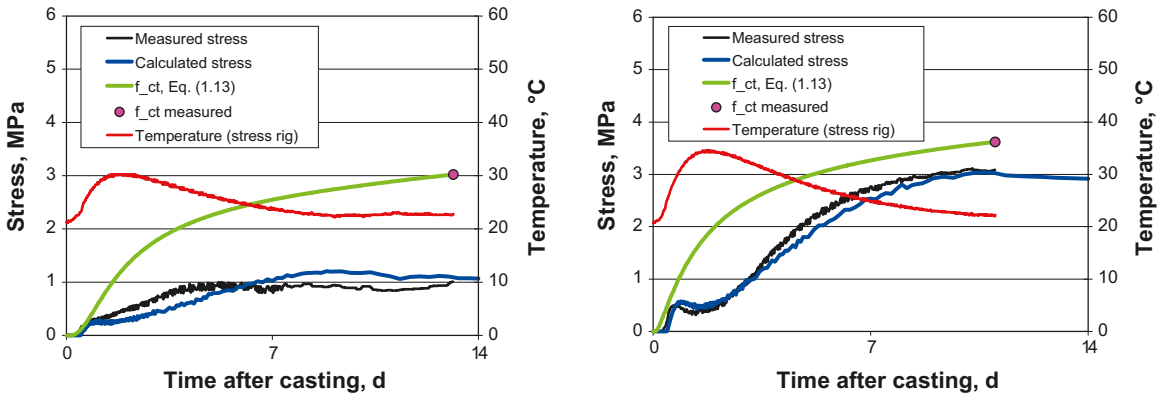

a) B200 b) B300

Figure 5-11. *Stresses at full restraining (for a simulated wall with thickness 0.7 m) for concrete mixes B200 and B300. f_ct = f_{ct} = tensile strength.*

Table 5-10. Parameters for the tensile strength using Eq. (5-13) for concrete mixes B200 and B300.

Concrete mix	Parameters using Eq. (5-13)		
	β_1 [–]	f_{ct}^{ref} [MPa]	f_{cc}^{ref} [MPa]
B200	0.667	3.02	44.9
B300	0.667	3.62	85.7

From Figure 5-11 it can be seen that mix B200 has significantly lower tensile stresses than mix B300. This implies that, if a concrete body is restrained to some degree, concrete B200 is preferable. If a newly cast concrete body is free to deform, the result from the stress rig is not relevant information to classify the concretes with respect to early age stresses. In the latter situation the stresses are much lower, and probably the difference between the studied concrete mixes is less. Further structural analyses can contribute more detailed information.

5.3 Creep for higher loading ages

5.3.1 Creep tests in the hydraulic test rig

In section 5.2.6 creep has been analysed for loading ages up to about 7 days. Additionally, tests with the same "early age" creep rigs /Westman 1999/ have been performed after curing times of about one month (B200) and two months (B300), see Figure 5-13 and Figure 5-14. The specimens were sealed immediately after casting and remained sealed during the testing. The maximum load on the test specimen in these rigs is about 150 kN, which is produced by the dead weight of steel plates and transferred by a hydraulic pressure system to the sample, see Figure 5-12. The resulting Young's modulus, calculated for a time duration of 0.001d, see Eq. (5-6), are presented in Table 5-11.

The plot with linear increase of creep deformation in the logarithmic time scale is, up to the present knowledge, the best we can do for the trend behaviour of creep deformation /Bažant 1975, 1988/. This means that for practical applications we always have to define a loading age, say one month, and a decisive load duration, say 30 yrs. This situation can for practical engineers be described by an Young's modulus valid at the concrete age of one month together with the associated creep ratio describing the additional creep deformation after 30 yrs load duration. The creep ratios calculated from the results shown in Figure 5-14 are presented in Figure 5-15.

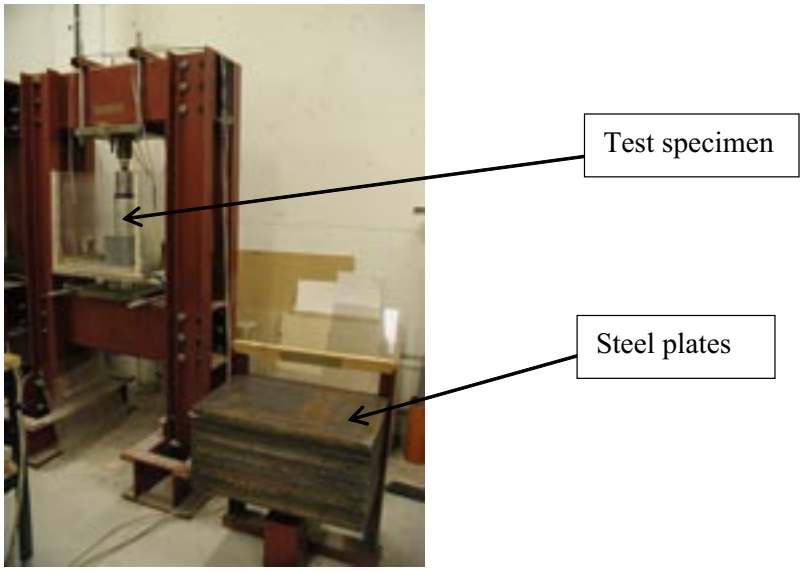

Figure 5-12. *Creep test in the "early age" creep rig with maximum loading.*

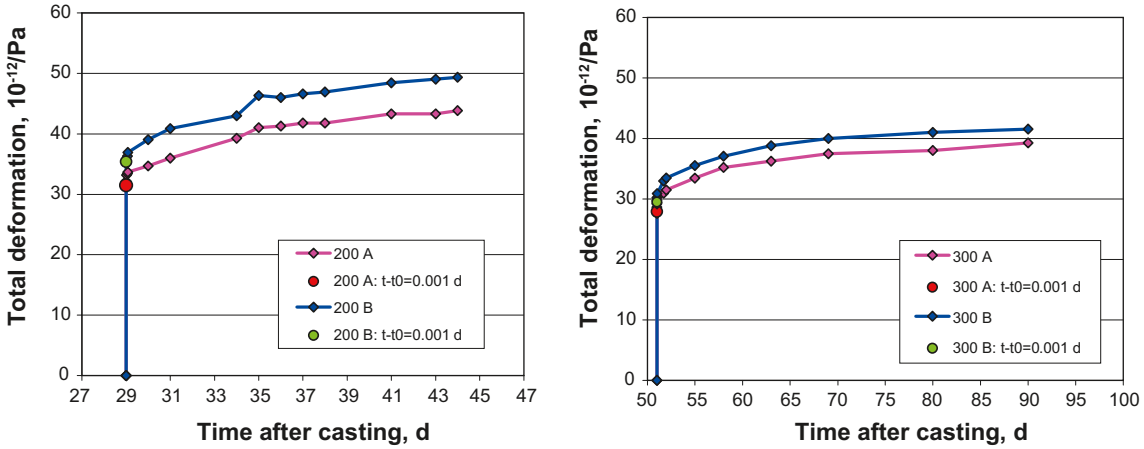

a) B200, loading age = 29 days b) B300, loading age = 51 days

Figure 5-13. *Creep for higher loading ages for concrete mixes B200 and B300. A and B denote two different samples.*

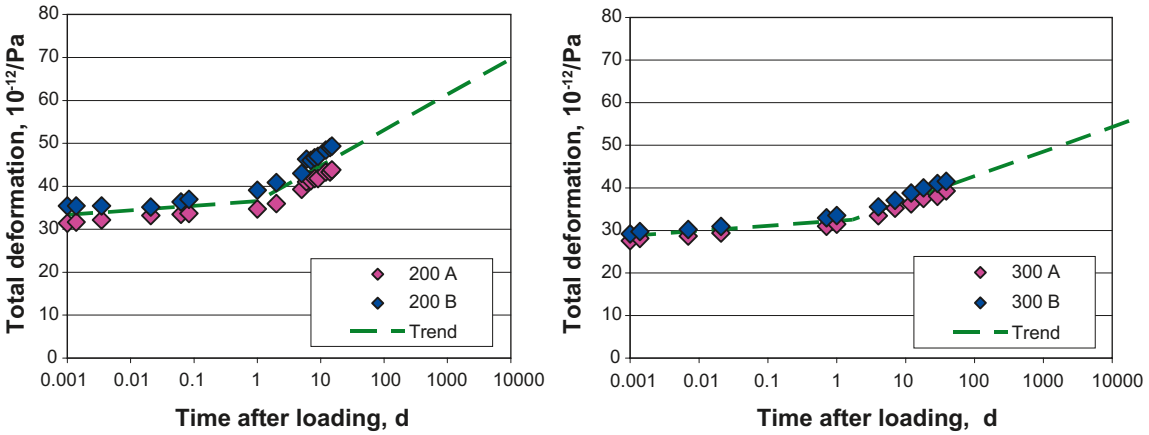

a) B200, loading age = 29 days b) B300, loading age = 51 days

Figure 5-14. *Creep for higher loading ages for concrete mixes B200 and B300. A and B denote two different samples.*

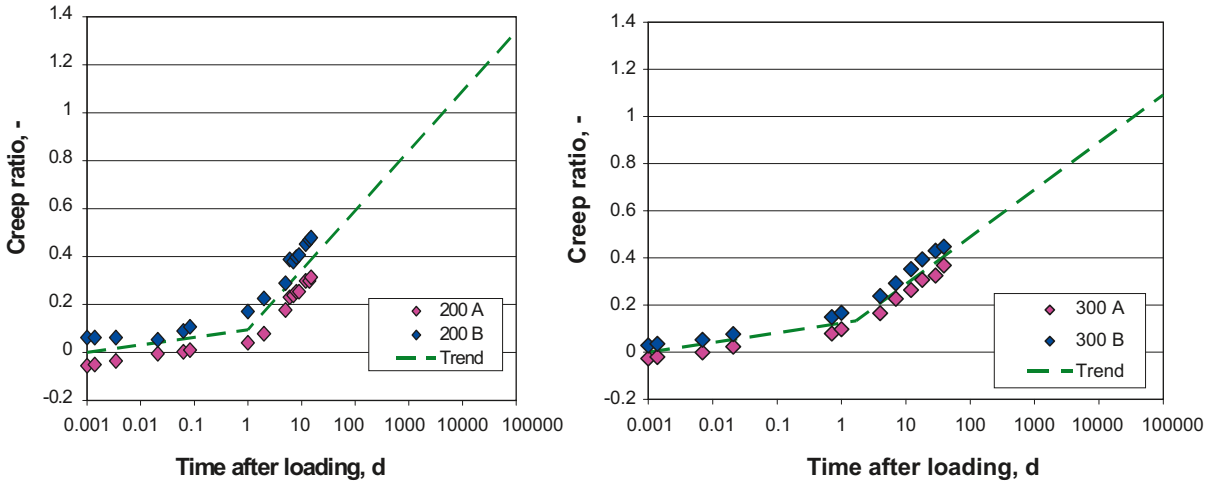

a) B200, loading age = 29 days

b) B300, loading age = 51 days

Figure 5-15. *Creep ratios for higher loading ages for concrete mixes B200 and B300. A and B denote two different samples for each tested concrete mix.*

Table 5-11. Young's modulus using Eq. (5-6) for concrete mixes B200 and B300 tested at loading ages 29 d and 51d, respectively. E_A and E_B denote two tested samples.

Concrete mix	Creep tests in "early age" rigs for higher loading ages			
	Loading age [d]	E_A [GPa]	E_B [GPa]	$E_{average}$ [GPa]
B200	29	31.72	28.22	30.0
B300	51	35.82	33.90	34.9

5.3.2 Creep tests in mechanical test rig

At loading times longer than two months the creep is tested on sealed specimens in mechanical tests rigs, the testing arrangement is shown in Figure 5-16. A spring plate maintains the load (Figure 5-17).

The evaluated Young's modulus from tests in the mechanical creep rig for loading age = 99 d is presented in Table 5-12, and the associated creep ratios are given in Figure 5-18.

The tests in the mechanical creep rig for sample age about one year are still ongoing, the results to 99 d are presented here; see the evaluated Young's modulus in Table 5-13, and the associated creep ratios in Figure 5-19.

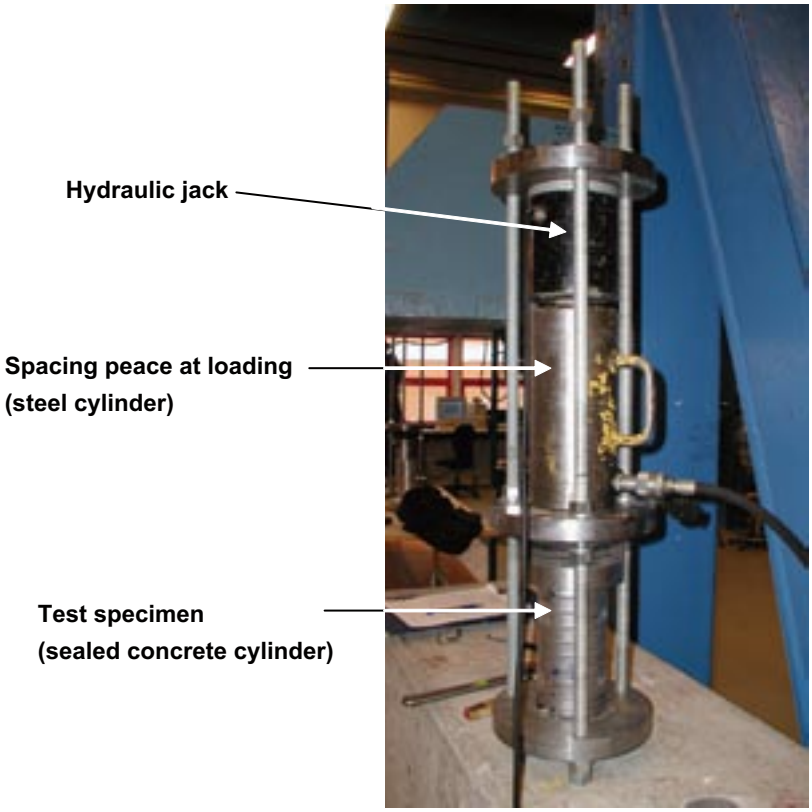

Figure 5-16. *Loading of test specimens in the mechanical creep rig.*

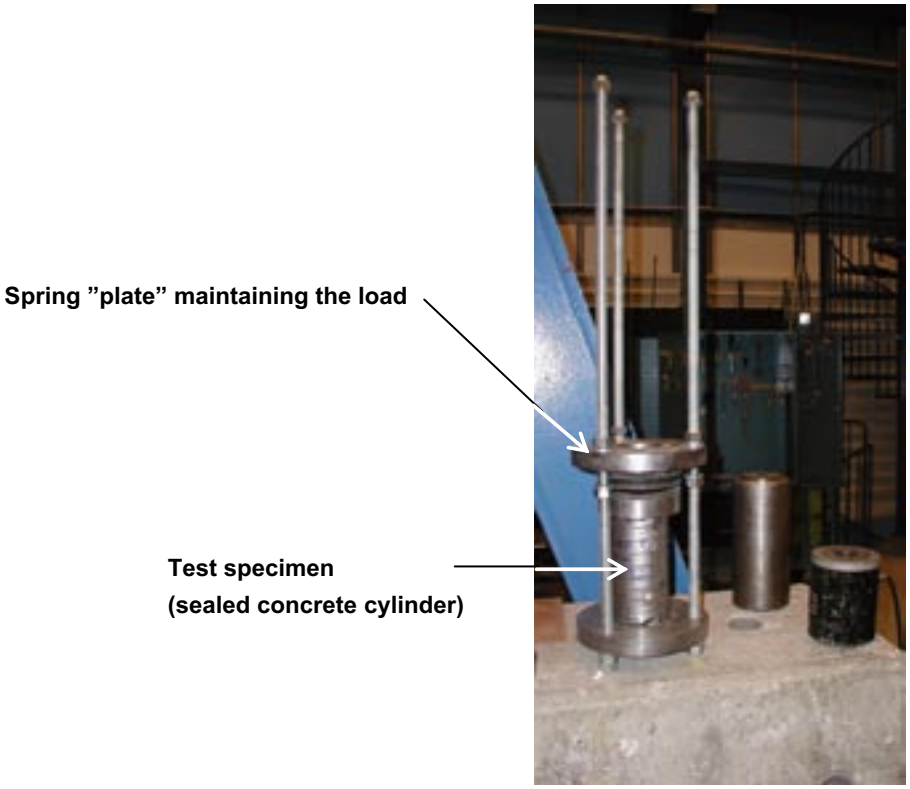

Figure 5-17. *Measurement of deformations maintaining the load in the mechanical creep rig. The deformations are measured in three lines for each specimen by a Steager instrument (mechanical extensometer), which show strains with an accuracy of about* 1×10^{-6}.

Table 5-12. Young's modulus for concrete mixes B200 and B300 tested at loading age 99d in mechanical test rigs. E_A and E_B denote two tested samples.

Concrete mix	Creep tests in mechanical rigs for sample age = 99 d			
	Sample age [d]	E_A [GPa]	E_B [GPa]	$E_{average}$ [GPa]
B200	99	34.45	34.23	34.3
B300	99	36.67	37.92	37.3

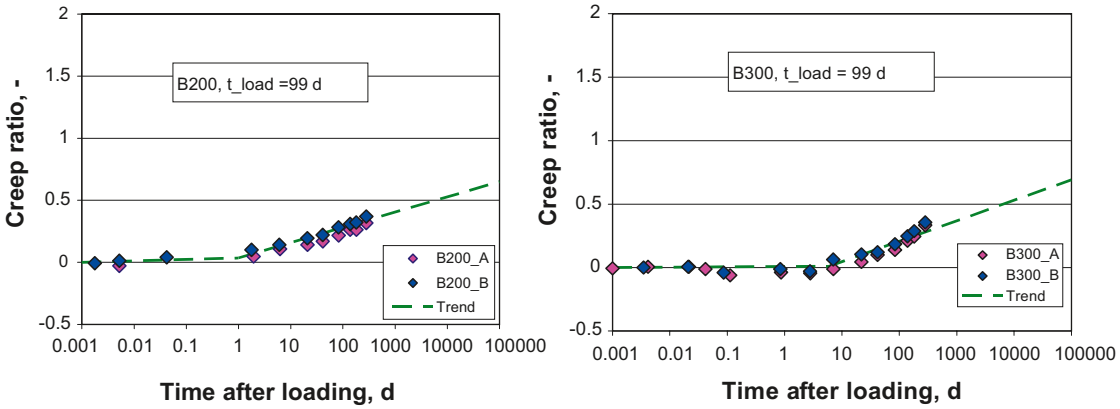

a) B200, loading age = 99 days b) B300, loading age = 99 days

Figure 5-18. *Creep ratios for 3 months sample ages for concrete mixes B200 and B300.*

Table 5-13. Young's modulus for concrete mixes B200 and B300 tested at sample age about one year in mechanical test rigs. E_A and E_B denote two tested samples.

Concrete mix	Creep tests in mechanical rigs for sample age 1 year			
	Sample age [d]	E_A [GPa]	E_B [GPa]	$E_{average}$ [GPa]
B200	385	37 .55	36.83	37.2
B300	387	39.36	39.36	39.4

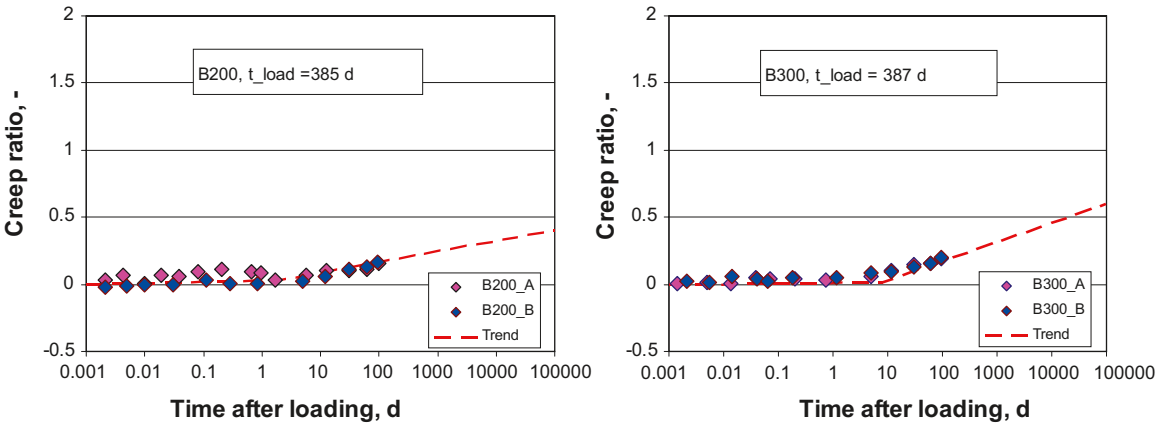

a) B200, loading age = 385 days b) B300, loading age = 387 days

Figure 5-19. *Creep ratios at loading age one year for concrete mixes B200 and B300.*

5.4 Young's modulus and Poisson´s ratio (short-term loading)

The Young's modulus may also be called elastic or elasticity modulus or simply E-modulus. The general technical meaning is that it denotes the material parameter that shall be used to calculate the "elastic deformation" at short-term loading. For very fast loading, like fast dynamic loads, we may also define a dynamic Young's modulus. Besides, the Young's modulus in reality is not a strict material parameter, although it is used a lot in structural calculations in engineering practice. It is always related to the rate of loading, and how long after (start of) loading we want to have information on the deformation response. In ordinary "static" load situations it might be relevant to use the load duration 0.001d /Westman 1999/ and defining that response as the "elastic deformation", which has been done here when calculating the developments of Young's modulus in Figure 5-9. The true information of the background for structural behaviour with respect to both "elastic" and creep" response of the material in question is the total deformation (Figure 5-10).

Well aware of the problems defining an Young's modulus, several standardized procedures have been developed to give strict rules for test procedures when measuring an Young's modulus. For concrete in compression such a procedure is described in /SS 13 72 32 2005/, which is used here with the purpose of producing a *key value of Young's modulus*, which can be used as a characterizing parameter of the elastic behaviour of the concrete as a *quality parameter*. However, this parameter alone is not primarily aimed to be used in structural calculations. It had been possible to use it as a *formal* Young's modulus when dividing the total deformation into an "elastic" and a "creep" part, but that is not possible here as the use of SS 13 72 32 is not suitable for young age concrete.

The test procedure in accordance with SS 13 72 32 has been used for a concrete of about 4 months age, see Table 5-14. The Young's modulus in compression is now a quality parameter, but the measured Young's modulus from the test in tension has no formal status, as SS 13 72 32 only regulates the condition for concrete in compression. The tensile test has been performed in a similar manner with the test specimen glued to end plates, which means that the tensile tests represent the load case of uniaxial tension.

The test performed at LTU according to the test procedures in SS 13 72 32 are presented in Figure 5-21 and Figure 5-22. For the concrete mixes B200 and B300 the parameters in Table 5-14 may be regarded as key values when studying short-term loading. Note that the Young's modulus determined from the total deformation at a specified load duration in Section 5.2.6 and 5.3 will in general differ from the Young's modulus determined according to SS 13 72 32.

One significant result for all tests in this section is that the tested stress-strain curves are linear up to about 80 per cent of the compressive strength; see Figure 5-20 to Figure 5-23. This indicates that linear creep might be a sufficient approximation up to the level of about 60 per cent of the compressive strength. In normal strength concrete the stress-strain curve is linear up to about 60 per cent of the compressive strength, and for these concretes the linear creep behaviour is usually applied for stresses up to about 40 to 50 percent of the compressive strength.

Table 5-14. Representative parameters for short-term loading at concrete age of almost 4 months.

Concrete mix	Young's modulus [GPa]	Compressive strength [MPa]	Tensile strength [MPa]	Poisson´s ratio [–]
B200	38	88	3.3	0.27
B300	42	113	3.8	0.27

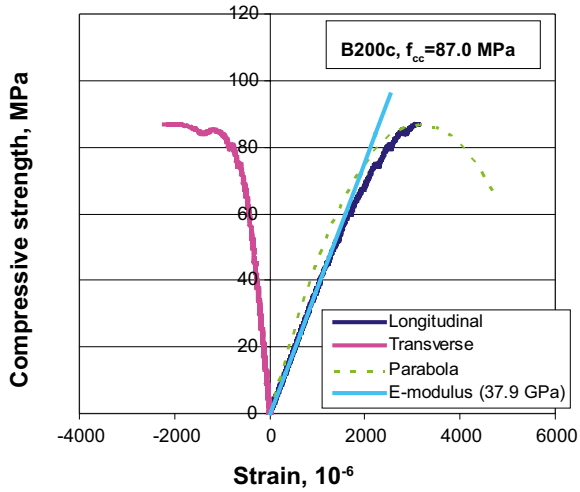

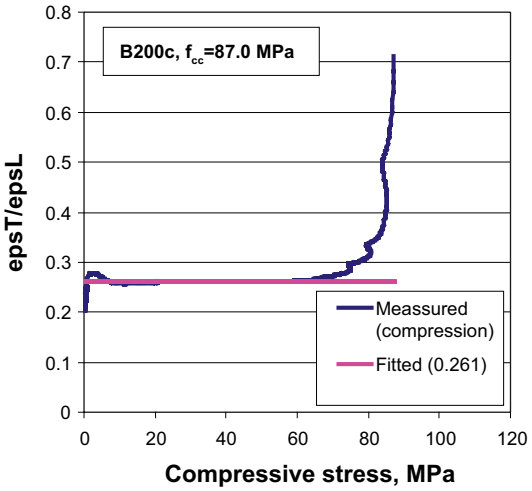

a) Sample 1 of concrete B200 in compression

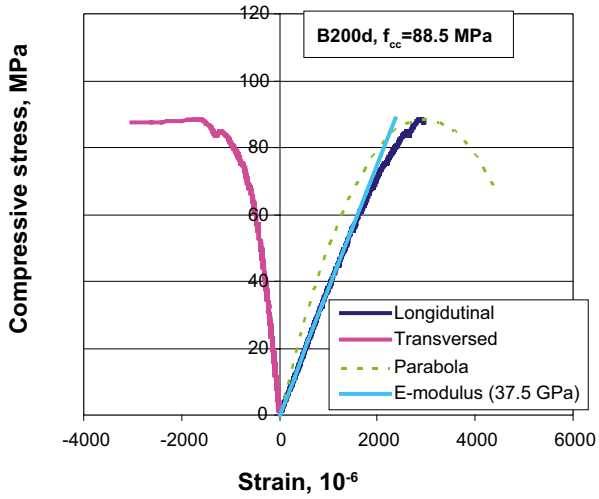

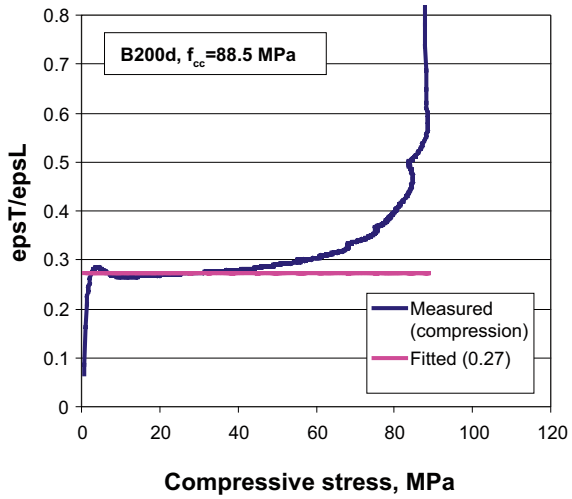

b) Sample 2 of concrete B200 in compression

Figure 5-20. *Test results for concrete mix B200 according to SS 13 72 32 (compression).*

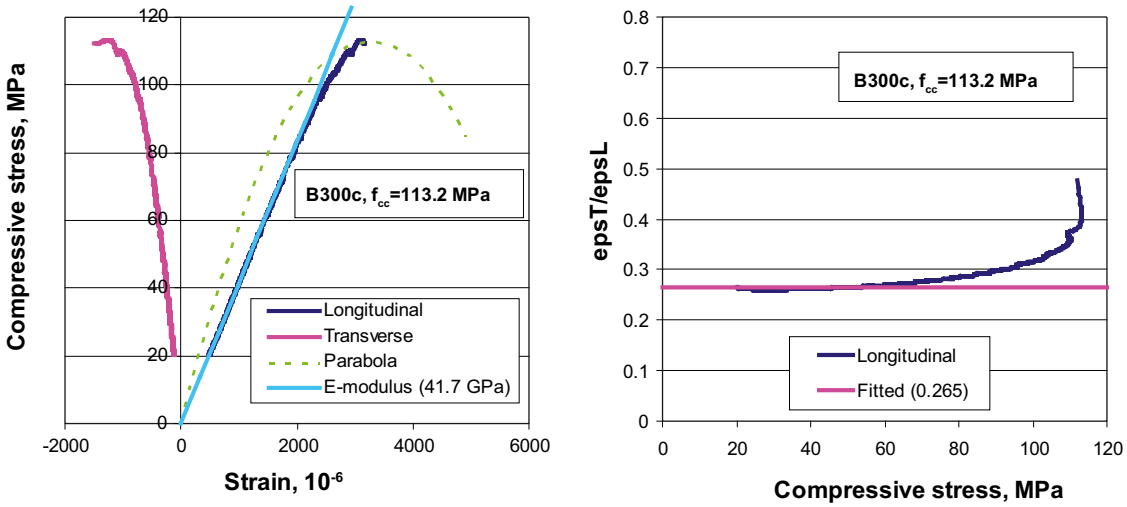

a) Sample 1 of concrete B300 in compression

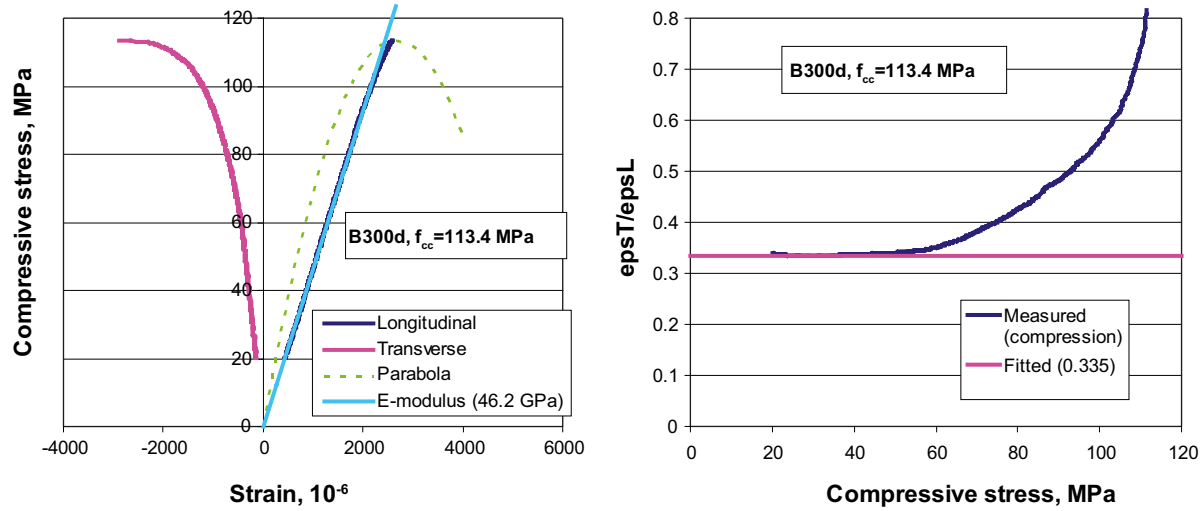

b) Sample 2 of concrete B300 in compression

Figure 5-21. *Test results for concrete mix B200 according to SS 13 72 32 (compression).*

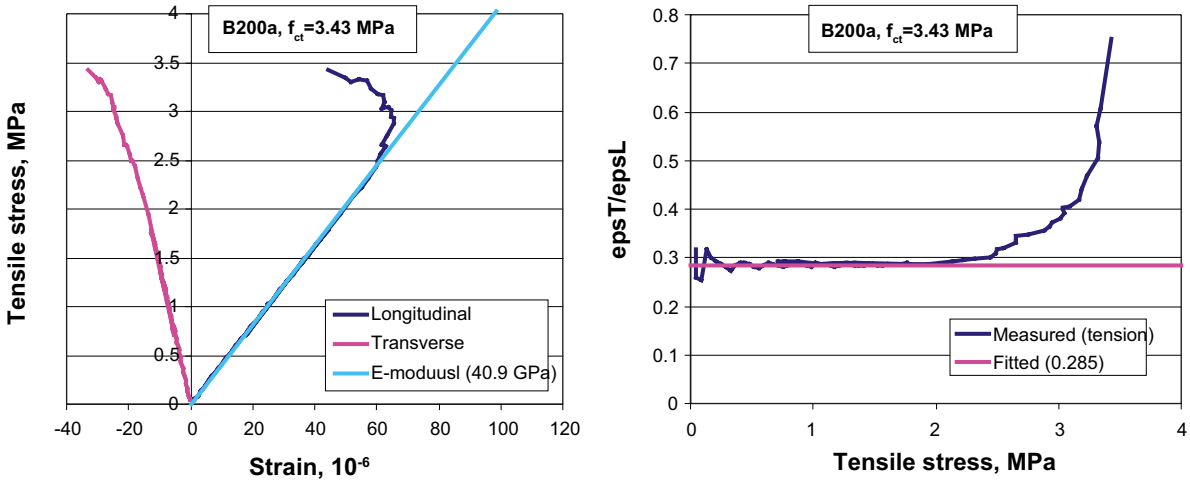

a) Sample 1 of concrete B200 in tension

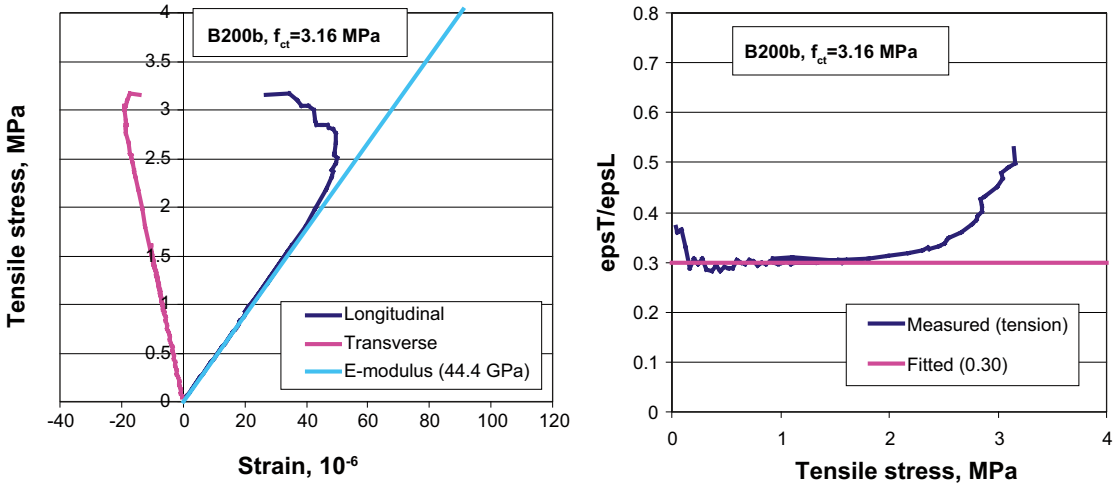

b) Sample 2 of concrete B200 in tension

Figure 5-22. *Test results for B200 in tension.*

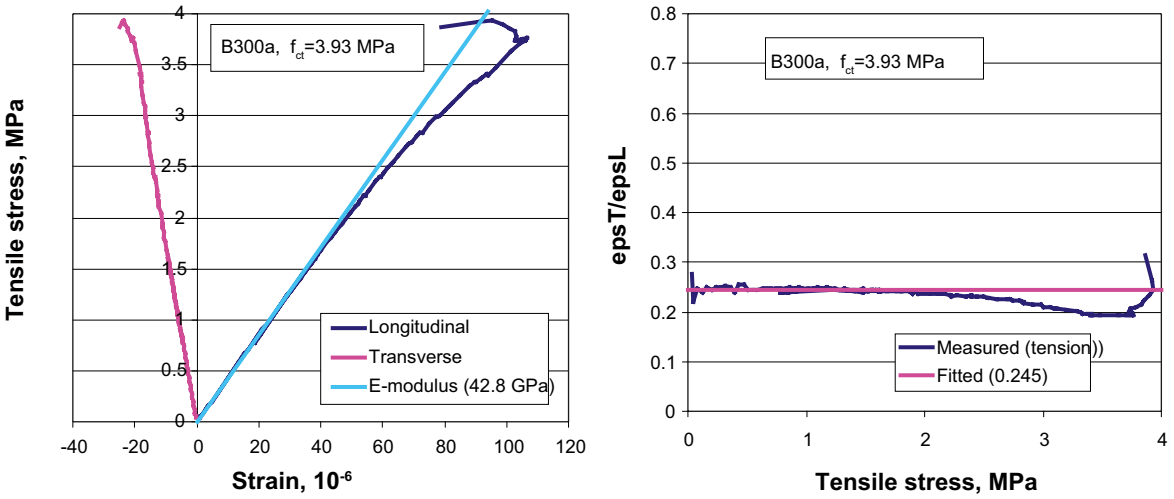

a) Sample 1 of concrete B300 in tension

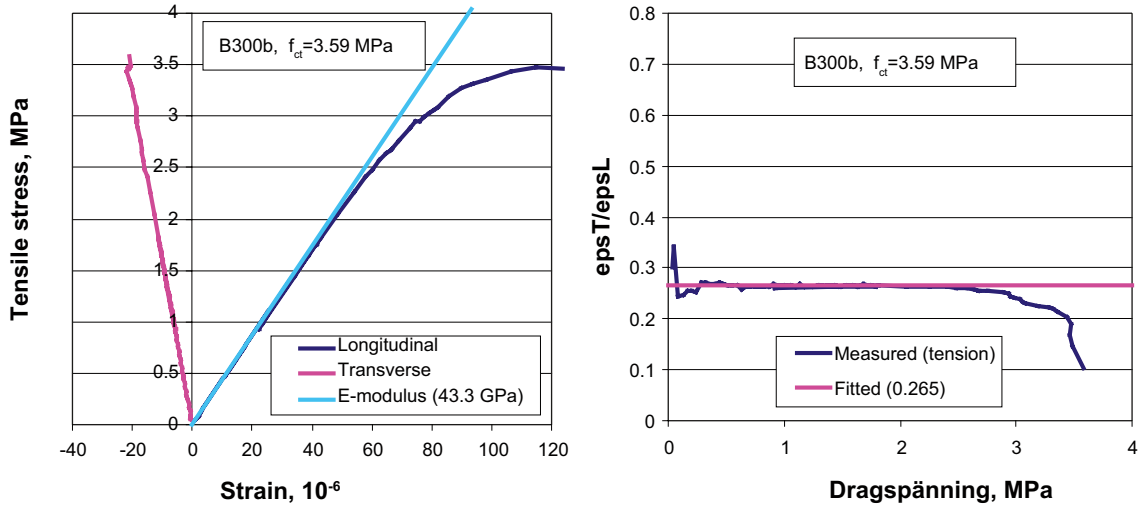

b) Sample 2 of

Figure 5-23. *Test results for B300 in tension.*

5.5 Trend values of compressive strength growth, Young's modulus and creep behaviour for studied concretes

The tested strength growth, Young's modulus and creep deformations are summarised as trend values in Figure 5-24 to Figure 5-29. Equivalent time is defined in Eq. (5-1).

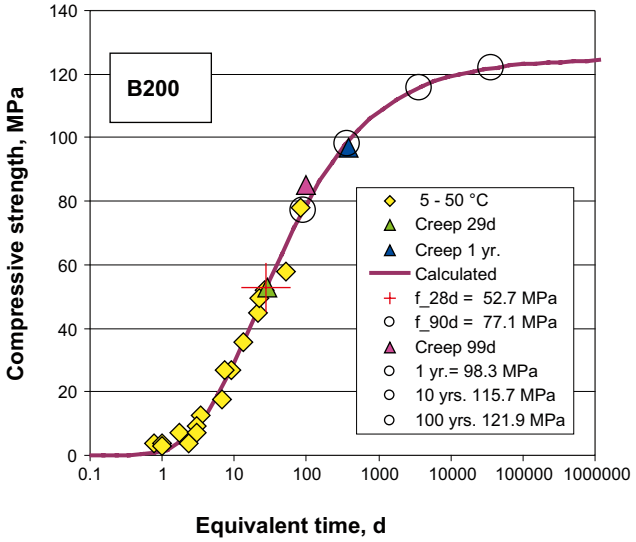

Time at loading	$f_{cm,cube}$, MPa
28 d	53
90 d	77
1 yr.	98
10 yrs.	116
100 yrs.	122

Figure 5-24. *Trend compressive strength curve (recalculated to 150 mm cubes) for concrete mixes B200.*

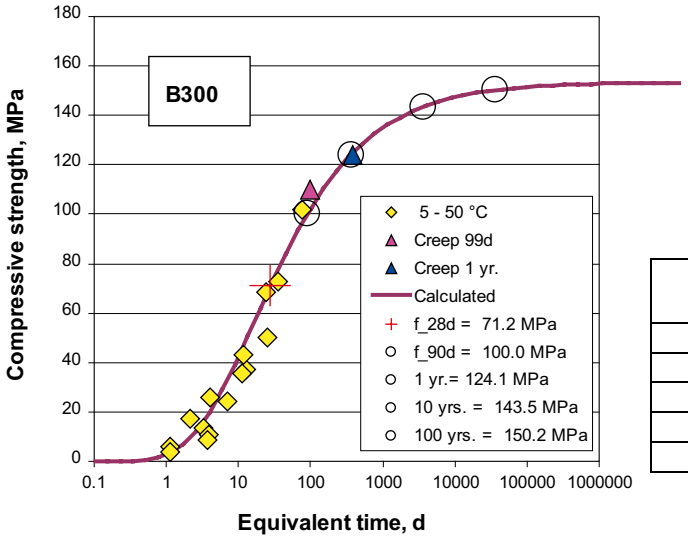

Time at loading	$f_{cm,cube}$, MPa
28 d	71
90 d	100
1 yr.	124
10 yrs.	143
100 yrs.	150

Figure 5-25. *Trend compressive strength curve (recalculated to 150 mm cubes) for concrete mixes B300.*

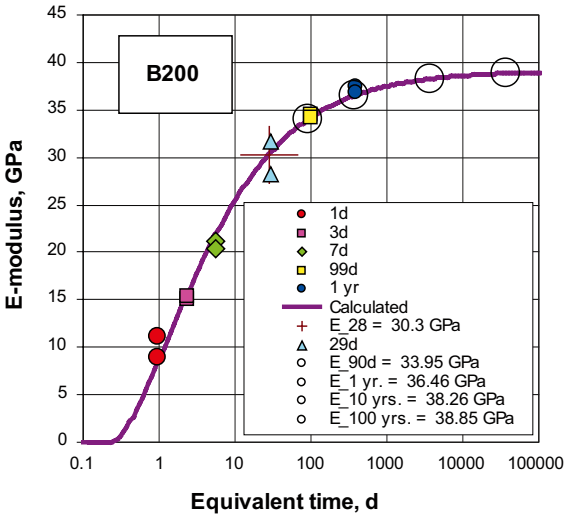

Time at loading	E_{cm}, GPa
28 d	30.3
90 d	33.9
1 yr.	36.5
10 yrs.	38.3
100 yrs.	38.8

Figure 5-26. *Trend of Young's modulus curve for concrete mixes B200.*

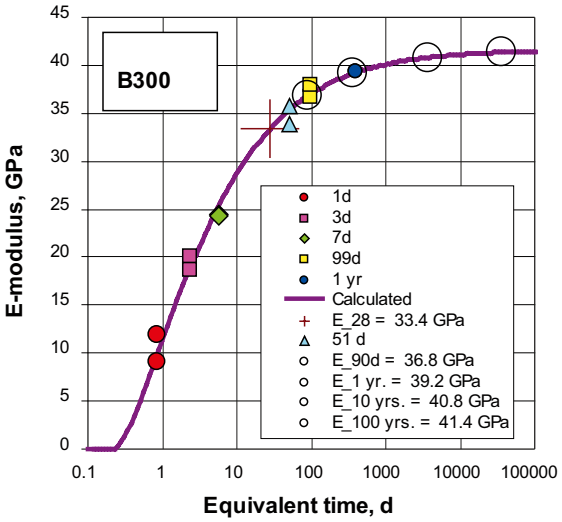

Time at loading	E_{cm}, GPa
28 d	33.4
90 d	36.8
1 yr.	39.2
10 yrs.	40.8
100 yrs.	41.4

Figure 5-27. *Trend of Young's modulus curve for concrete mixes B300.*

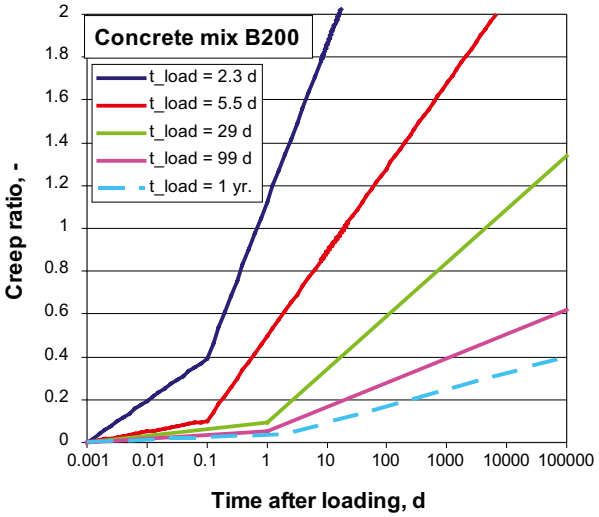

Loading at 90 d ≈ 99 d		
Time duration	Creep ratio φ'	$\chi \cdot \varphi'$
90 d	0.27	0.22
1 yr.	0.34	0.27
10 yrs.	0.46	0.36
100 yrs.	0.57	0.46

Figure 5-28. *Trend creep ratio curve at tested loading ages for concrete mixes B200.*

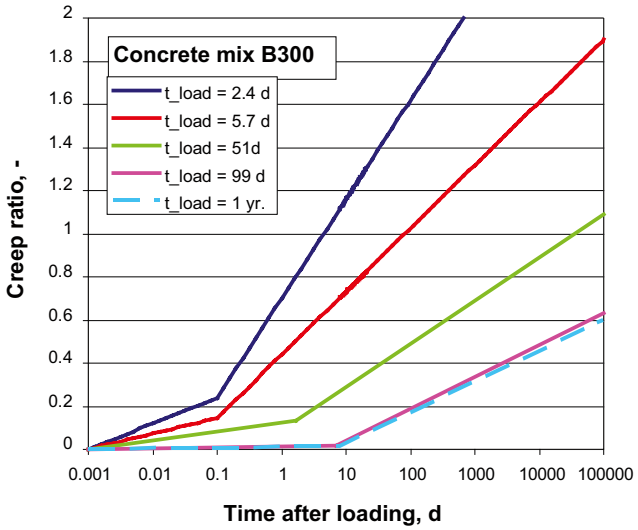

Loading at 90 d ≈ 99 d		
Time duration	Creep ratio φ'	$\chi \cdot \varphi'$
90 d	0.18	0.14
1 yr.	0.24	0.19
10 yrs.	0.42	0.34
100 yrs.	0.55	0.44

Figure 5-29. *Trend creep ratio curve at tested loading ages for concrete mixes B300.*

5.6 Summary young and mature concrete

Some properties of young low pH SCC are different compared to traditional concrete. The heat development and also the compressive strength development during the first days of curing are low. The compressive strength increases to high values with increasing age. At 28 days of curing, the compressive strength was 53 MPa (B200) and 71 MPa (B300). Unlike conventional concrete, the compressive strength keeps increasing after 28 days of curing. After 3 months, B200 has a compressive strength of about 75 MPa and B300 of 100 MPa. The early volume changes are higher than for conventional concrete. Despite the differences in behaviour, the evaluation of the obtained results was possible and mathematical concepts, established for traditional concrete, could be used. The use of the obtained parameters in thermal stress analysis is possible.

The properties of mature low pH SCC do not differ remarkably from conventional concrete other than a higher ultimate strength development. The established models for Young's modulus, compressive strength, tensile strength, stress-strain and creep are valid. The creep ratio is low when the concrete is mature. There is no large difference between the two mix designs; the mix B300 has a higher final compressive strength, Young's modulus and tensile strength. The higher early volume changes of B300 lead to higher stresses at young age when fully restrained.

6 Summary of material parameters for structural calculations

6.1 General background

The mechanical properties of low pH SCC for curing times greater than 3 months are summarised here. All necessary values are presented for the concrete denoted B200, and in a few cases data for concrete B300 is added.

6.2 Compressive strength

Compressive strength values are based on tests performed at Luleå University of Technology. Characteristic material data are presented to be used in the structural analysis for the long-term behaviour.

Figure 5-24 shows the strength development by time, and yellow symbols shows results using several test specimens (≥ 3 per symbol), while green, pink and blue symbols are based on one test specimen. The spread in test results was shown to be small, and the later ages with only one specimen are also evaluated to be sufficient for description of the strength.

The line marked "calculated" is in line with Eq. (5-5) to predict strength growth, and the agreement is satisfactory between calculated and measured values. Large circles represent expected compressive strengths at the ages 28 days, 90 days, 1 year, 10 years, and 100 years.

With respect to the uncertainty that might be present for long-term concrete with high silica content, the compressive strength is here limited to the value at 90 days:

$f_{cm,cube} = 77\ MPa$

where $f_{cm,cube}$ = mean compressive strength for a 150 mm cube [MPa].

Recalculation to compressive strength for cylinders gives:

$f_{cm} = f_{cm,cube}/1.25 = 62$ MPa

where f_{cm} = mean compressive strength for a cylinder with 150 mm diameter and height 300 mm [MPa].

Calculation of characteristic compressive strength, f_{ck}, in accordance with /EN 1992-1-1 2004/ gives:

$f_{ck} = f_{cm} - 8 = 54$ MPa

For the calculation the following is valid: $f_{ck} = 54$ MPa

In this investigation the on-going formation of gel-products (hydration and puzzolanic activity) is taken into account by the test procedure and the extrapolation by the formulas used. In addition, there is a so called long-term "aging effect" meaning some redistribution of the chemical products (like polymerization). The effects of the aging effect is for normal concrete very small (strength loss less than ten per cent), but for this low pH SCC there is no experience in the literature. One way of overcoming this uncertainty is to use 90 days as the design age, and "set off" the strength growth after 90 days with the aging effect. This process is estimated to be on the safe side with respect to strength.

6.3 Tensile strength

Tensile strengths are selected on uniaxial tensile tests performed at Luleå University of Technology. Characteristic material data are presented to be used in the structural analysis for the long-term behaviour. Material data are measured from cylinders with 68.5 mm diameter at the age of about 115 days. Only two specimens are tested for each concrete type. In spite of the limited amount of test data, real tensile data are preferable compared with data from splitting tests or data calculated based on the compressive strength. The reason is that the tensile strength has to be recalculated with some adjustment factor using splitting test results. Such factors show a wide spread in the literature, and direct tensile tests are used for this calibration. Such calibration tests are not performed here.

As only two test specimens exist for each concrete type, it is formally not possible to perform a statistical evaluation. Based on the observation that the spread in material strength has been low for the compressed concrete, an approximate technique to assess the spread in tensile strength is performed.

The standard deviation is based on $f_{ctm,1}$, $f_{ctm,2}$ and $f_{ctm,12} = (f_{ctm,1} + f_{ctm,2})/2$,

where $f_{ctm,}$ = mean tensile strength [MPa]; $f_{ctm,1}$ = mean tensile strength in test specimen 1 [MPa]; $f_{ctm,2}$ = mean tensile strength in test specimen 2 [MPa]; $f_{ctm,12}$ = average mean tensile strength for test specimens 1 and 2 [MPa].

The result is presented in Table 6-1.

The denotation *s* means the standard deviation, and $f_{ctk,0.05}$ is the 5% fraction value representing the characteristic tensile strength for the concrete in question.

The following values are chosen: $f_{ctk,B200}$ = 2.9 MPa, $f_{ctk,B300}$ = 3.3 MPa.

The level of the crack safety ratio, ξ /see BBK04 2008/, is accounted for to define the tensile strength to be used in the structural analyses.

The tensile strength will be used to assess whether cracking will occur in the numerical model. If cracking occurs, only compressed concrete will be considered.

Table 6-1. Obtained and calculated tensile strength values for low pH SCC.

Concrete	Parameter	f_{ctm}, MPa	s = std. dev., MPa	$f_{ctk,0.05}$, MPa
B200	$f_{ctm,1}$	3.43	0.14	2.94
	$f_{ctm,2}$	3.16		
	$f_{ctm,12}$	3.30		
B300	$f_{ctm,1}$	3.93	0.17	3.31
	$f_{ctm,2}$	3.59		
	$f_{ctm,12}$	3.76		

6.4 Young´s modulus

Young's modulus values are based on tests performed at Luleå University of Technology, see Figure 5-26. Average material data are presented to be used in the structural analysis for the long-term behaviour.

Again, like for the compressive strength in Section 6.2, to counteract the elasticity modulus increase due to formation of gel-products with possible, if any, elasticity modulus decrease due to aging, the first choice is to use the Young's modulus at 90 d in the numerical calculations. If the numerical calculations for some cases show that a higher Young's modulus would be unfavourable in some respect, a value direct taken from Figure 5-26 for larger ages than 90 days can be used.

6.5 Poisson´s ratio

Poisson´s ratios (i.e. lateral deformation in relation to the deformation in line with the load) are based on tests performed at Luleå University of Technology. Average material data to be used in the structural analysis for the long-term behaviour are presented in Table 6-1. Tests are performed for both compression and tension, see Table 6-2. Test data show consistently a Young's modulus (E) and a higher Poisson´s ratio (υ) for tension compared with compressive loading.

The following is chosen:	$\upsilon = 0.27$ (taken from the compression test as in compression it is a standardized test procedure, and the numerical calculations demand one value both for compression and tension).

Table 6-2. Poisson's ratio for B200.

Concrete mix of low pH SCC	Test	E [GPa]	υ [–]	$\upsilon_{average}$ [–]
B200	Tension	40.9	0.285	
	Tension	44.4	0.300	0.29
	Compression	37.9	0.262	
	Compression	37.5	0.270	0.27

6.6 Creep ratio

Chosen creep ratios are based on tests performed at Luleå University of Technology. Average material data to be used in the structural analysis for the long-term behaviour are presented in Figure 5-28. Creep ratios are evaluated with the aim of calculation of an effective elastic modulus to be used in a one-step calculation.

It has been shown in many one-step calculations that it is efficient to use the Trost-Bažant Method /Bažant 1972/, which is expressed by:

$E_{cm,ef} = E_{cm}/(1+\chi \cdot \varphi')$

where $\chi = 0.8$ and φ' is the creep ratio at maintained load, see Figure 5-28.

6.7 Shrinkage

The shrinkage was tested on sealed beam specimens. Shrinkage values presented in Figure 6-1 are zeroed at 24 h (ε_{cs}). The shrinkage used in the structural calculation for the long-term analyses is based on shrinkage starting at 90 d ($\varepsilon_{cs,90d}$), as the plug construction is supposed to be practically stress free at 90 d.

The evaluated shrinkage values are presented in Figure 6-1. Including the shrinkage for concrete mix B300 as an alternative is one way of taking the "maximum" shrinkage variation of B200 into account.

Values selected for calculations are:	$\varepsilon_{cs\,,90d} = 0.00$ ‰, $\varepsilon_{cs,1yr} = 0.07$ ‰, $\varepsilon_{cs10yrs} = 0.17$ ‰, $\varepsilon_{cs,100yrs} = 0.28$ ‰

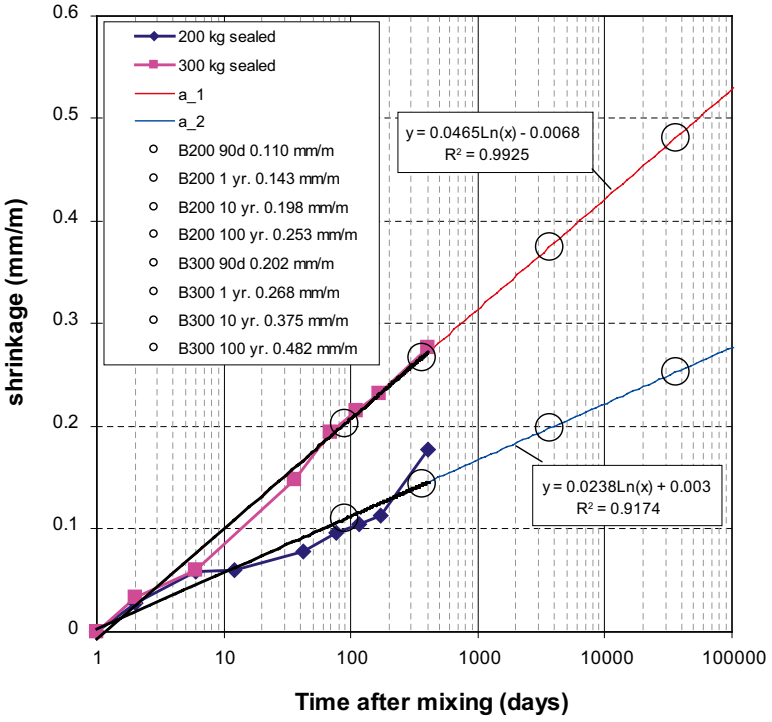

Concrete mix B200		
Time	ε_{cs}, ‰	$\varepsilon_{cs,90}$, ‰
90 d	0.11	0.00
1 yr.	0.14	0.03
10 yrs.	0.20	0.09
100 yrs.	0.25	0.14

Concrete mix B300		
Time	ε_{cs}, ‰	$\varepsilon_{cs,90}$, ‰
90 d	0.20	0.00
1 yr.	0.27	0.07
10 yrs.	0.37	0.17
100 yrs.	0.48	0.28

Figure 6-1. *Measured sealed shrinkage for concrete mixes B200 and B300.*

6.8 Permeability coefficient

Using the results from the water penetration test according to /SS-EN 12390-8 2000/ and a concept presented in /Neville 1994/, the calculation of the water permeability coefficient is possible. The permeability can be described by:

$$K = \frac{e^2 v}{2ht}$$

where e = measured depth of water penetration in the concrete in meters, h = hydraulic head in meters, t = time under pressure in seconds and v = fraction of volume of concrete occupied by pores, typically between 0.02 and 0.06. The calculated results are shown in Table 6-3.

The permeability coefficient (K) of the material in the plug is supposed to be not higher than the permeability coefficient of the surrounding rock, which means the material should have a permeability coefficient within the interval $10^{-12} \leq K \leq 10^{-11}$ m/s. The water permeability coefficient of the low pH SCC is much lower than this.

Value selected for calculations is: K = 10^{-11} m/s.

Table 6-3. Calculated water permeability coefficients for low pH SCC.

Concrete	*e* m	υ, –	*h* m	*t* s	*K* m/s
B200	0.005	0.04	50	259200	$3.9\ 10^{-14}$
B300	0.003	0.04	50	259200	$1.4\ 10^{-14}$

7 Conclusions

Workable mix designs of low pH self compacting concrete were developed. The open time and the self-compacting properties are sufficient for use in the tunnel plugs. The mix composition used incorporate limestone filler, Ordinary Portland cement, densified silica fume, superplasticizer, high quality natural fine aggregates and average quality crushed coarse aggregate. Two mix designs, B200 and B300, were investigated more thoroughly. The amount of binder was lowered as much as possible, while maintaining good stability of the fresh concrete.

The properties of young and hardening low pH SCC differ to some extend from traditional concrete. The early volume changes (< 24 hours) were high, up to 0.8 mm/m. The total shrinkage (drying shrinkage and autogenous shrinkage) is of the same magnitude for the two mix designs. The B200 has a lower autogenous shrinkage but a higher drying shrinkage compared to the B300. Both, the drying shrinkage as well as the shrinkage under sealed conditions are remarkably low, if the high volume changes during the first 24 hours are neglected. The heat development and also the compressive strength development during the first days of curing are very low. Unlike conventional concrete, the compressive strength keeps increasing after 28 days of curing. The strength increases to more than 100 MPa after one year of curing. The properties of mature low pH SCC do not differ remarkably from conventional concrete, other than higher final strength and lower permeability. The established models for Young's modulus, compressive strength, stress-strain and creep are valid. The creep ratio is low when the concrete is mature. There is no big difference between the two mix designs; the mix with 300 kg of binder has higher final compressive strength, Young's modulus and tensile strength. Both mix designs have very good resistance to water penetration. Longer term strength tests are still underway. The long term durability of both mixes should be assessed.

The evaluation of the obtained results using mathematical concepts, established for traditional concrete, was possible. A setup of input data for FE-calculations was established. To what extend the differences between the two mix designs influence the development of stresses and consequently the crack risk needs to be evaluated by FE-calculations.

The results of the factory tests show that mixing and pumping at full scale even using rather inefficient equipment can be done. The importance of correct determination of aggregate moisture and correct mixing order was shown, as improper determination of aggregate moisture content and order of adding materials effected the workability of the concrete and its hardened properties. It was found that similar hardened concrete properties were achieved in factory tests as those achieved in laboratory tests.

8 References

Atrushi D S, 2003. *Tensile and Compressive Creep of Early Age Concrete: Testing and Modelling*. Doctoral Thesis, Norwegian University of Science and Technology, 2003:17, 314 pp.

Bažant Z P, 1972. *Prediction of Concrete Creep Effects Using Age-Adjusted Effective Modulus Method* . ACI Journal, April 1972, pp 212–217.

Bažant Z P, 1975. *Theory of Creep and in Concrete. A Précis of Recent Developments.* Mechanics Today, Vol. 2, pp 1–93.

Bažant Z P, Chern J, 1985. *Concrete Creep at Variable Humidity: Constitutive law and Mechanisms*. Materials and Structures, vol. 18, pp. 1–20.

Bažant Z P /editor/, 1988. *Mathematical Modelling of Creep and Shrinkage of Concrete.* (Fourth RILEM Int. Symp. on Creep and Shrinkage of Concrete: Mathematical Modelling. Northwestern University, August 26–29, 1986). John Wiley and sons.

BBK04, 2008. *Boverkets handbook om betongkonstruktioner* (in Swedish). Handbook from Boverket on Concrete Structures. Can be downloaded from: http://www.boverket.se/upload/publicerat/bifogade%20filer/2004/boverkets_handbok_om_betongkonstruktioner_BBK_04.pdf.

Bergström S G, 1953. *Curing Temperature, Age and Strength of Concrete*. Magazine of Concrete Research, Vol. 4, pp. 61–66.

Betonghandbok Material, 1994. AB Svensk Byggtjänst, in Swedish.

Bjøntegaard Ø, 2000. *Thermal Dilation and Autogenous Deformation as Driving Force to Self-Induced Stresses in High Performance Concrete*. Doctoral Thesis, Norwegian University of Science and Technology, 1999, ISBN 82-7984-002-8.

Bosnjak D, 2001. *Self-induced Cracking Problems in Hardening Concrete Structures*. Doctoral Thesis, Norwegian University of Science and Technology, 2001, ISBN 82-7984-151-2.

Byfors J, 1980. *Plain concrete at early ages*. Swedish Cement and Concrete Research Institute, Fo/Research 3:80, Stockholm, 462 pp.

Carlswärd J, 2006. *Shrinkage Cracking of Steel Fibre Reinforced Self Compacting Concrete Overlays – Test Methods and Theoretical Modelling.* Division of Strucural engineering, Luleå University of Technology, Doctoral Thesis 2006:55, 248 pp.

ConTeSt Pro, 2008. *User's Manual*. Produced by JEJMS Concrete AB, Luleå.

Dahlström L-O, Gueorguiev G, Johansson M, Magnusson J, 2008. *Feasibility study of a concrete plug made of low pH concrete (draft)*, R08-0X.

EFNARC, 2005. *The European guidelines for self compacting concrete*, www.efnarc.org, 2005.

Ekerfors K, 1995. *Mognadsutveckling i ung betong, temperaturkänslighet, hållfasthet och värmeutveckling* (in Swedish). Maturity development for young concrete, temperature sensitivity, strength growth and heat evolution. Luleå University of Technology, Division of Structural Engineering. Licentiate thesis 1995:34 L.

Ekerfors K, Jonasson J-E, 2000. *Maturity Development in Young Concrete – Temperature Sensitivity, Strength and Heat Development*. Nordic Concrete Research, Publication No. 25, 2/2000, ISBN 82-91341-41-9, pp 35–47.

Emborg M, 1989. *Thermal Stress in Concrete Structures at Early Ages*. Doctoral Thesis 1989:73D, Division of Structural Engineering, Luleå University of Technology, Luleå 1989.

EN 1992-1-1:2004, 2004. *Eurocode 2: Design of concrete structures – Part 1-1: General rules and rules for buildings*, European Committee for Standardization, (ICS 91.010.30, 91.080.40).

Esping O, 2007. *Early age properties of self-compacting concrete- Effects of fine aggregate and limestone filler*, doctoral thesis, 2007, Chalmers University of Technology, Göteborg, Sweden.

Freisleben Hansen P, Pedersen E J, 1977. *Måleinstrument til control af betons haerdning* (in Danish), Maturity computer for controlled curing and hardening of concrete. Journal of the Nordic Concrete Federation, No. 1:1977, Stockholm, pp 21–25.

Groth P, 2000. *Fibre Reinforced Concrete – Fracture Mechanics Methods Applied on Self-Compacting Concrete and Energetically Modified Binders.* Division of Structural Engineering, Luleå University of Technology, Doctoral Thesis 2000:04 pp. 204.

Hedlund H, 2000. *Hardening concrete- Measurements and evaluation of non-elastic deformation and associated restraint stresses.* Division of Structural Engineering, Luleå University of Technology, Doctoral Thesis 2000:25, 394 pp.

Ji G, 2008. *Cracking Risk of Concrete Structures in The Hardening Phase*. Doctoral Thesis, Norwegian University of Science and Technology, 2008:198, 244 pp.

Jonasson J-E, 1984. *Slipform construction – Calculations for Assessing Protection Against Early Freezing.* Swedish Cement and Concrete Research Institute, Stockholm, CBI Forskning/ Research 4.84, 69 pp.

Jonasson J-E, 1994. *Modelling of Temperature, Moisture and Stresses in Young Concrete*. Division of Structural Engineering, Luleå University of Technology, Doctoral Thesis 1994:153D, 225 pp.

Jonasson J-E, Westman G, 2001. *Conversion of Creep Data to Relaxation Data by the Program RELAX.* Division of Structural Engineering, Luleå University of Technology, IPACS Report, ISBN 91-89580-45-1, 25 pp.

Kanstad T, Hammer T A, Bjøntegaard Ø, Sellevold E J, 1999. *Mechanical Properties of Young Concrete – Evaluation of Test Methods for Tensile Strength and Modulus of Elasticity – Determination of Model Parameters.* NOR-IPACS report STF22 A99762. ISBN 82-14-01062-4.

Lagerblad B, Utkin P, 1993. *Silica granulates in concrete-dispersion and durability aspects*, CBI-report 3-93, 1993, Stockholm, Sweden.

Larsson M, 2003. *Thermal Crack Estimation in Early Age Concrete – Models and Methods for Practical Application.* Division of Structural Engineering, Luleå University of Technology, Doctoral Thesis 2003:20, 190 pp.

Larson M, Jonasson J-E, 2003. *Linear Logarithmic Model for Concrete Creep – I. Formulation and Evaluation*. Journal of Advanced Concrete Technology, Vol. 1, No. 2, July 2003, Japan Concrete Institute, pp172–187.

Lea, edited by Hewlett P C, 2000. *Lea's Chemistry of Cement and Concrete, 4th edit.* Arnold, 2000.

Neville, 1994. *Properties of concrete, 4th ed*.

Nilsson M, 2003. *Restraint Factors and Partial Coefficients for Crack Risk Analyses of Early Age Concrete Structures.* Division of Structural Engineering, Luleå University of Technology, Doctoral Thesis 2003:19, 170 pp.

Nurse R W, 1949. *Steam Curing of Concrete*. Magazine of Concrete Research, Vol. 1, pp 79–88.

Reinhardt H W, Wuestholz T, 2007. *Tensile deformation behaviour of self compacting concrete under sustained loading*, 5th International RILEM Symposium on Self-Compacting Concrete2007, Ghent, Belgium.

Saul A G A, 1951. *Principles Underlying the Steam Curing of Concrete at Atmospheric Pressure*. Cement and Concrete Research, Vol. 2, pp 216–224.

SS-EN 197-1, 2000. *Cement – Part 1: Composition, specifications and conformity criteria for common cements*, European Committee for Standardization, Brussels.

SS-EN 206-1, 2001. *Concrete – Part 1: Specification, performance, production and conformity*, European Committee for Standardization, Brussels.

SS-EN 12620, 2008. *Aggregates for concrete*, European Committee for Standardization, Brussels.

SS-EN 12390-3, 2001. *Testing hardened concrete – Part 3: Compressive strength of test specimens*, European Committee for Standardization, Brussels.

SS-EN 12390-6, 2000. *Testing hardened concrete – Part 6: Tensile splitting strength of test specimens*, European Committee for Standardization, Brussels.

SS EN 12390-8, 2000. *Testing hardened concrete – Part 8: Depth of penetration of water under pressure*, European Committee for Standardization, Brussels.

SS 13 72 15, 2000. *Concrete testing – Hardened Concrete – Shrinkage*, SIS Förlag AB, in Swedish.

SS 13 72 32, 2005. *Concrete testing – Hardened Concrete – Modulus of elasticity in compression*, SIS Förlag AB, in Swedish.

Taylor H W F, 1997. *Cement chemistry, 2nd ed.*, Thomas Telford, 1997, London, UK.

Thelandersson S, 1987. *Modelling of Combined Thermal and Mechanical Action in Concrete*. Journal of Engineering Mechanics, Vol.113, Issue 6, ASCE, pp 893–906.

Wallevik O, 2007. *Rheology of cement-based materials*, material for DTU-RILEM course, Aug 2007.

Westman G, 1999. *Concrete Creep and Thermal Stresses – New Creep Models and their Effects on Stress Development*. Doctoral Thesis 1999:10, Division of Structural Engineering, Luleå University of Technology, Luleå 1999.

List of abbreviations

a_1	Inclination, dependent on the loading ages, in the linear-logarithmic plot of the creep behaviour
a_2	Inclination, dependent on the loading ages, in the linear-logarithmic plot of the creep behaviour
a	Cooling ratio
α_{ct}	Upper limit of the linear stress-strain at 1st loading
α_T	Thermal dilation coefficient
β_Δ	Adjustment factor to be used for different admixtures [–]
β_T	Temperature sensitivity factor
β_1	Exponent
c_c	Specific heat capacity of the concrete by cement weight
Δ	Change associated with a time step
Δt_0	“elastic” time duration, here 0.001 day
Δl_{load}	$t - t_0$ = load duration
$\Delta J(\Delta t_{load}, t_0)$	“creep” part of the total deformation
Δt_1	Time duration for the distinct break point in the creep behaviour
ΔT	Change in temperature
e	Measured depth of water penetration in the concrete
ε_0	Strain related to a linear behaviour up to $\sigma = f_{ct}$
ε_{cs}	Strain in concrete related to shrinkage
ε_m	Strain related to stresses in concrete
ε_{tot}	Measured strain
ε_T^o	Stress free strain related to changes in temperature
ε_{SH}^o	Stress free strain not related to changes in temperature
ε_{s1}	Fitting parameter
ε_{s2}	Fitting parameter
ε_T	Strain related to a temperature variation at a stress level of σ/f_{ct} (≥ 0)
ε_φ	Strain not related to a temperature variation at a stress level of σ/f_{ct} (≥ 0)
$E(t_0)$	Young’s modulus at loading age
E_{28}	Young’s modulus at equivalent time = 28d
E_{cm}	Average Young’s modulus of concrete cylinders
φ'	Creep ratio at maintained load
f_A	Compressive strength at $t_e = t_A$
f_{cc}	Compressive strength as a function of equivalent time
$f_{cc,28}$	28-days compressive strength
f_{ct}	Tensile strength
f_{cc}^{ref}	Reference compressive strength
f_{ct}^{ref}	Reference tensile strength
$f_{cm,cube}$	Average compressive strength of cubes
f_{cm}	Average compressive strength for cylinders
f_{ck}	Characteristic compressive strength
f_{ctm}	Average tensile strength of cylinders
$f_{ctk,0.05}$	5% percentile value of tensile strength of cylinders
h	Hydraulic head
$J(0.001, t_0)$	Measured deformation 0.001d
$J(\Delta t_{load}, t_0)$	Total deformation
χ	Factor in the Trost-Bažant Method
κ_1	Fitting parameter
κ_3	Fitting parameter
K	Permeability coefficient

λ_1	Fitting parameter
η_{SH}	Fitting parameter
υ	Poisson's ratio
θ	Activation energy divided by general gas constant
θ_{ref}	Fitting parameter
ρ_c	Concrete density
σ	(uniaxial) stress in the concrete
s	Fitting parameter
s_E	Shape parameter for the growth of the Young's modulus
t_0	equivalent age at loading
t_A	Start time, here 1.5 h
t	Clock time
t_e,	temperature equivalent time
$t_{e,0}$	starting time of t_e (at t = 0)
t_1	Fitting parameter
t_S	Fitting parameter
t_{SE}	equivalent time, where deformations start to create stresses
t_{s1}	Fitting parameter
t_{s2}	Fitting parameter
t_{SH}	Fitting parameter
T	Temperature
T_{air}	Environmental temperature in the air
T_{start}	Starting concrete temperature
v	Fraction of volume of concrete occupied by pores
W_B	Generated heat by weight of binder as a function of equivalent time
W_{tot}	Generated heat at testing
W_U	Ultimate generated heat by weight of binder

AEA	Air entraining agent
B200	Low pH SCC with 200 kg of binder per cubic meter concrete
B300	Low pH SCC with 300 kg of binder per cubic meter concrete
CEM I	Ordinary Portland Cement
EDX	Energy-dispersive X-ray spectroscopy
EN	European Standard
LA	Low alkali
LVDT	Linear variable displacement transducer
MH	Moderate heat
MPa	Mega Pascal
pH	Measure of the acidity or basicity of a solution
RH	Relative humidity
SCC	Self compacting concrete
SEM	Scanning Electron Microscope
SR	Sulphate resistant
SS	Swedish Standard
VMA	Viscosity modifying agent
w/b	Weight of water divided by weight of binder (cement + silica fume)
w/c	Weight of water divided by weight of cement
w/p	Weight of water divided by weight of powder (cement + silica fume + filler)